Lecture B2 and C3a: Superconductive RF

Cavity Fundamental
SRF Fundamental
Cavity Fabrication

T. Saeki (KEK)

LC school 2015

27 Oct. - 6 Nov. 2015, Whistler, Canada

ILC Overview

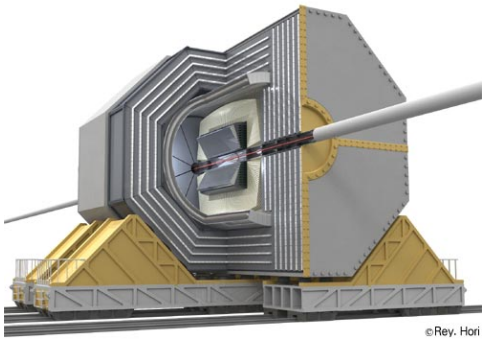

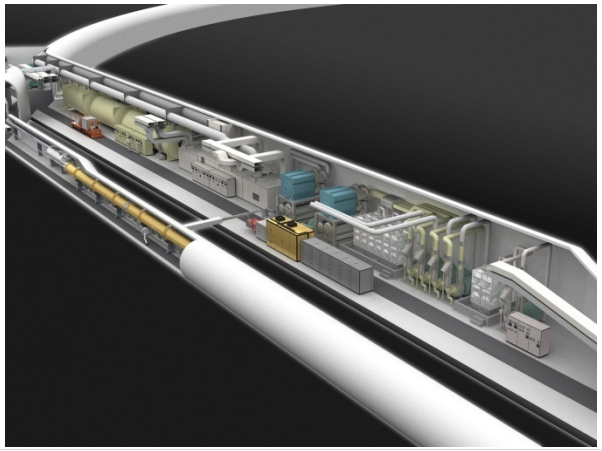

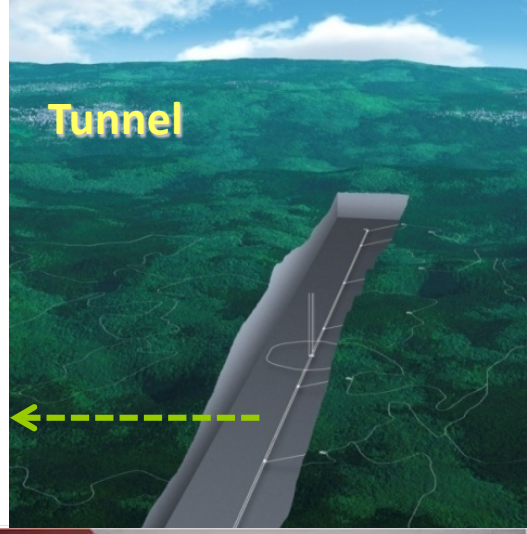

Detector

# of SRF cavities ~16000

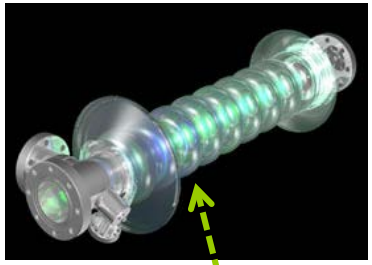

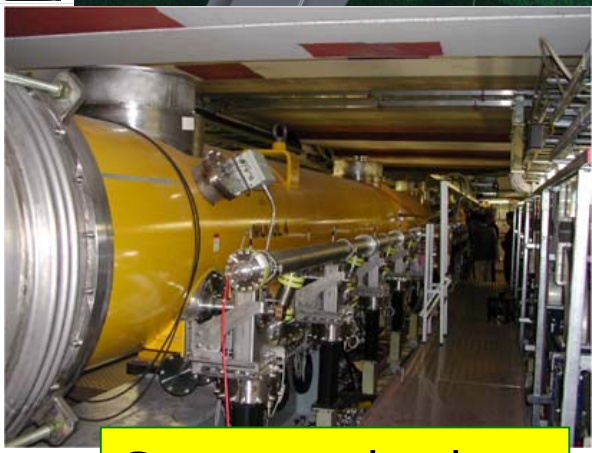

Superconducting RF accelerator

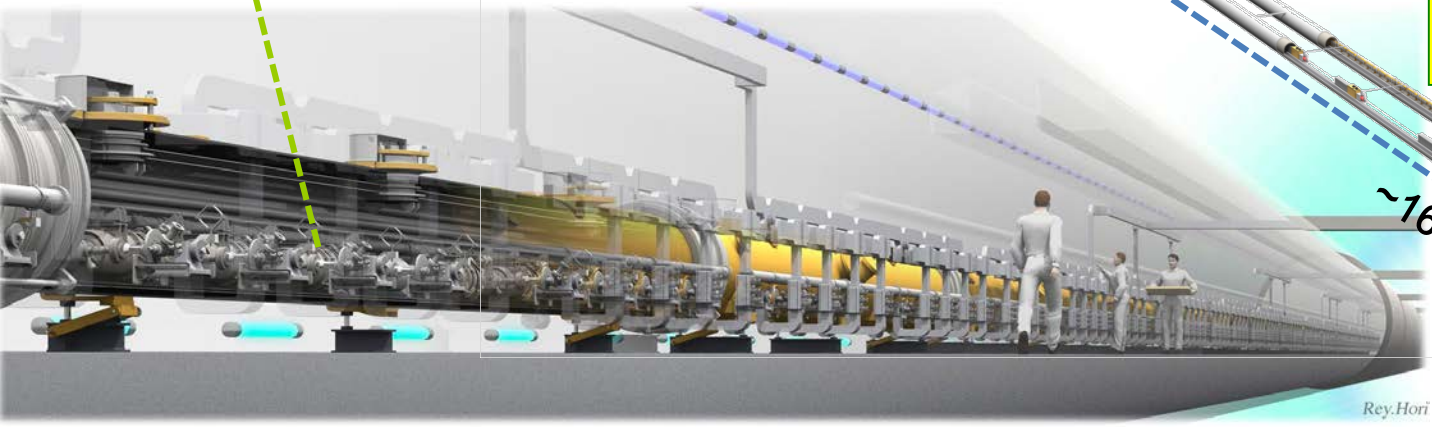

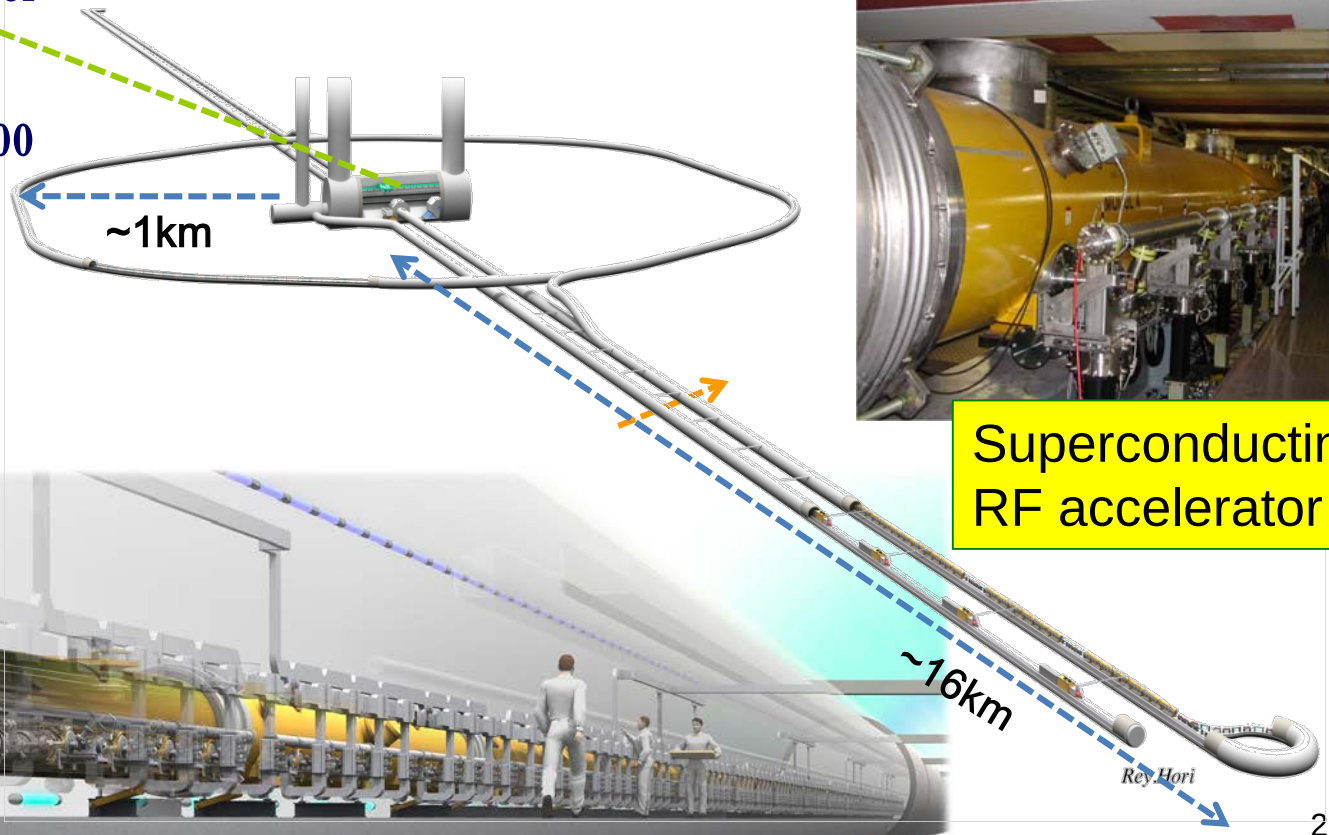

European XFEL

Civil Construction for the European XFEL

3.4km

Slide by H. Weise

European XFEL

Accelerator Complex for 17.5 GeV

100 + 1 accelerator modules

808 accelerating cavities
1.3 GHz / 23.6 MV/m

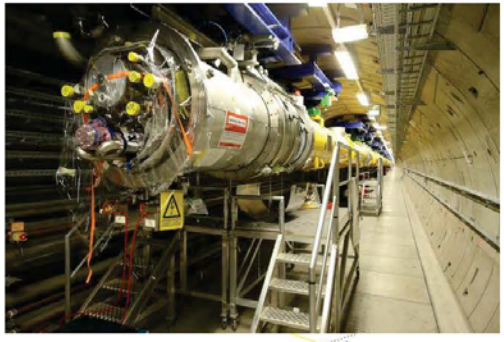

25 + 1 RF stations
5.2 MW each

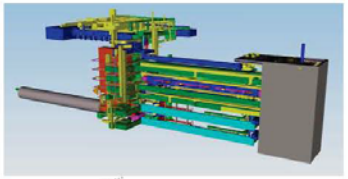

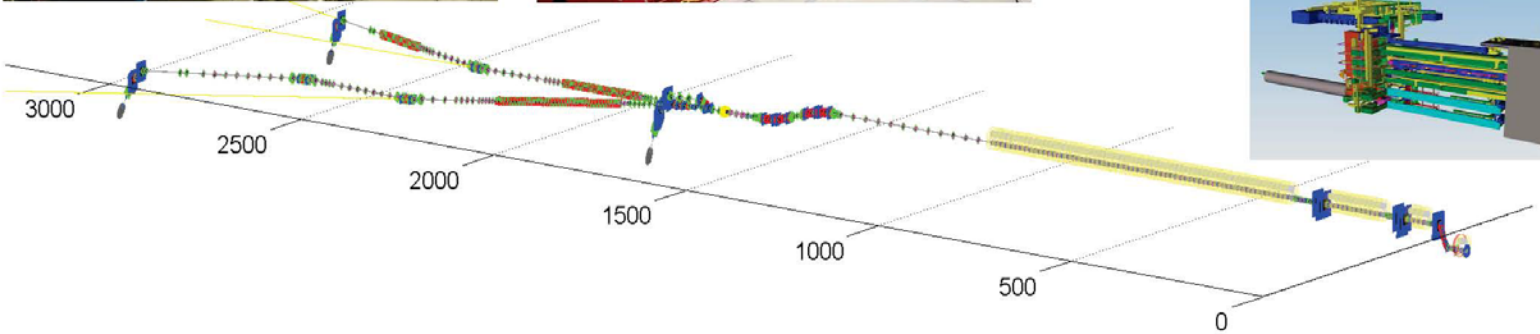

Accelerator technology - collaborative effort

Industrial study module assembly (M6 done, M8 autumn 2007)

Superferric magnet (CIEMAT)

BPM (Saclay)

2 more cryostats (TTF3/INFN) delivered

# of 9-cell cavities = 800

Integrated HOM absorber

Length quantized n·λ/2 (possibility of ERL)

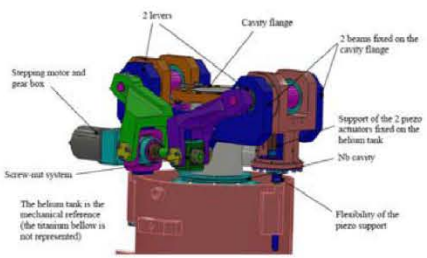

Tuner w/piezo (Saclay)

Industrialization in preparation

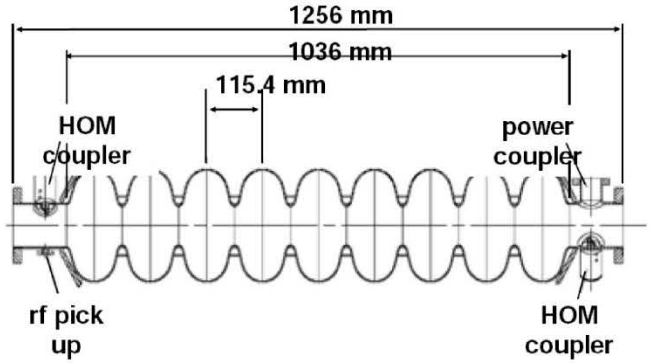

LLRF development (collab. Warsaw/Lodz)

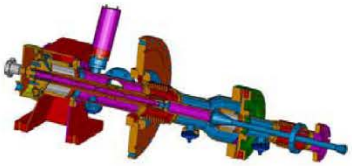

TTF3-type coupler

Industrialization launched (Orsay)

Almost the same technology as ILC

Installation Progress XTL

European XFEL

34 Modules installed
6 Modules parked

1 RF-Station ready
5 RF-Station in preperation

Status: 04.09.2015

1

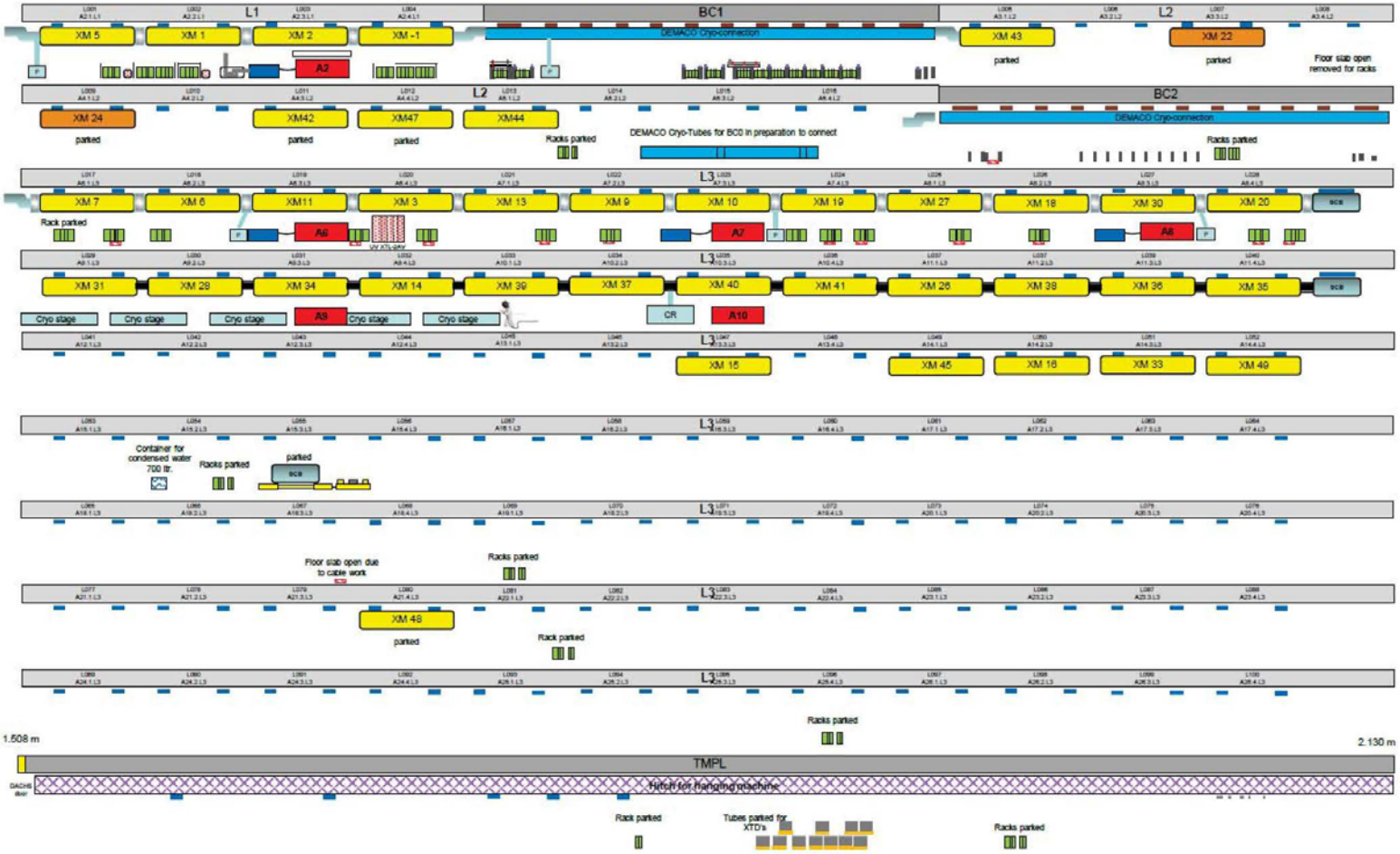

Fabrication of 9-cell Cavity

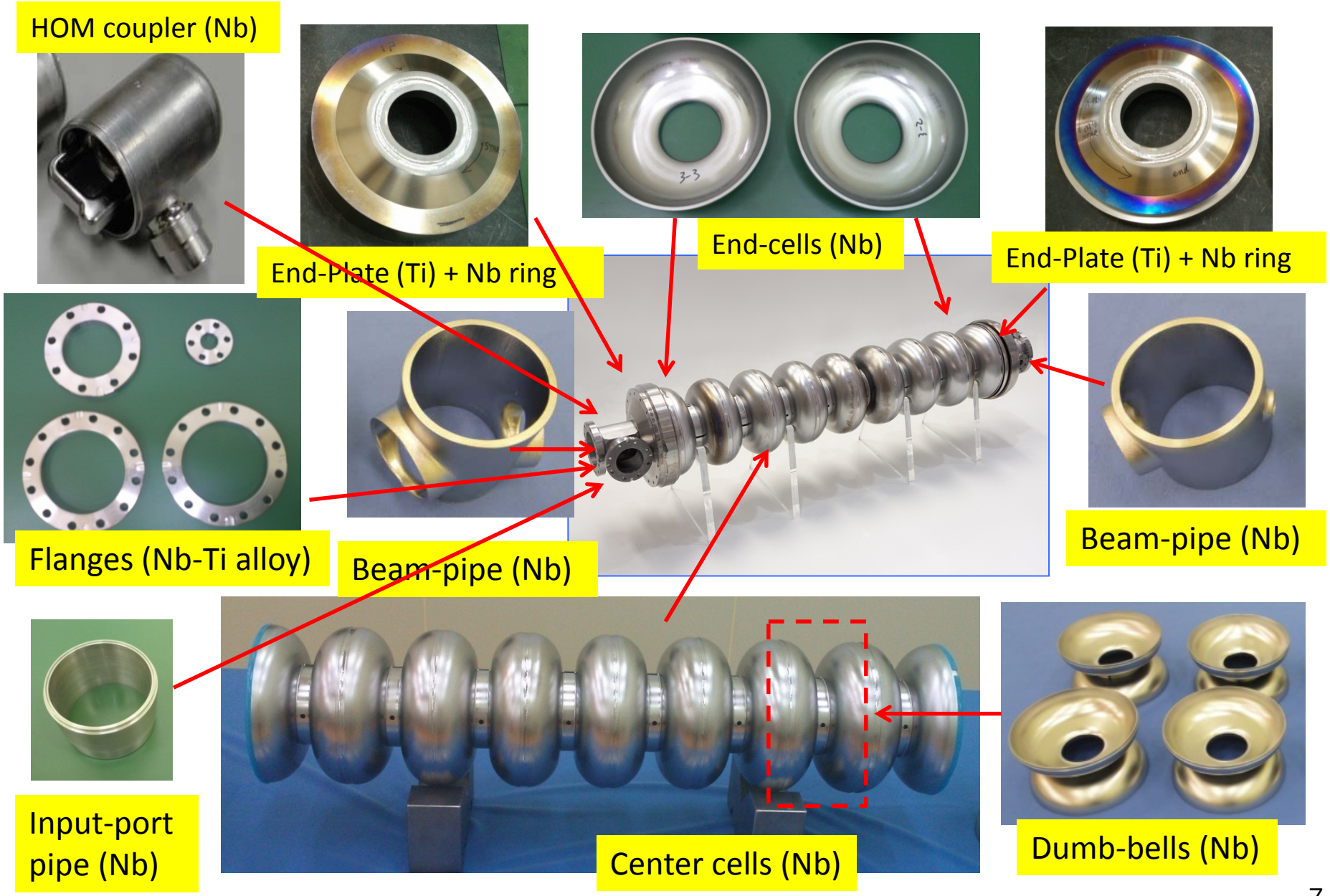

Inner Surface Preparation of SC Cavity

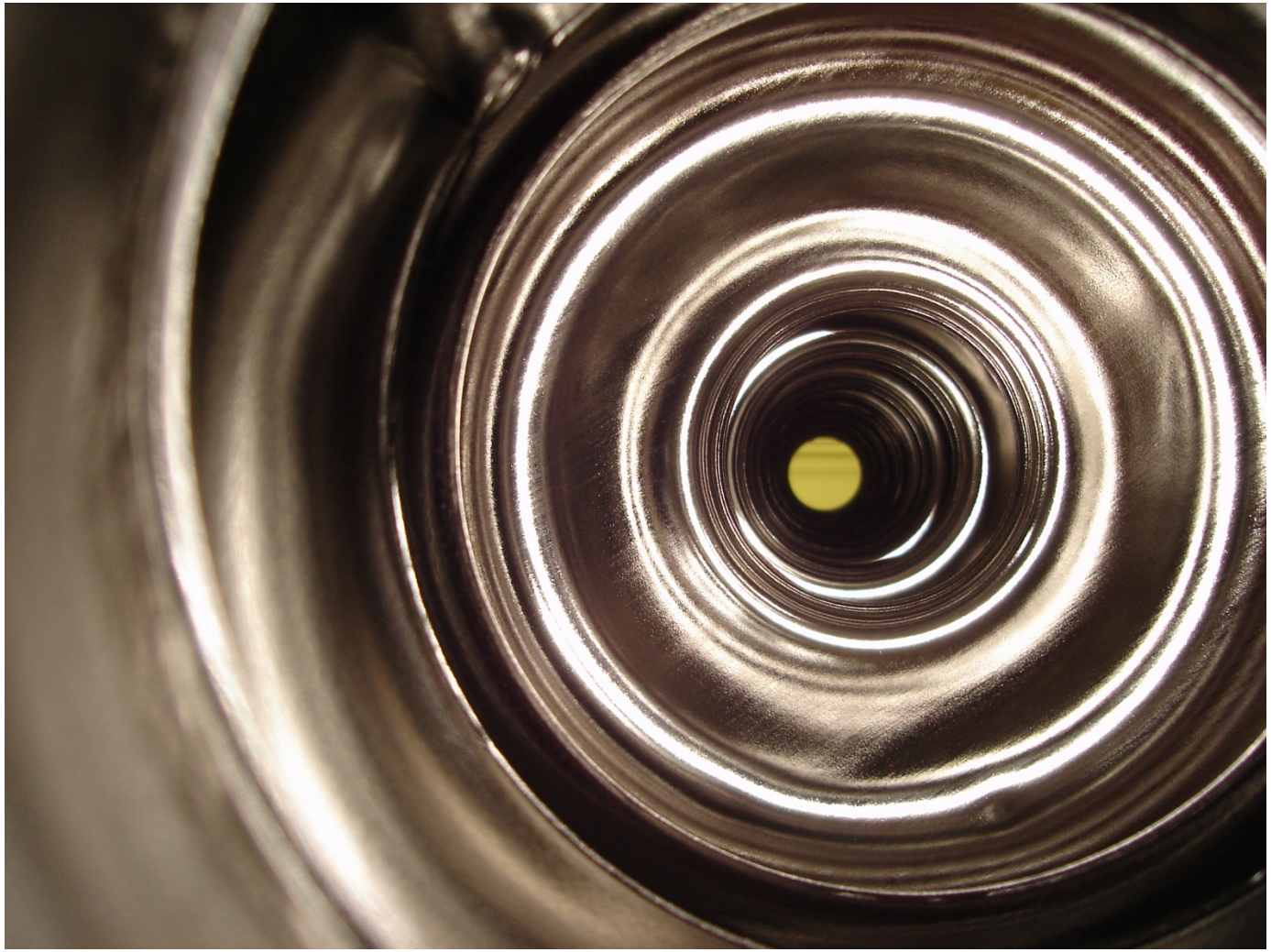

Status of Euro-XFEL (E.U.)

European XFEL

Treatment: European XFEL treatment recipe was worked out on prototype cavities

Prior surface treatment.

EP 110-140 µm (main EP), outside BCP, ethanol rinse, 800° C annealing, tuning

Final surface treatment - two alternative options

1. Final EP of 40 µm, ethanol rinse, high pressure water rinsing (HPR) and 120° C bake
2. Final BCP of 10 µm (BCP Flash), HPR and 120° C bake.

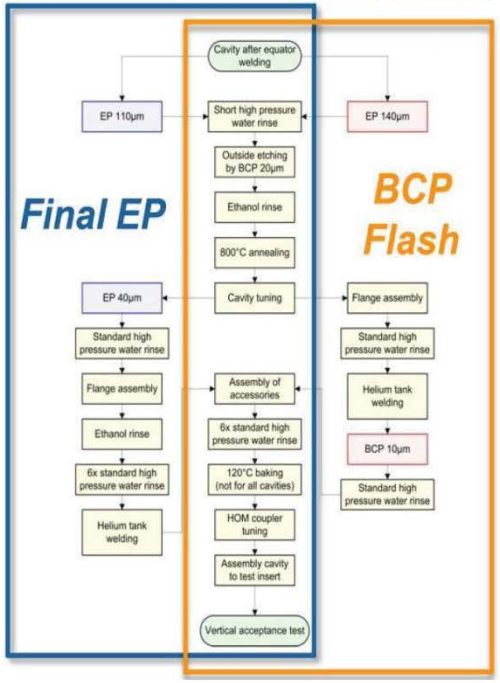

Integration of the helium tank, assembly of HOM, pick up and high Q antennas and shipment to DESY for 2K RF acceptance test

Slide by W. Singer / DESY

RI: 380 cavities / 2 year
Zanon: 380 cavities / 2 year
Total 760 cavities / 2 year

DESY

String Assembly

Saclay

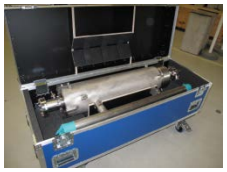

RI Germany

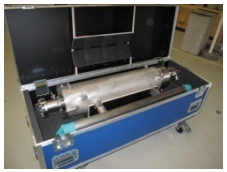

Z Italy

Cavity Fabrication

Acceptance
Vertical RF Test

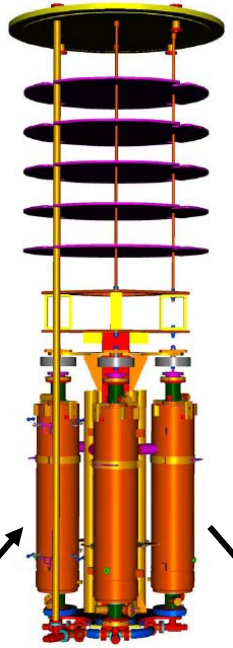

DESY Germany

IRFU /CEA France

DESY takes care of installation / dismounting of cavities into / from test insert
Transport to CEA in transport boxes as well

Slide by H. Weise

Cavity-String Assembly in Clean Room (DESY)

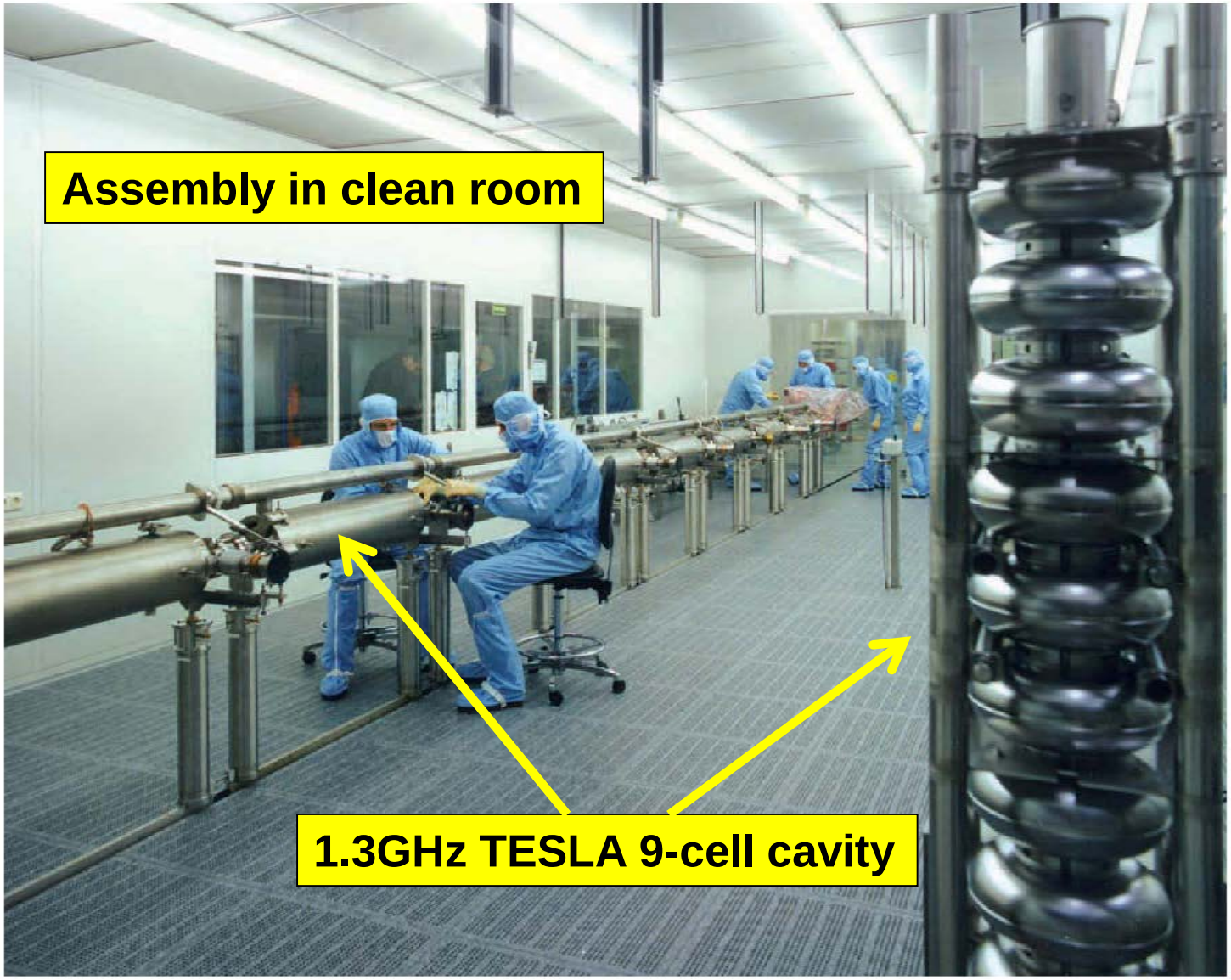

Saclay (March 2011)

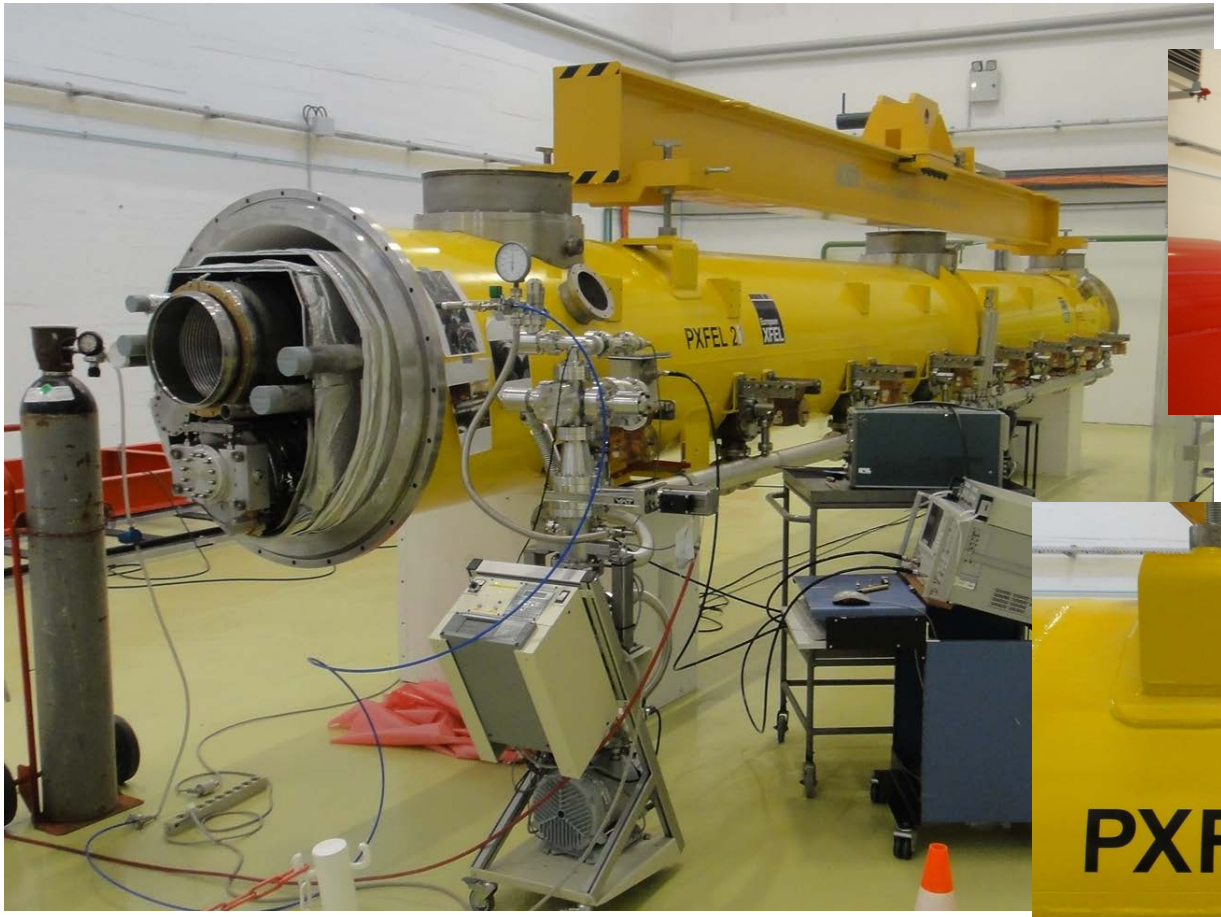

7 March 2011 at Saclay

PXFEL 2.1 (DESY >>> Saclay >>> transportation to DESY within a few weeks)

European XFEL

The finished L1 section

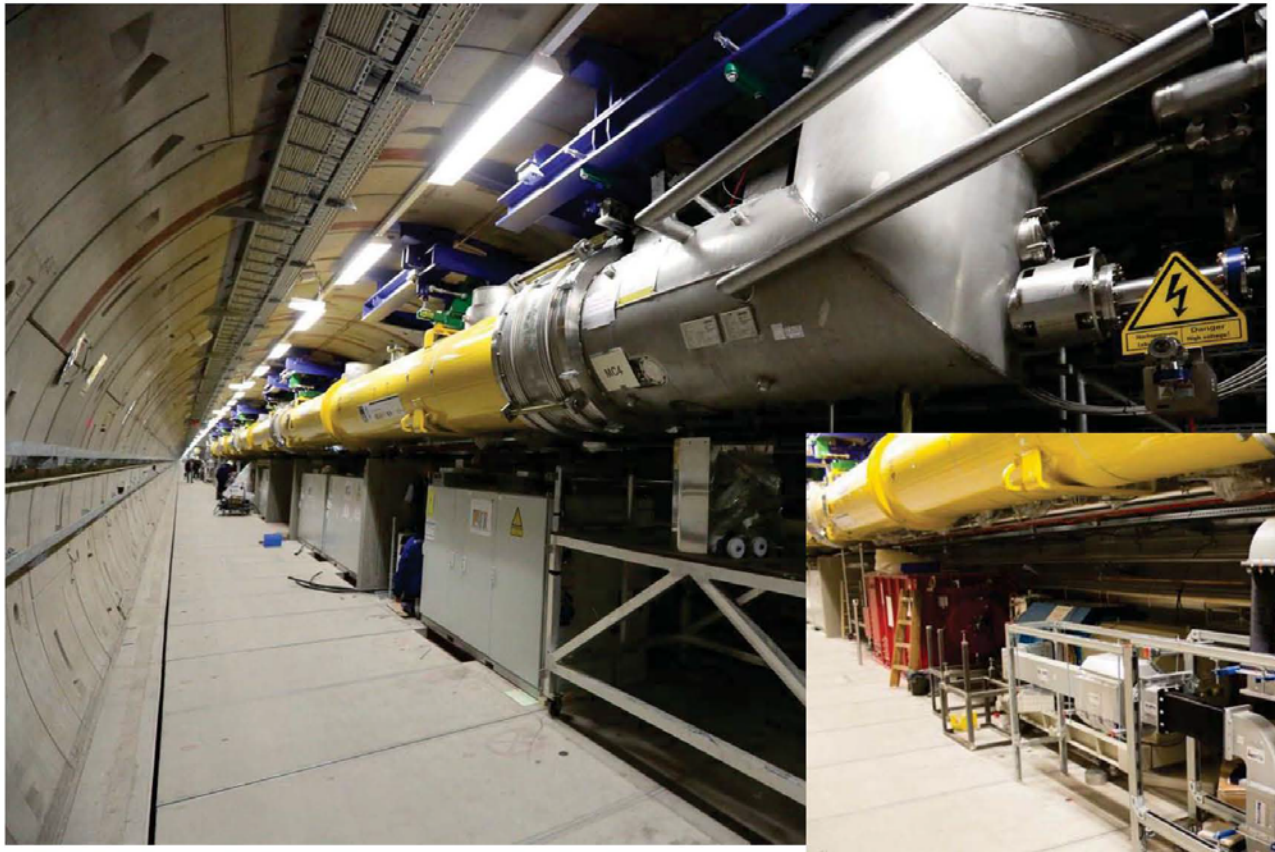

Lecture B and C3a: Superconducting RF

Cavity Fundamental

1.3 GHz elliptical 9-cell cavity

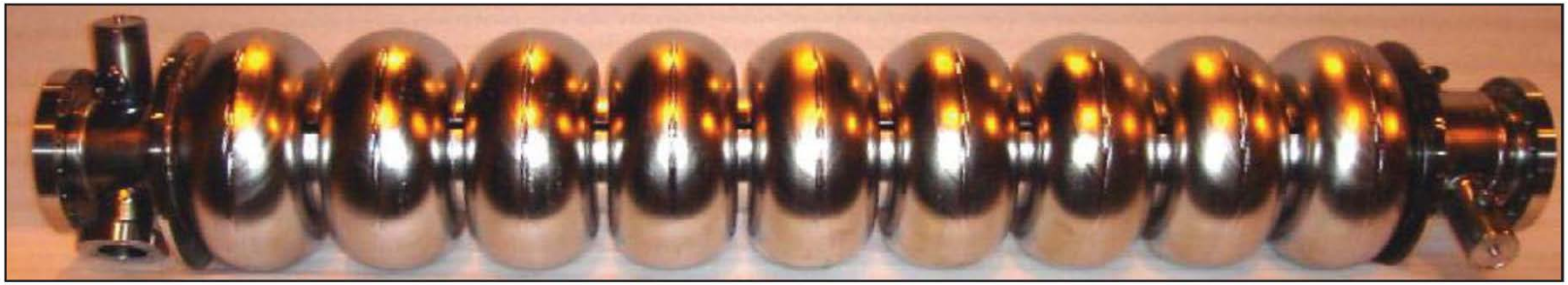

Pill Box Cavity

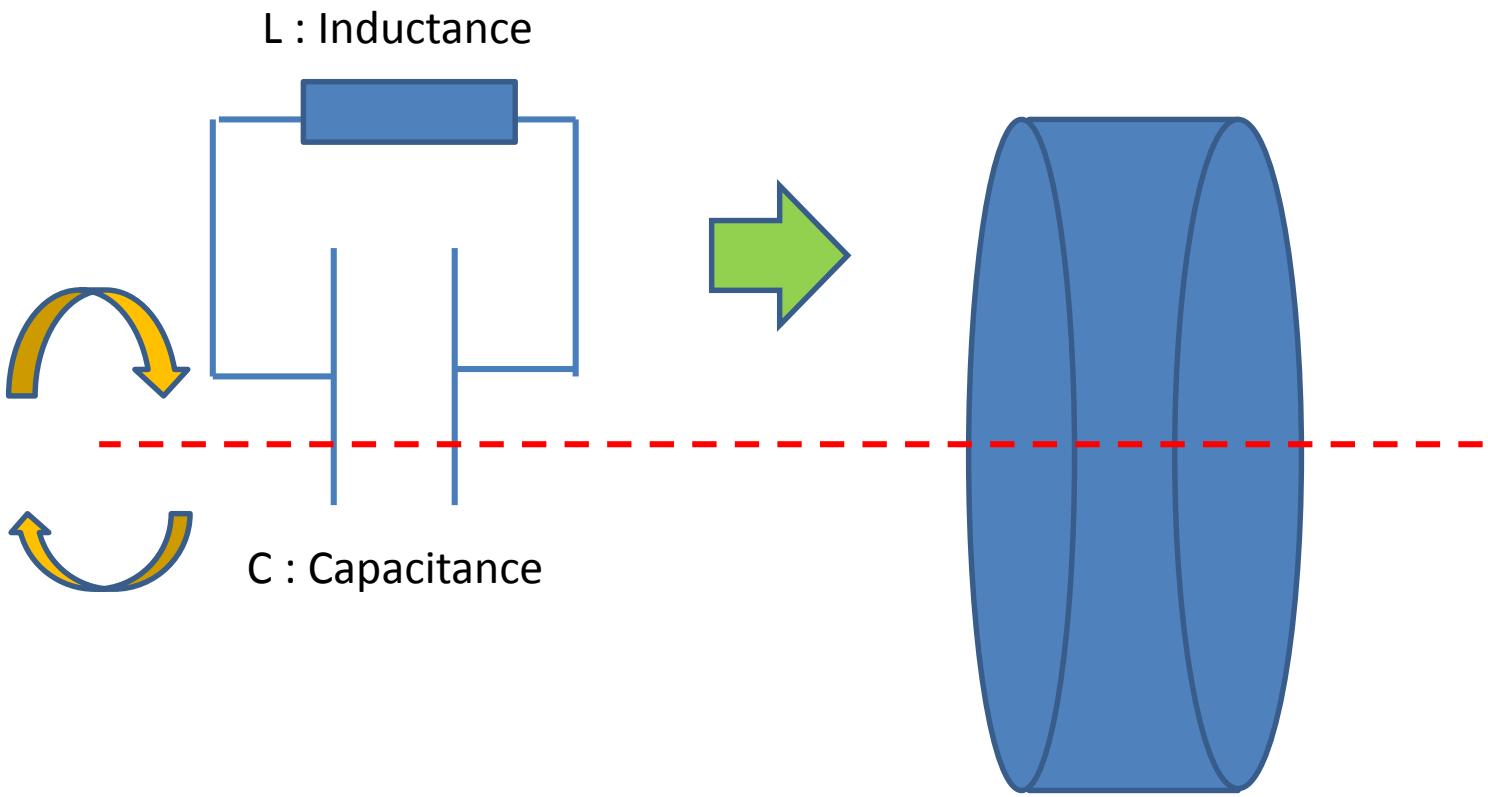

Pill Box Cavity

Hollow right cylindrical enclosure

Operated in the TM_{010} mode $H_z = 0$

TM_{010} mode

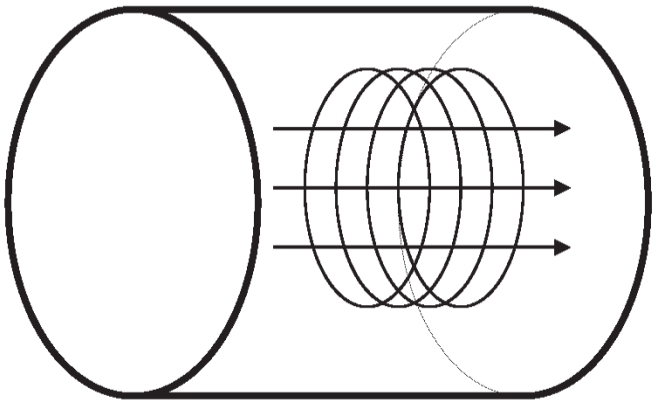

$$\frac{\partial^2 E_z}{\partial^2 r} + \frac{1}{r}\frac{\partial E_z}{\partial r} = \frac{1}{c^2}\frac{\partial^2 E_z}{\partial^2 t} \qquad \omega_0 = \frac{2.405c}{R}$$

$$E_z(r,z,t) = E_0 J_0\left(2.405\frac{r}{R}\right)e^{-i\omega_0 t}$$

$$H_\varphi(r,z,t) = -i\frac{E_0}{\mu_0 c}J_1\left(2.405\frac{r}{R}\right)e^{-i\omega_0 t}$$

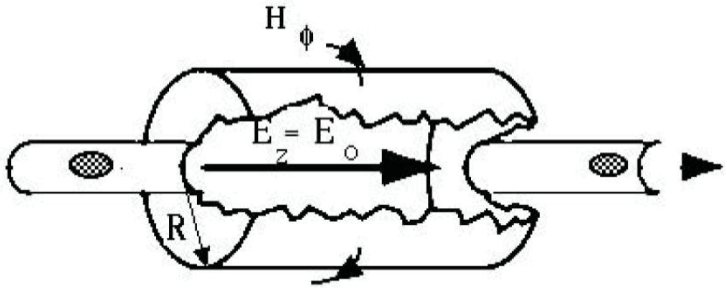

Modes in pill-box cavity

- TM_{010}
  - Electric field is purely longitudinal
  - Electric and magnetic fields have no angular dependence
  - Frequency depends only on radius, independent on length
- TM_{0mn}
  - Monopoles modes that can couple to the beam and exchange energy
- TM_{1mn}
  - Dipole modes that can deflect the beam
- TE modes
  - No longitudinal E field
  - Cannot couple to the beam

Pill-box cavity to real cavity

Beam tubes reduce the electric field on axis

- **Gradient decreases**
- **Peak fields increase**
- **R/Q decreases**

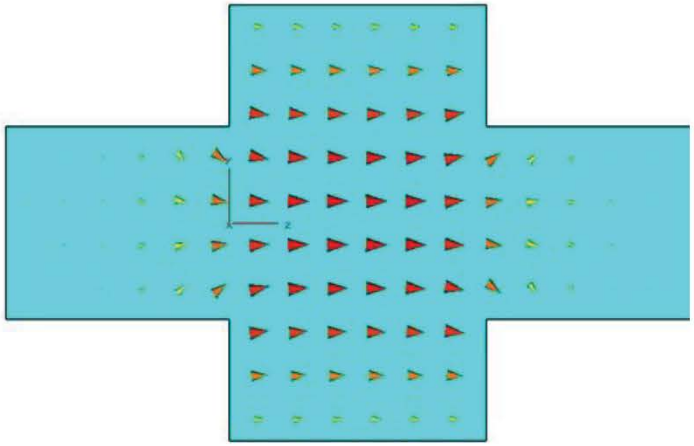

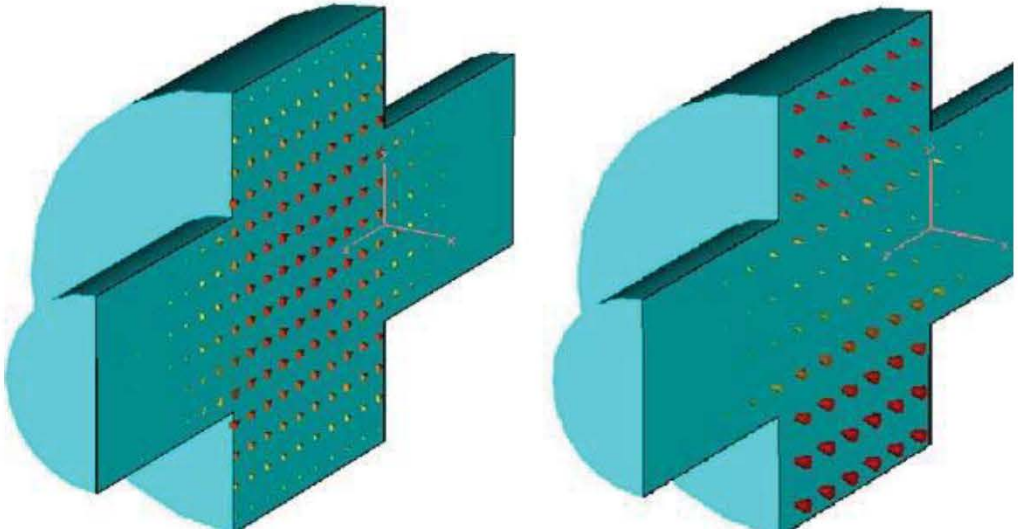

Pill-box cavity to real cavity

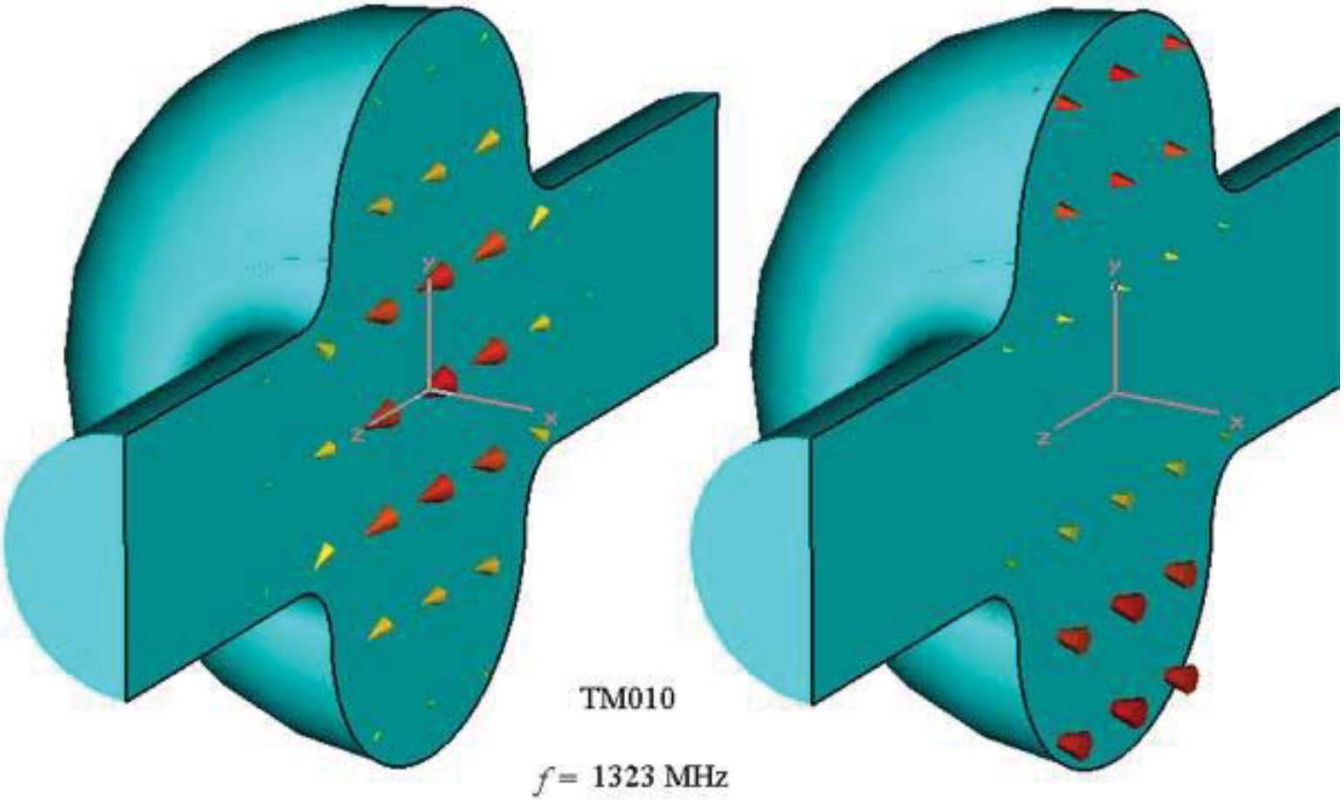

Single-cell cavity

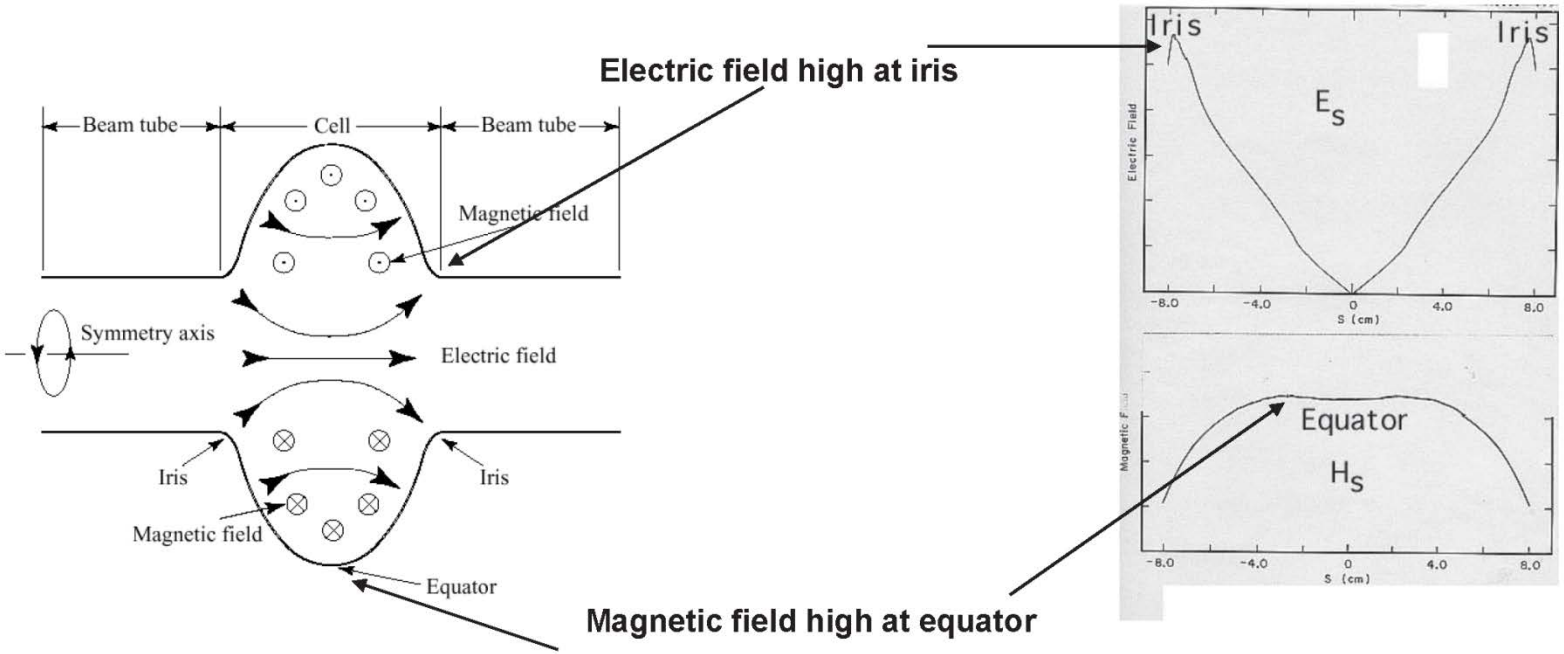

Single-cell cavity

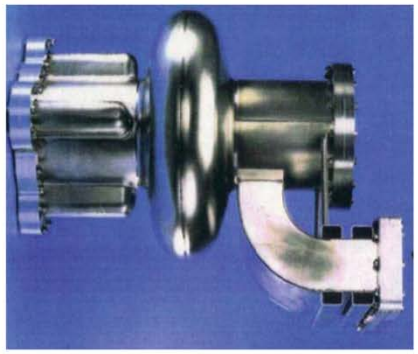

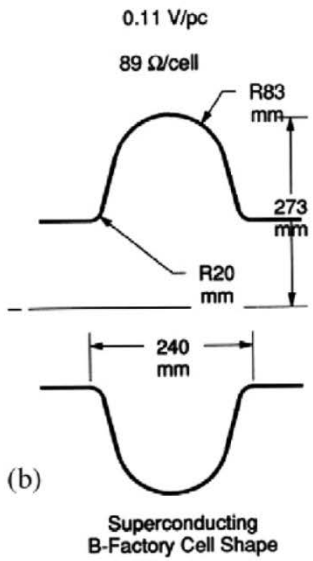

Quantity	**Cornell SC 500 MHz**	Pillbox
G	**270 ohmΩ**	257 Ω
R_a/Q_0	**88 ohm/cell**	196 Ω/cell
E_{pk}/E_{acc}	**2.5**	1.6
H_{pk}/E_{acc}	**52 Oe/MV/m**	30.5 Oe/(MV/m)

Cell shape design

- What is the purpose of the cavity?
- What EM parameters should be optimized to meet the design specs?

The "perfect" shape does not exist, it all depends on your application

Example: CEBAF upgrade

- "High Gradient" shape: lowest E_p/E_{acc}
- "Low Loss" shape: lowest cryogenic losses G(R/Q)

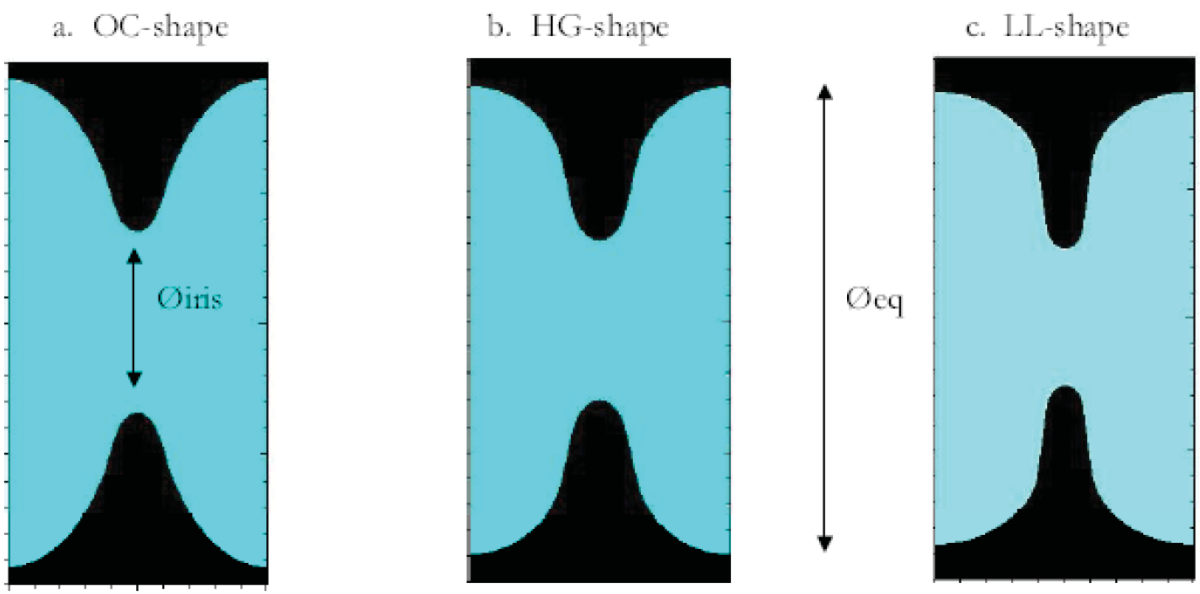

CEBAF upgrade cell-shape comparison

Table 1. Parameters of inner dumbbells

Parameters	Unit	OC-shape	HG-Shape	LL-Shape
Øeq	[mm]	187.03	180.50	174.00
Øiris	[mm]	70.00	61.40	53.00
k_{cc}	[%]	3.29	1.72	1.49
E_{peak}/E_{acc}	-	2.56	1.89	2.17
B_{peak}/E_{acc}	$[mT\cdot(MV/m)^{-2}]$	4.56	4.26	3.74
Lorentz factor*) k_L	$[Hz\cdot(MV/m)^{-2}]$	-1.35	-1.1	-1.2
R/Q	[Ω]	96.5	111.9	128.8
r/q = (R/Q)/length	[Ω/m]	965	1119	1288
G	[Ω]	273.8	265.5	280.3
R/Q*G	[Ω*Ω]	26421	29709	36102

CEBAF Upgrade: cryo-budget limit of 30W/cavity. Higher energy gain can be obtained using LL-shape.

Trend in TM-mode cavity design

- The **field emission is not a hard limit** in the performance of sc cavities if the surface preparation is done in the right way.

- Unlikely this, **magnetic flux on the wall** limits performance of a sc cavity (Q_0 decreases or/and quench). Hard limit **~180 mT** for Nb.

B_{peak} / E_{acc} should be low

1. Cavities may operate at higher gradients.

2. Cavities may operate at lower cryogenic load.

$$\frac{P_{dissipated}}{V_{acc}^2} \equiv \frac{R_s}{G \cdot (R/Q)}$$

New advanced shape for ILC

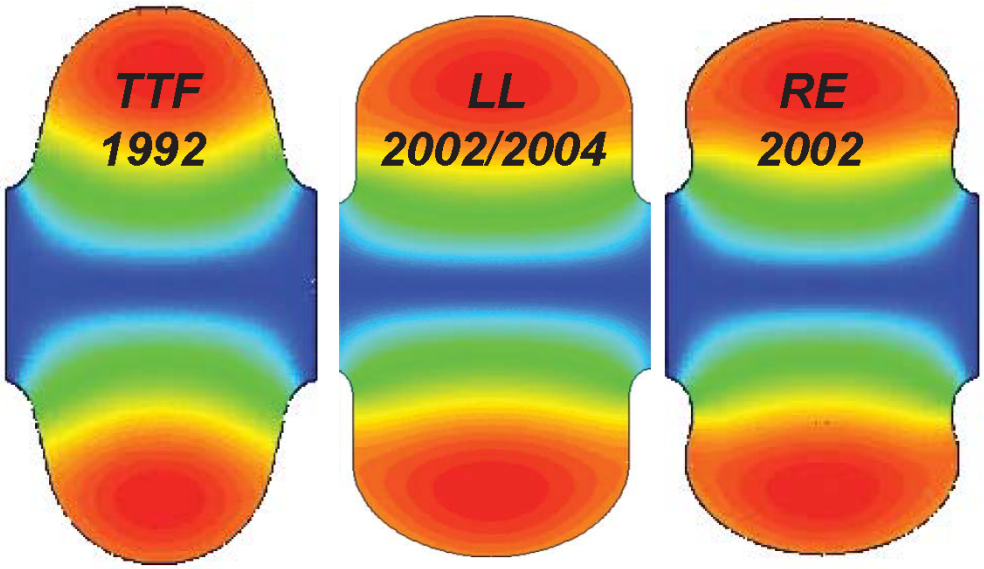

r_{iris}	[mm]	35	30	33
k_{cc}	[%]	1.9	1.52	1.8
E_{peak}/E_{acc}	-	1.98	2.36	2.21
B_{peak}/E_{acc}	[mT/(MV/m)]	4.15	3.61	3.76
R/Q	[Ω]	113.8	133.7	126.8
G	[Ω]	271	284	277
R/Q*G	[Ω*Ω]	30840	37970	35123

RF Test of LL single-cell cavity / Eacc = 53.5 MV/m

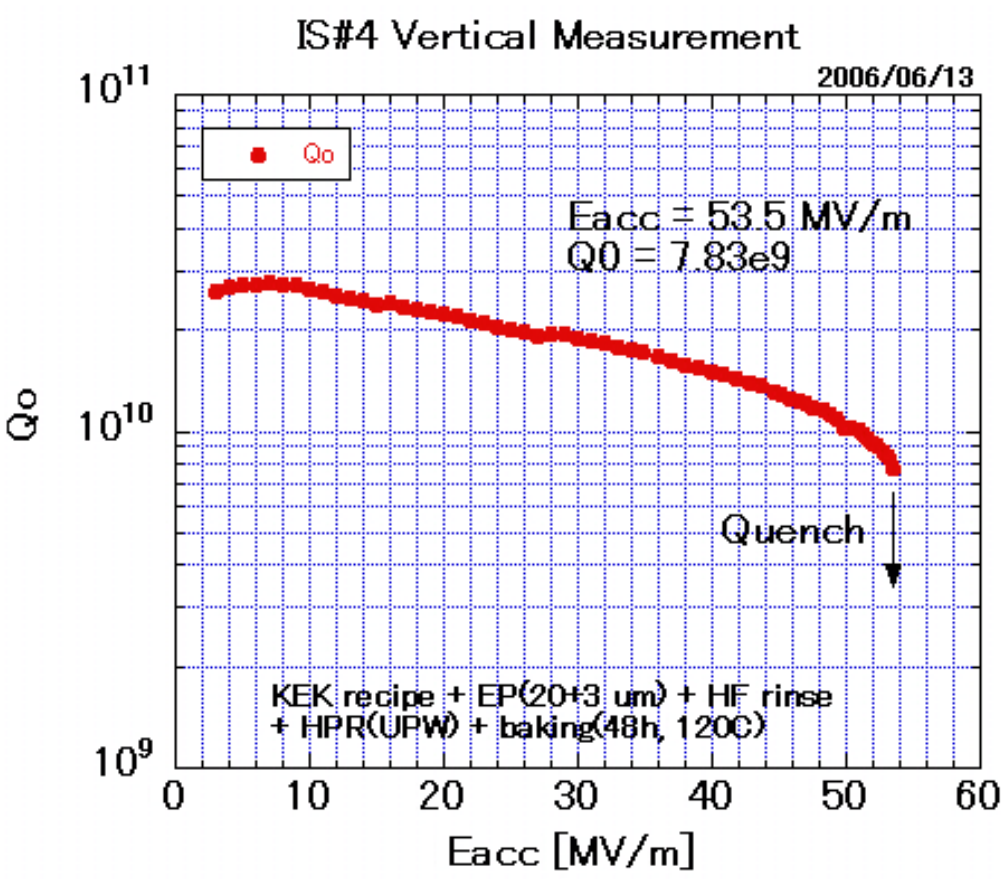

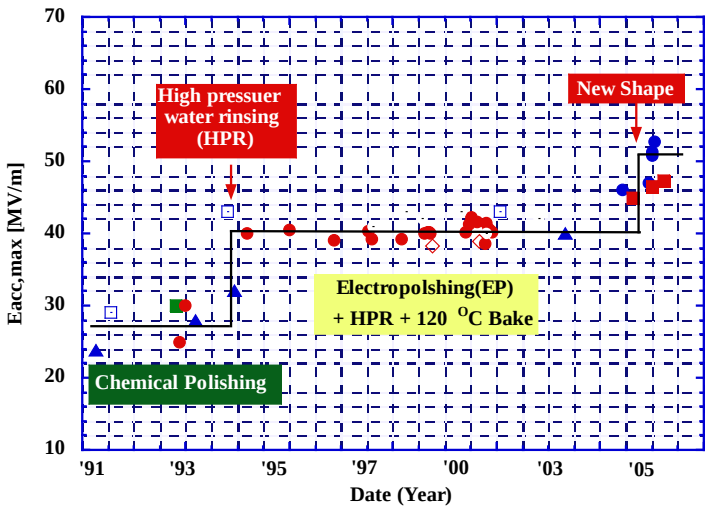

Press release

’05 28th Sept. NHK news, “Good morning Japan”
’05 12th Oct. Nikkan Kogyo News
’05 21st Oct. Energy News Weekly
’05 1st Nov. Daily Yomiuri
’06 24th Jan. Nihon Keizai News

Eacc = 53.5 MV/m was achieved.
This had been the world record until RE single-cell cavity reached beyond.

RF test of RE-shape single-cell cavity fabricated by Cornell Univ.

		RE
f_{π}	[MHz]	1278.6
E_{peak}/E_{acc}	-	2.19
B_{peak}/E_{acc}	[mT/(MV/m)]	3.79
R/Q	[Ω]	126.0
G	[Ω]	278
$Ø_{iris}$	[mm]	68

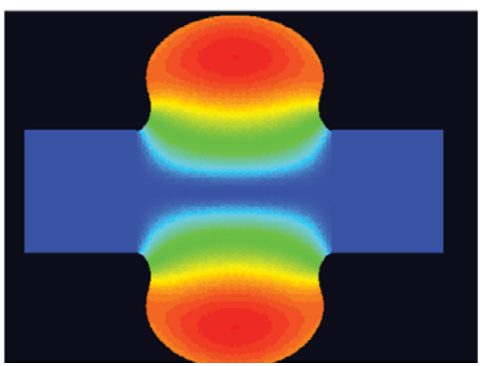

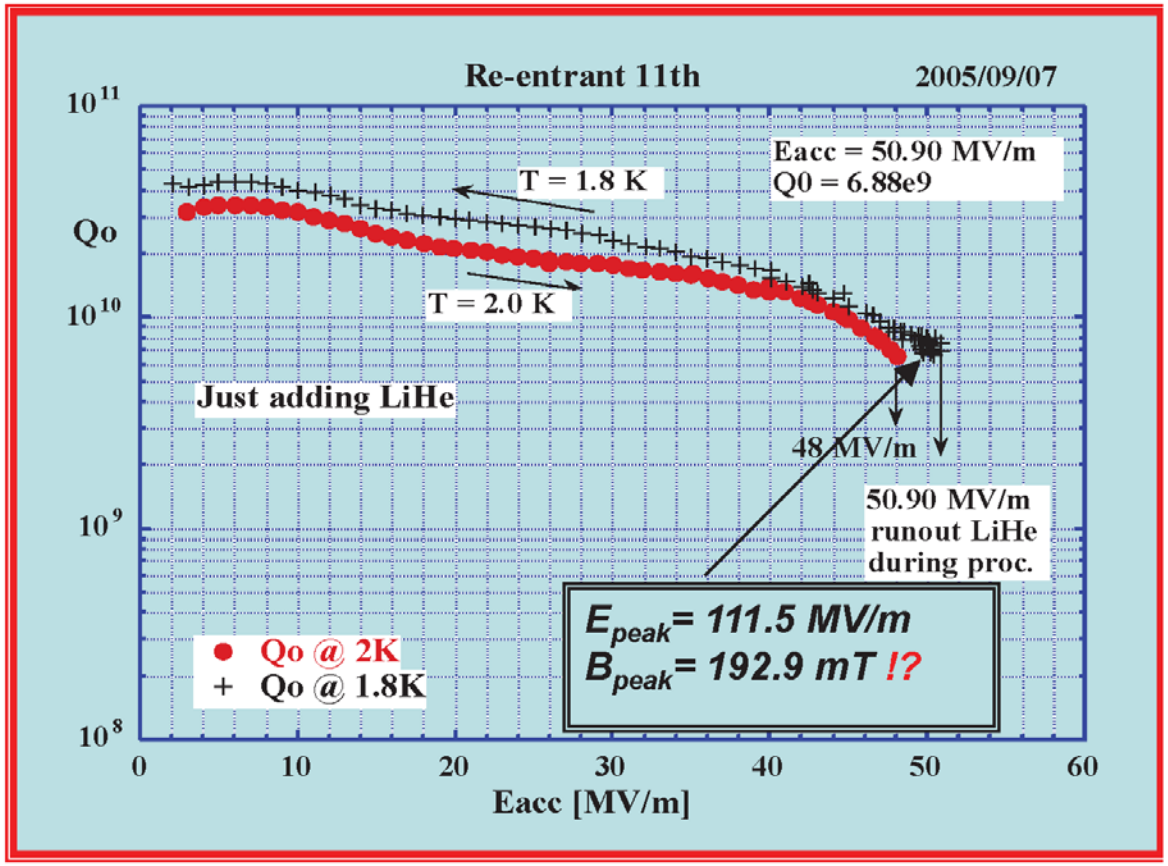

This cavity reached Eacc > 60 MV/m. I believe this cavity might be the world-record holder of highest Eacc. Sorry, I could not find the plot, that I, F. Furuta, and K. Saito measured at KEK…

Multi-cell cavities

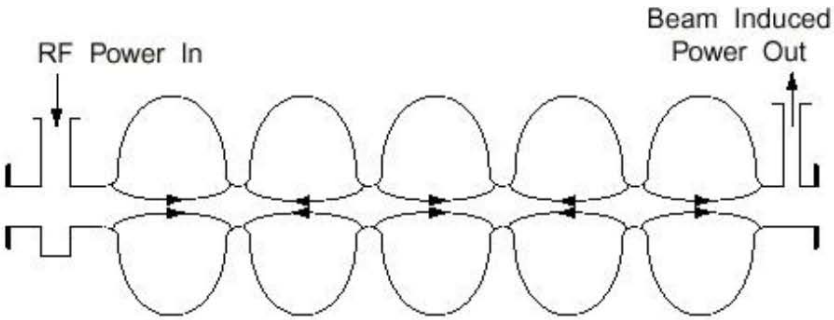

(c)

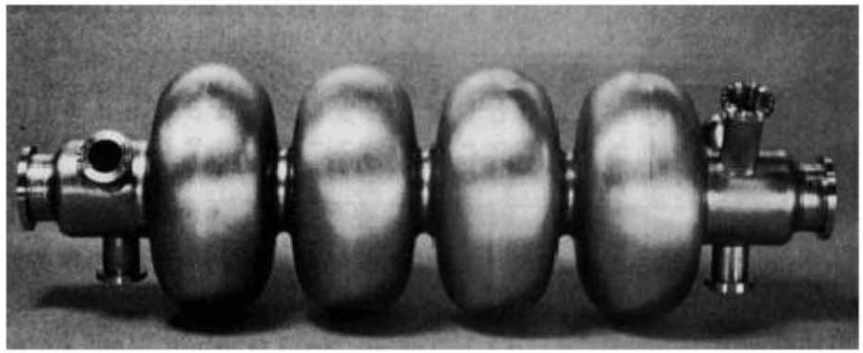

Multi-cell cavities

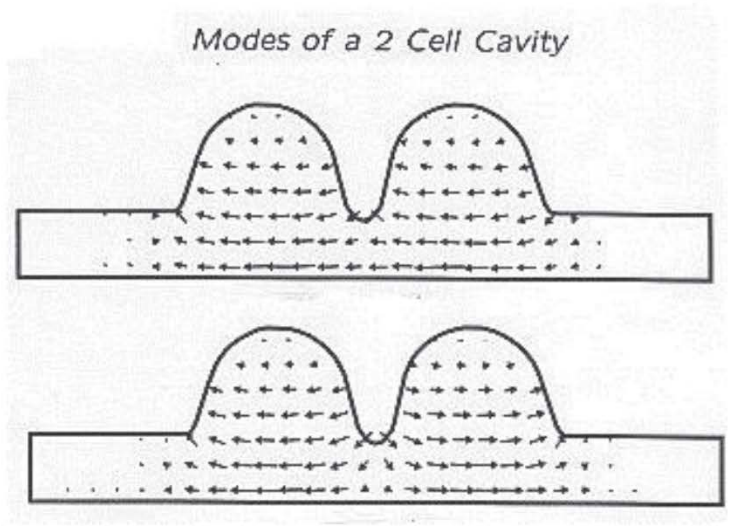

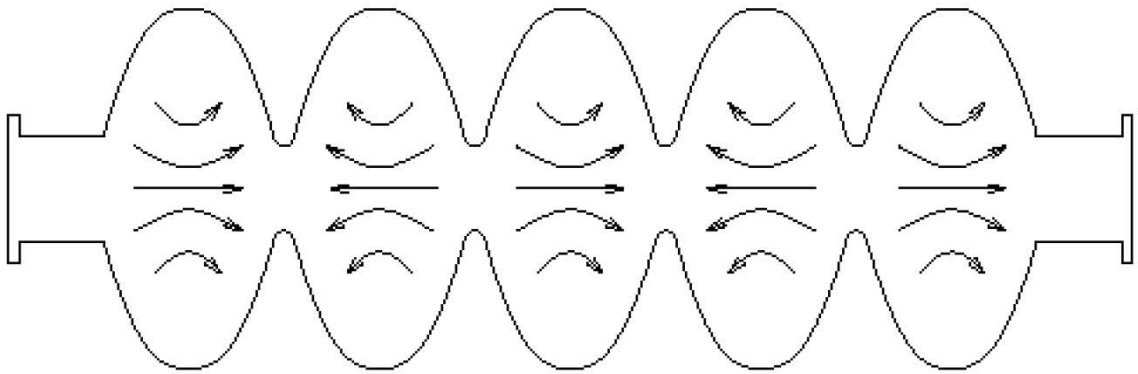

: Sketch of the electric field lines of the π-mode of a 5-cell

Multi-cell cavities

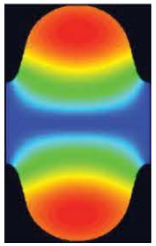

Single-cell is attractive from the RF-point of view:

- **Easier to manage HOM damping**
- **No field flatness problem.**
- **Input coupler transfers less power**
- **Easy for cleaning and preparation**

- ***But it is expensive to base even a small linear accelerator on the single cell. We do it only for very high beam current machines.***

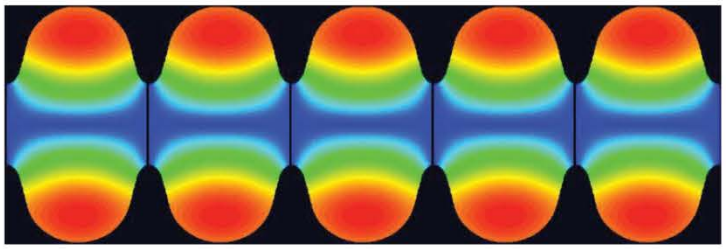

A multi-cell structure is less expensive and offers higher real-estate gradient but:

Field flatness (stored energy) in cells becomes sensitive to frequency errors of individual cells

- ***Other problems arise: HOM trapping…***

Pros and cons of Multi-cell cavities

- Cost of accelerators are lower (less auxiliaries: LHe vessels, tuners, fundamental power couplers, control electronics)
- Higher real-estate gradient (better fill factor)

- Field flatness vs. N
- HOM trapping vs. N
- Power capability of fundamental power couplers vs. N
- Chemical treatment and final preparation become more complicated
- The worst performing cell limits whole multi-cell structure

Coupling between cells

ω_o

ω_π

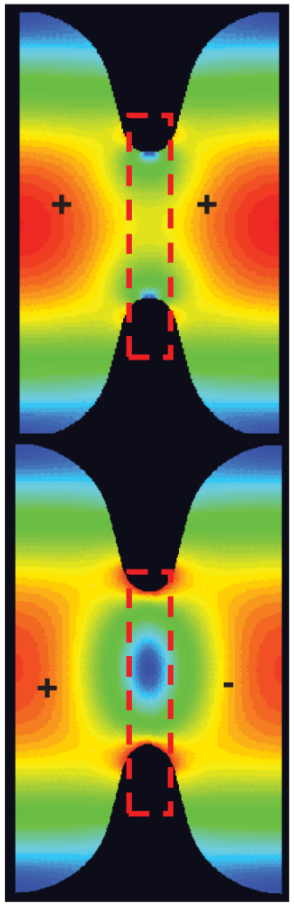

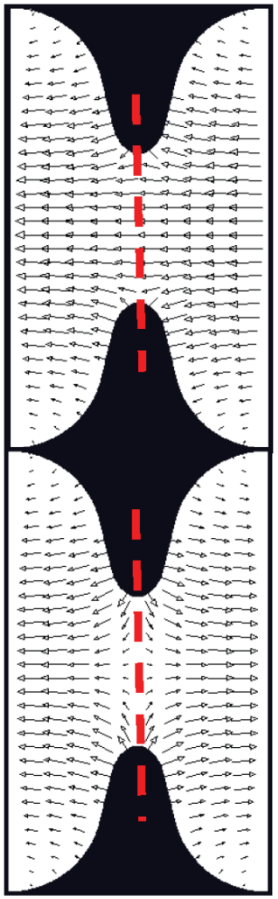

Symmetry plane for the H field

Symmetry plane for the E field which is an additional solution

The normalized difference between these frequencies is a measure of the energy flow via the coupling region

$$k_{cc} = \frac{\omega_\pi - \omega_0}{\frac{\omega_\pi + \omega_0}{2}}$$

Field flatness after pre-tuning of LL 9-cell cavity

π mode frequency 1298.774 MHz

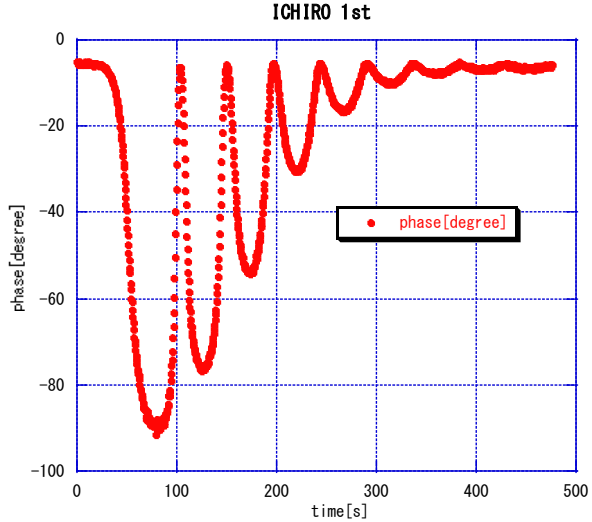

Field flatness = 0.1 %
(as delivered to KEK)

π mode frequency 1298.547 MHz

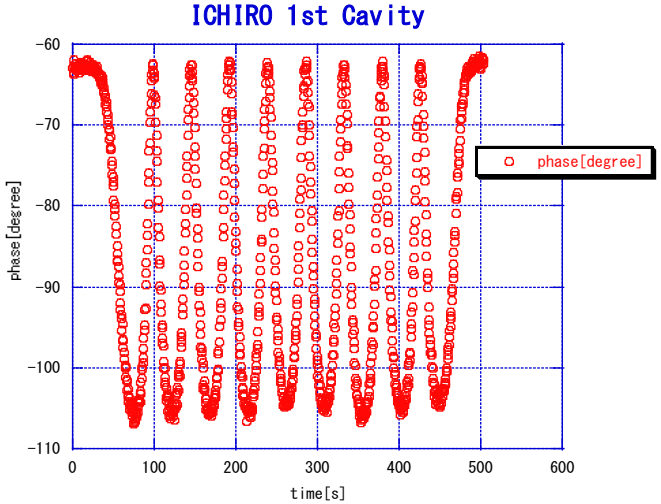

Field flatness = 98 %
(after pre-tuning)

Cavity	Field flatness (min/max) as delivered / after pre-tuning	Freq. target 1298.141 (MHz) @R.T. as delivered / after pre-tuning
1st	0.1% / 98%	1298.774 / 1298.547

Cell-to-cell coupling is as small as 1.6%, but no problem in pre-tuning.

RF Test of LL 9-cell cavity

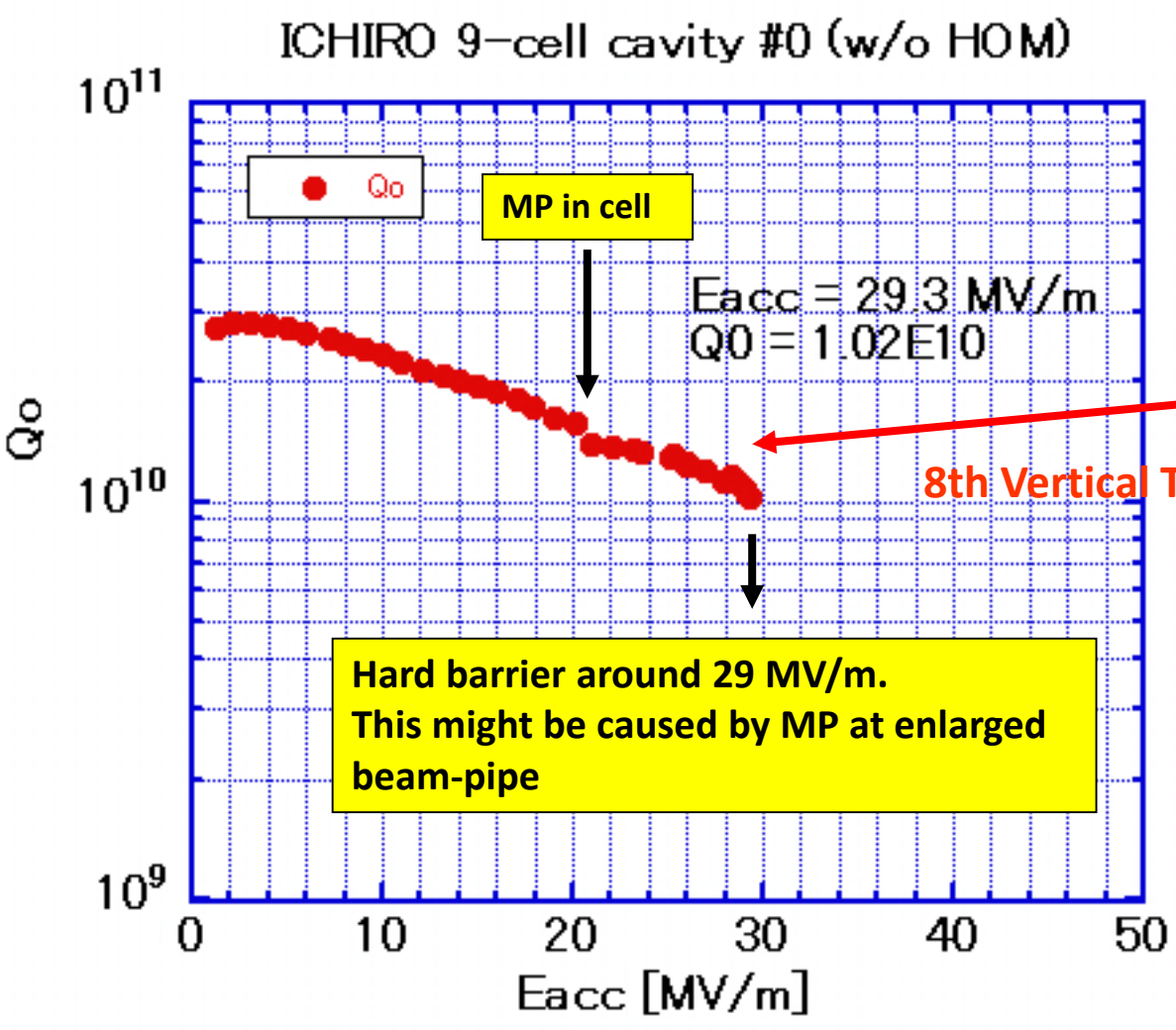

LL 9-cell 1st Cavity #0 w/o HOM

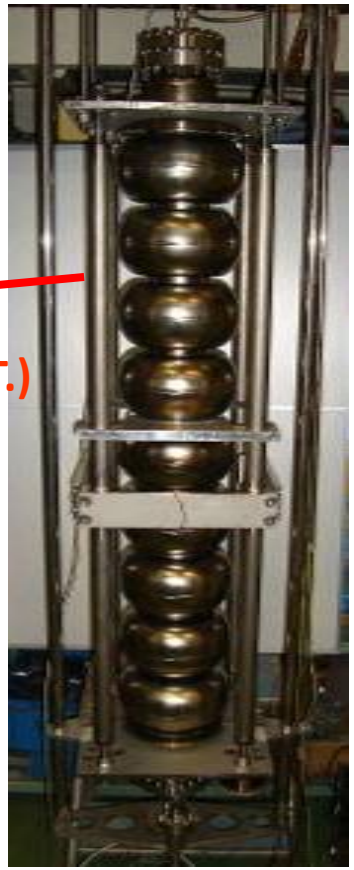

8th Vertical Test (V.T.)

No Q-disease was found.

Mechanical design

The mechanical design of a cavity follows its RF design:

- **Lorentz Force Detuning**
- **Mechanical Resonances**

$$P = \frac{\mu_0 H_s^2 - \varepsilon_0 E_s^2}{4}$$

Lorentz Force Detuning

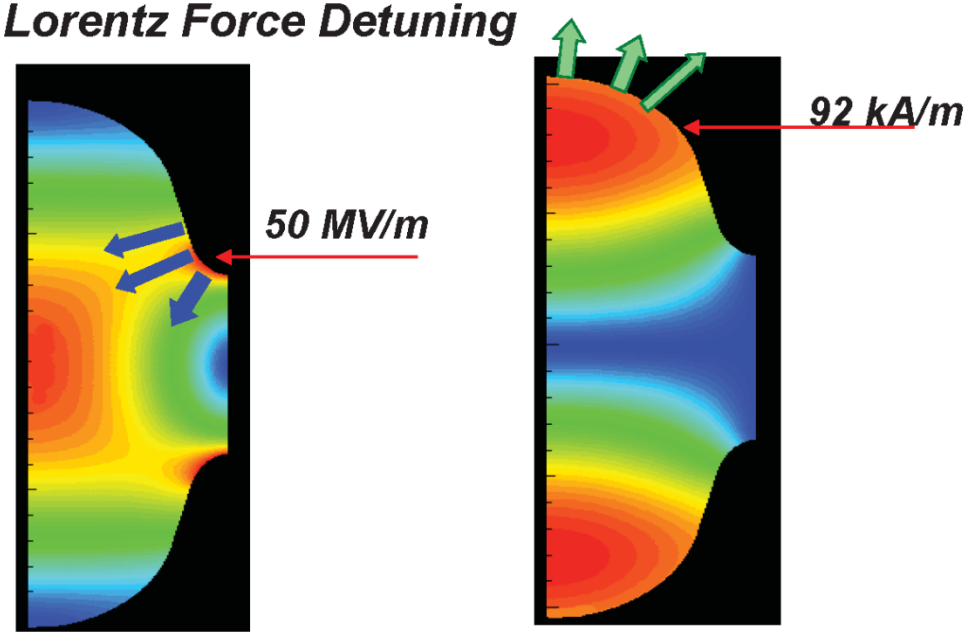

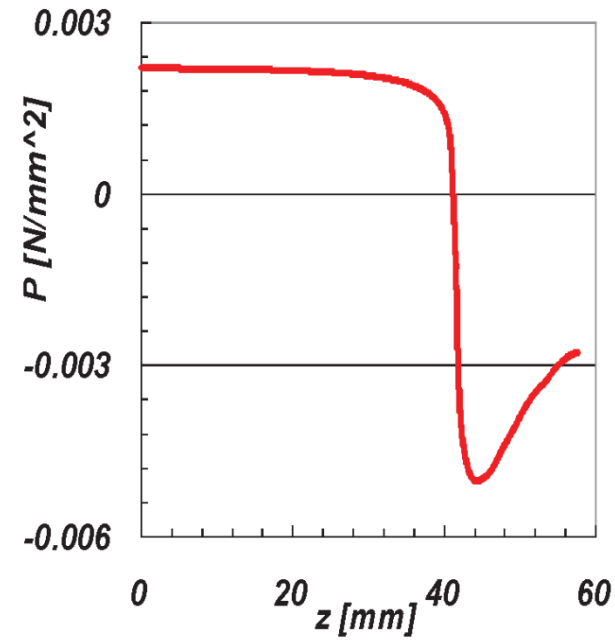

E and H at E_{acc} = 25 MV/m in TESLA inner-cup

Mechanical design

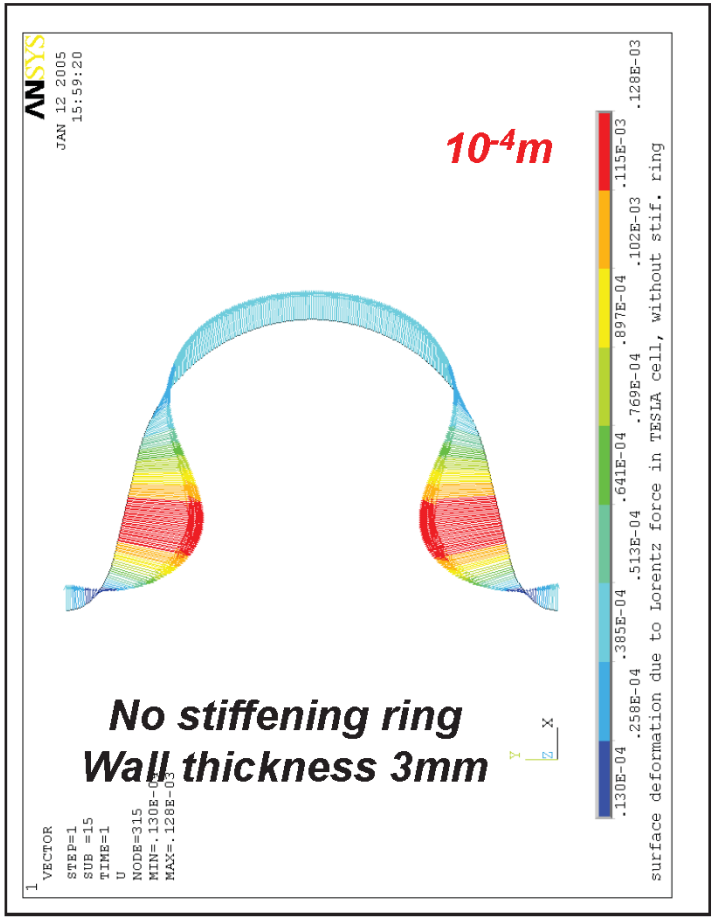

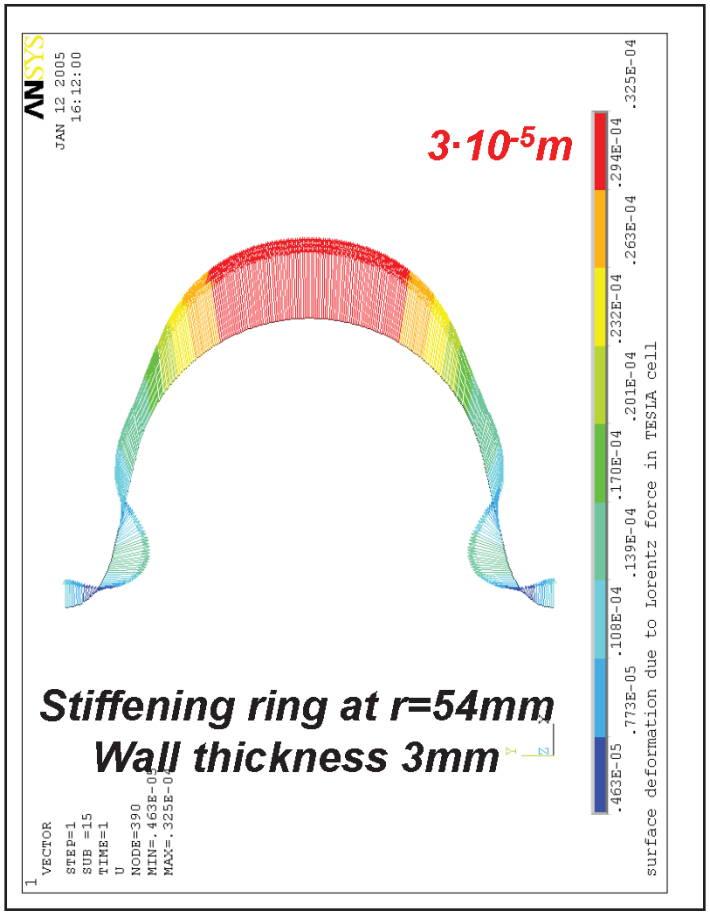

k_L = -1 Hz/(MV/m)^2

Essential for the operation of a pulsed accelerator

$$\Delta f = k_L (E_{acc})^2$$

Mechanical design

Mechanical Resonances of a multi-cell cavity

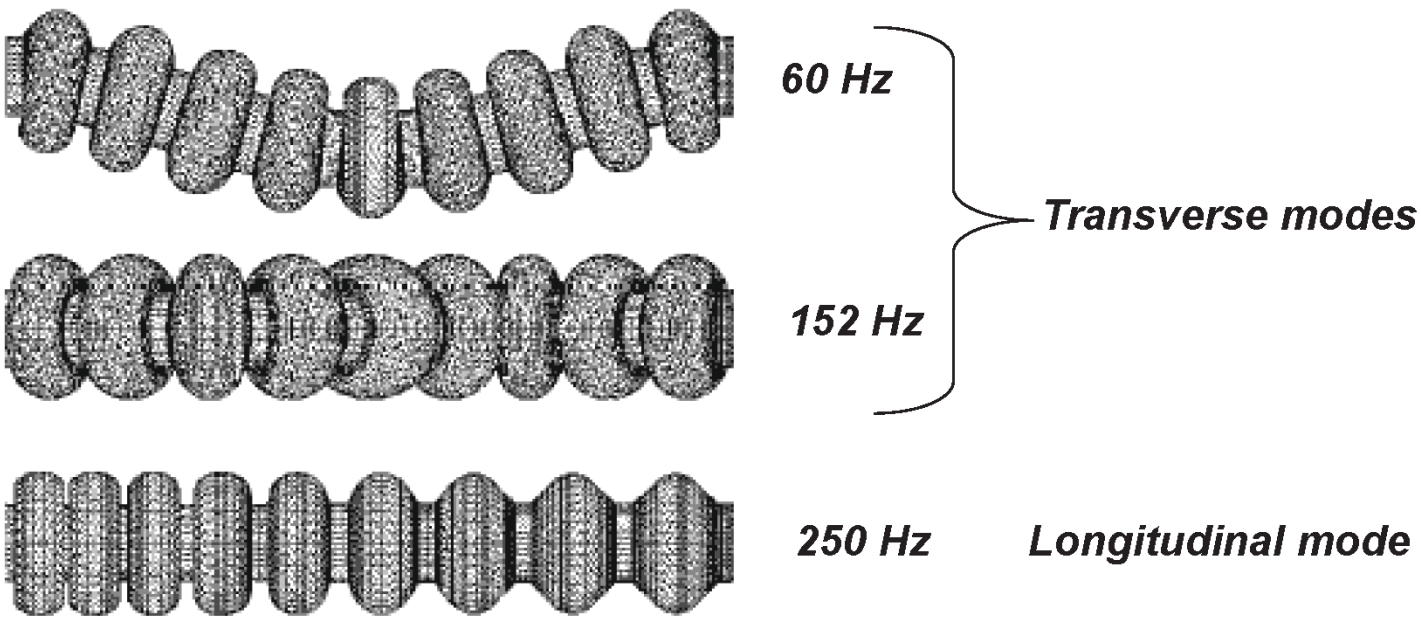

TESLA structure

The mechanical resonances modulate frequency of the accelerating mode.
Sources of their excitation: vacuum pumps, ground vibrations…

These mechanical resonant modes are also closely related to the microphonics.

RF Test of LL 9-cell cavity in Cryomodule

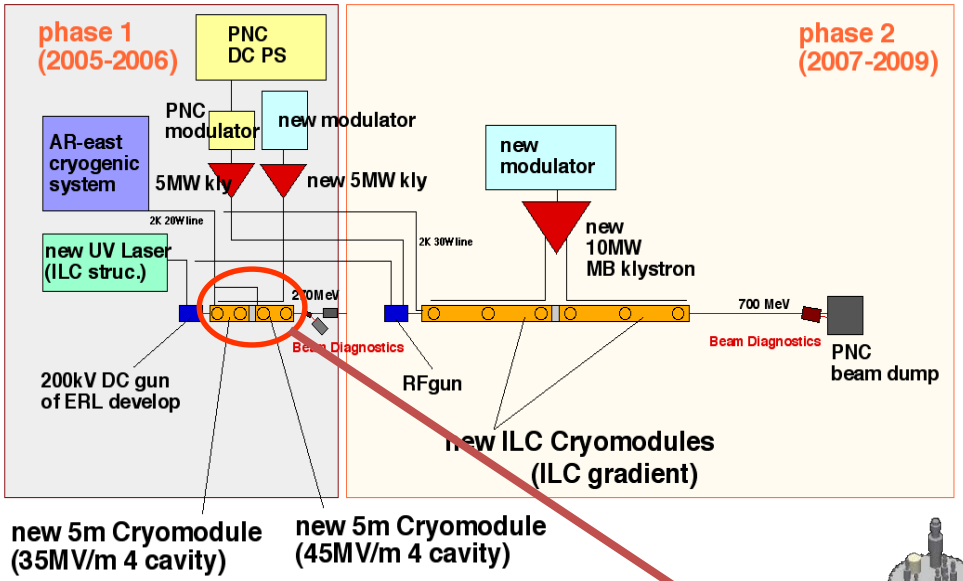

STF @ KEK

STF Phase 1

TESLA design cavities
Operation at 31.5 MV/m

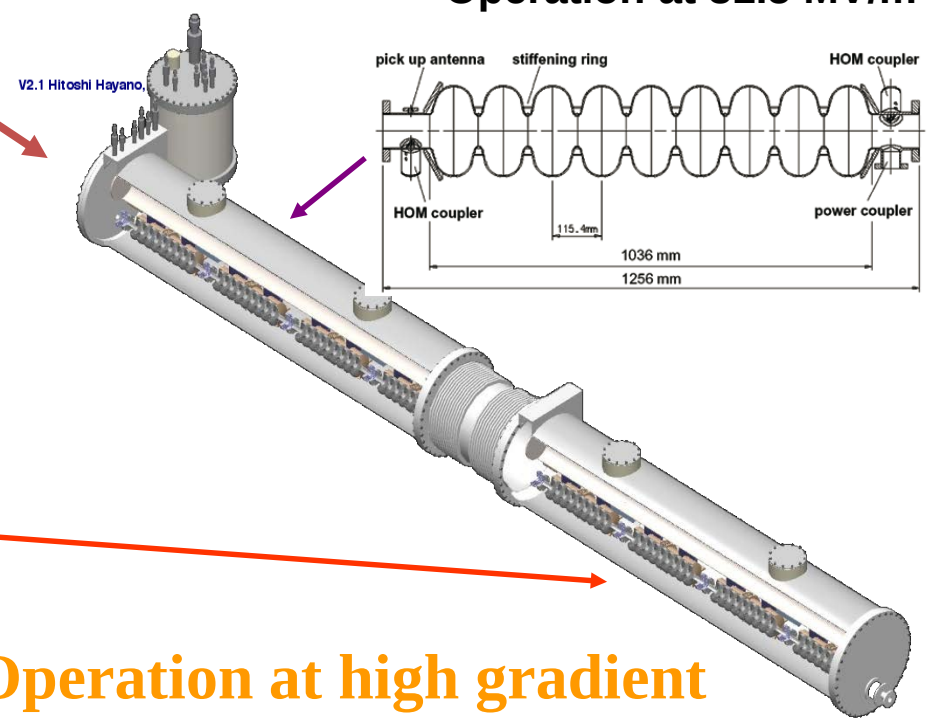

LL 9-cell cavity

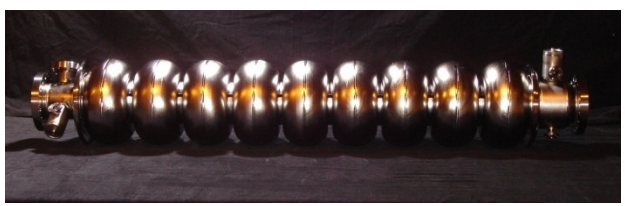

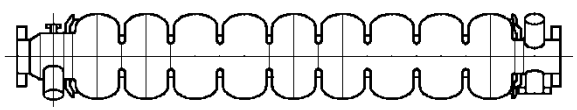

Already fabricated.

Operation at high gradient

I Q measurement by LLRF
(LL 9cell cavity in cryomodule)

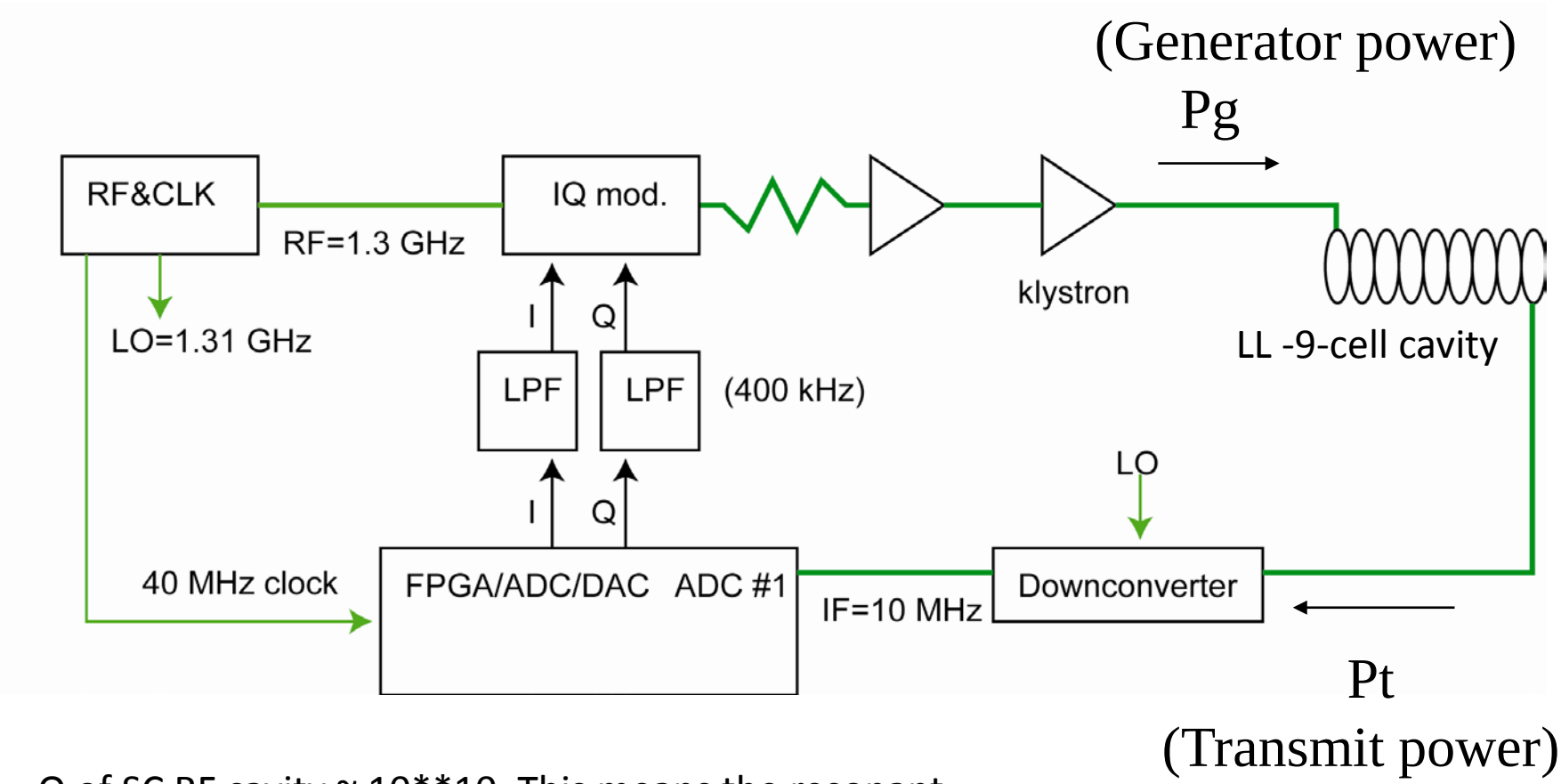

Q of SC RF cavity ~ 10**10. This means the resonant frequency of cavity should be controlled within a few Hz taking into account the vibration of cavity.

High-power RF Test of LL 9-cell cavity in cryomodule

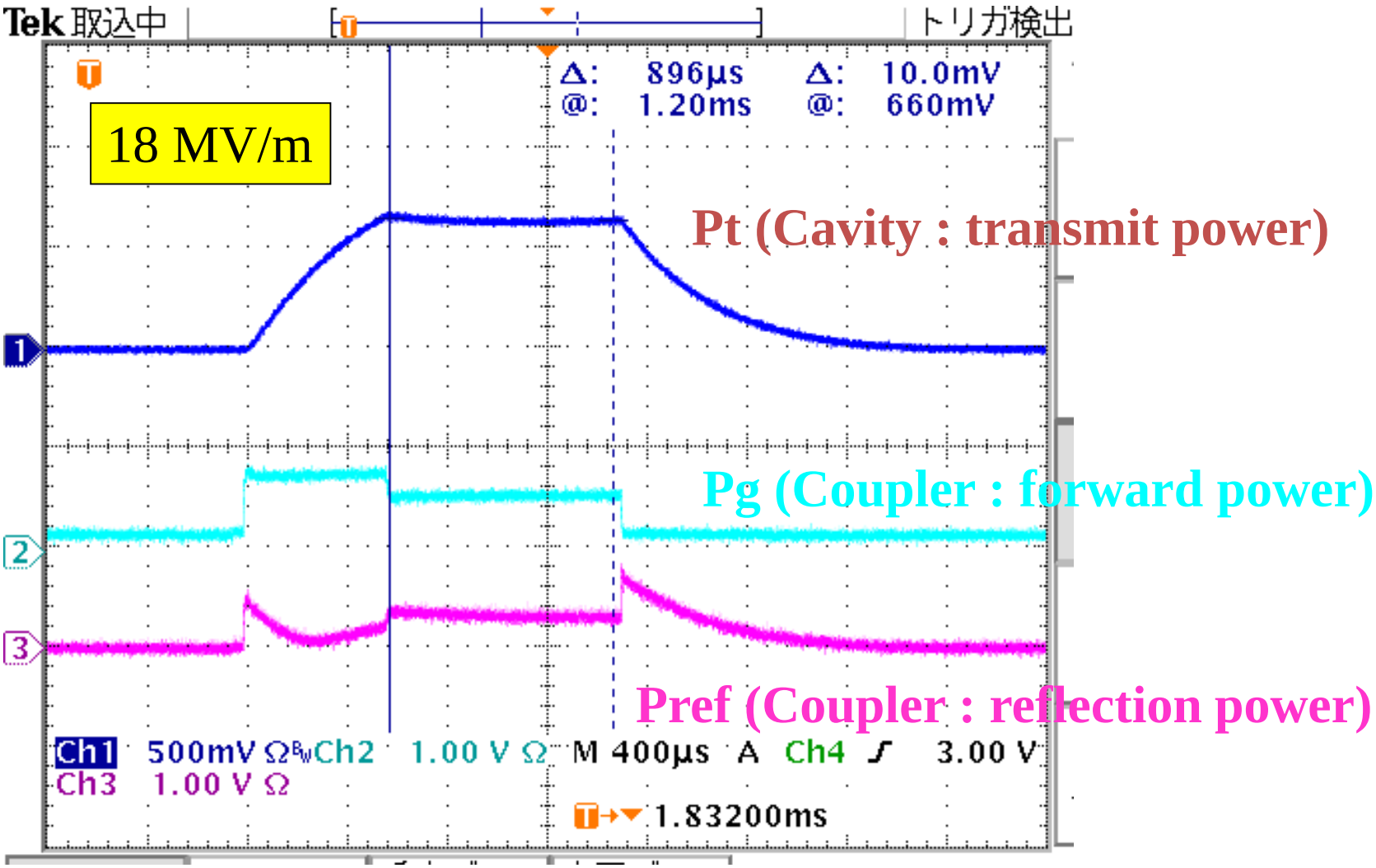

Evaluation of Microphonics (LL 9-cell cavity in CM)

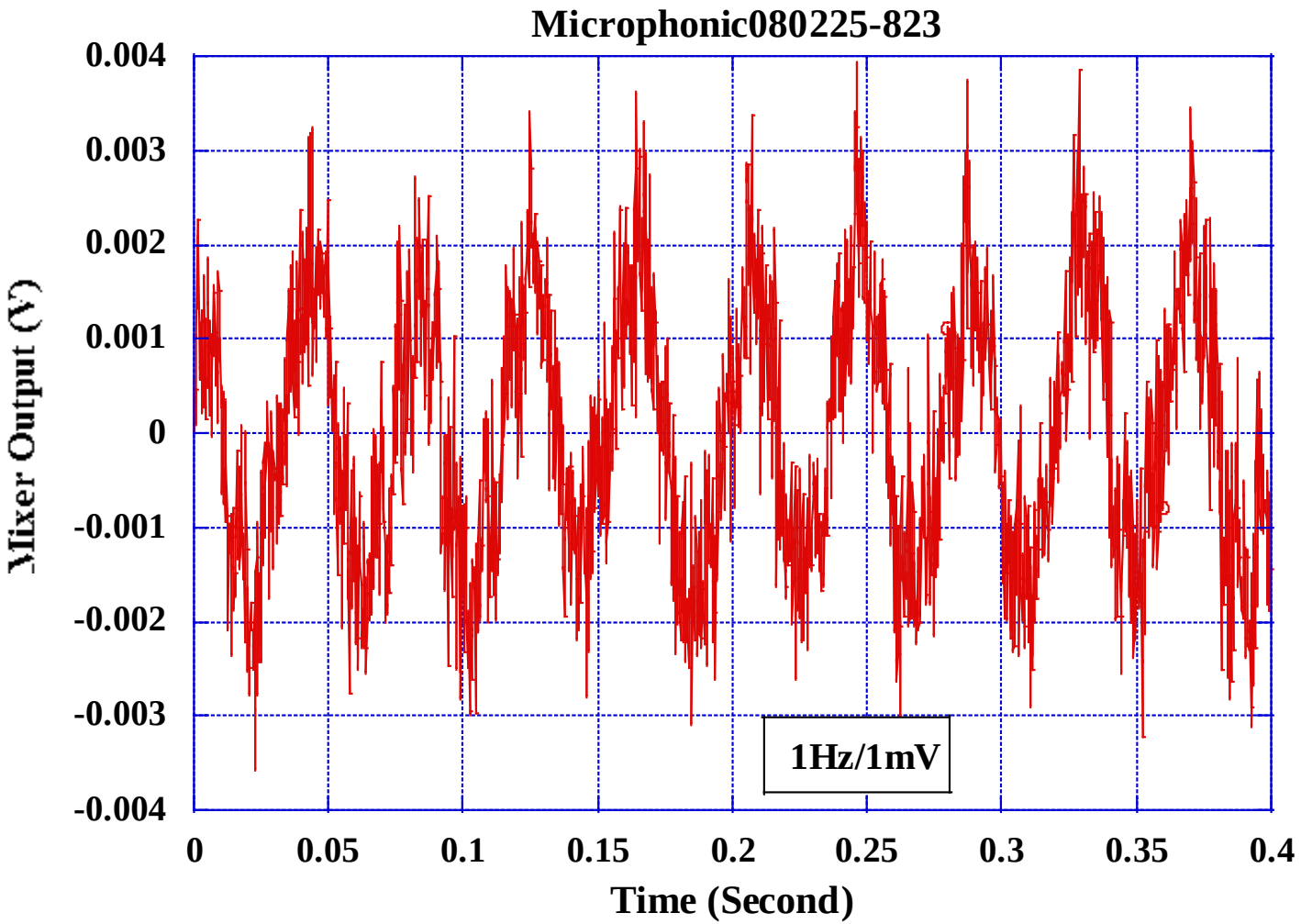

Microphonics is ± 3mV,
which corresponds to ± 3Hz in frequency and ±0.5^{O} in phase variation.

Lecture B2 and C3a: Superconducting RF

Superconductive RF fundamental

Reference books

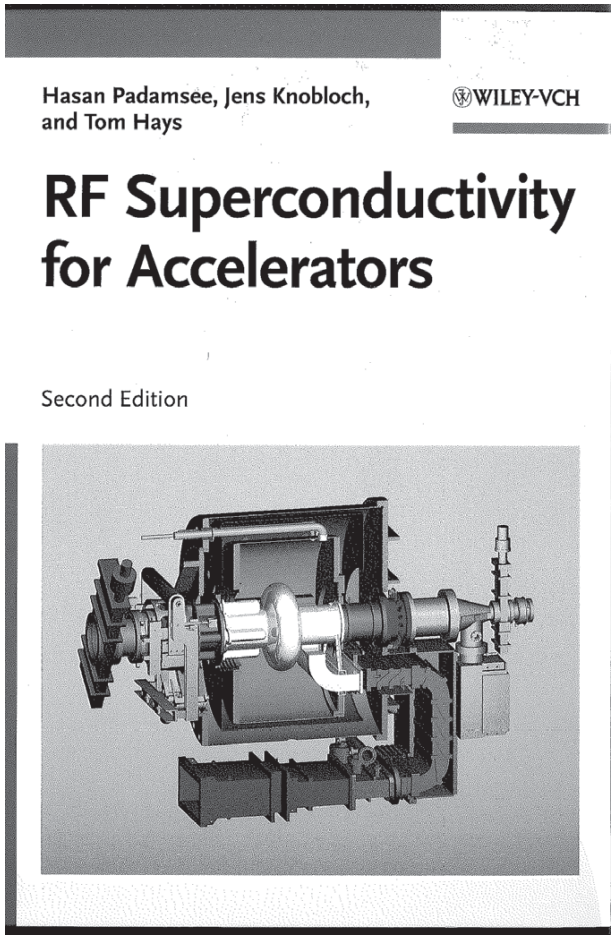

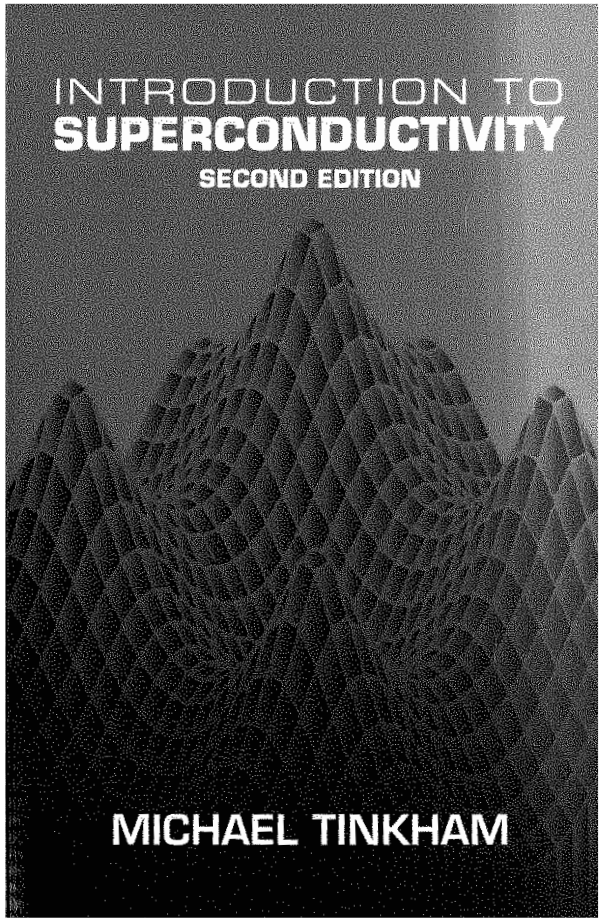

History of Superconductivity 1

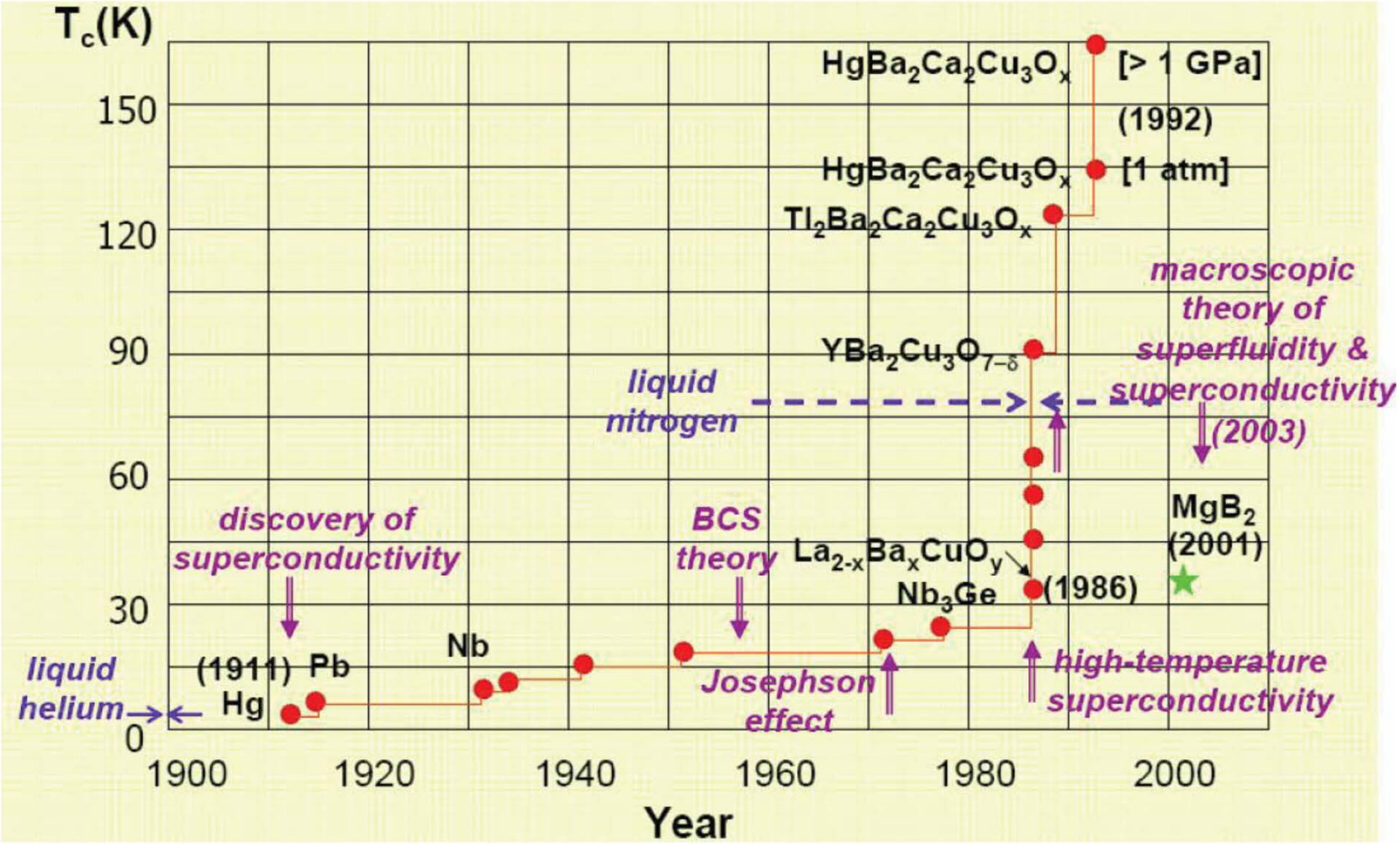

Superconductive materials

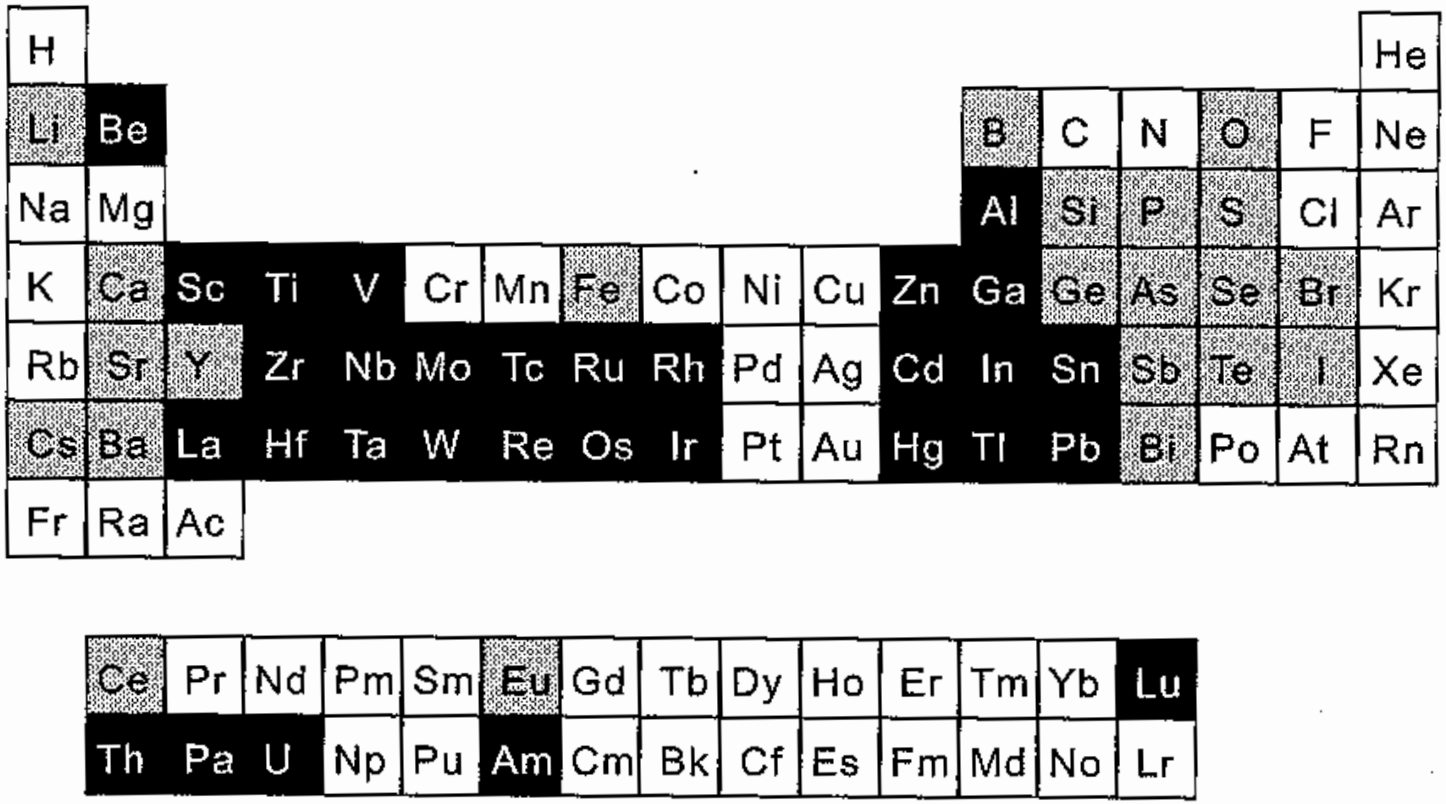

Al — SC materials in normal crystal condition

Si — SC materials only in special conditions like high pressure, amorphous, etc.

Cu — Materials for which SC phase has not been found yet.

Compound materials have also SC phase. ➡ High-temperature superconductivity materials.

Non superconductive materials

- Even if they are metal, alkaline metals and good metals with high conductivity are non SC materials.
- Even if they are metal, transition elements and Rare Earth Elements (REE) with magnetization are non SC materials.

History of Superconductivity 2 (1/2)

- 1908: H. K. Onnes and Van Der Waals liquefied He for the first time in Leiden.
- 1911: H. K. Onnes discovered superconductivity with Hg at 4.1 K in Leiden.
- 1914: H. K. Onnes discovered persistent current in loop superconductor.
- 1933: F. W. Meissner discovered Meissner effect.
- 1935: F. W. London and H. London established London equations which explained Meissner effect.
- 1935 – 37: L. V. Schvinikov, De Haas and Casimir-Jonker discovered two Hc's. Later this is called Hc1 and Hc2 of type-II superconductor.

History of Superconductivity 2 (2/2)

- 1950: V. L. Ginzburg and L. D. Landau established GL theory, introducing thermo-dynamical states in superconductor.
- 1952: A. Abrikosov predicted Type-II superconductor.
- 1953: Pippard introduced Pippard coherent length.
- 1953: SC phase of Nb3Sn was found with Tc = 17 K (at rather high temperature).
- 1957: J. Bardeen, L. N. Cooper, and J. R. Schrieffer established BCS theory (microscopic understanding of superconductivity).
- 1961: Nb3Sn was confirmed to be Type-II superconductor.
- 1980's: High-temperature SC materials were found.

Superconductivity in DC

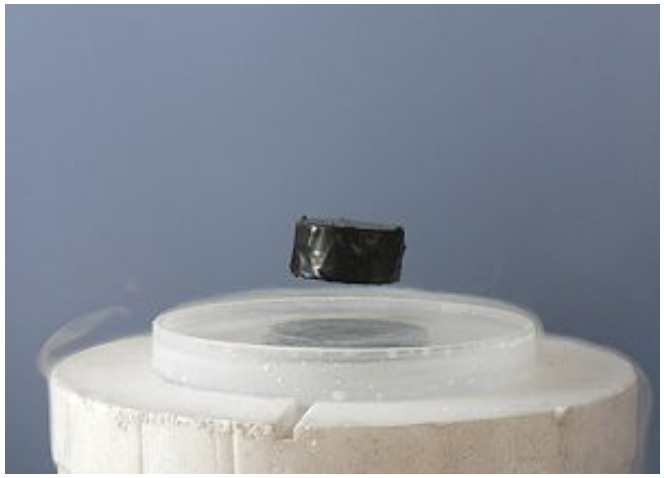

Persistent DC current

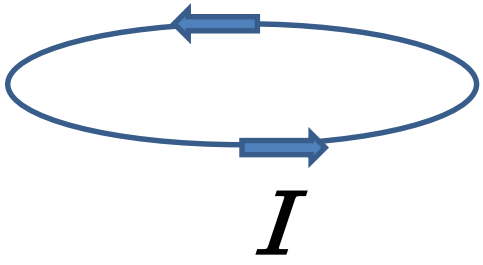

Decay time of DC superconductive current > 10^5 years

The perfect conductivity is the first hallmark of superconductivity.
But the superconductivity is not identical to the perfect conductivity.

Perfect conductivity

Tc = Critical temperature

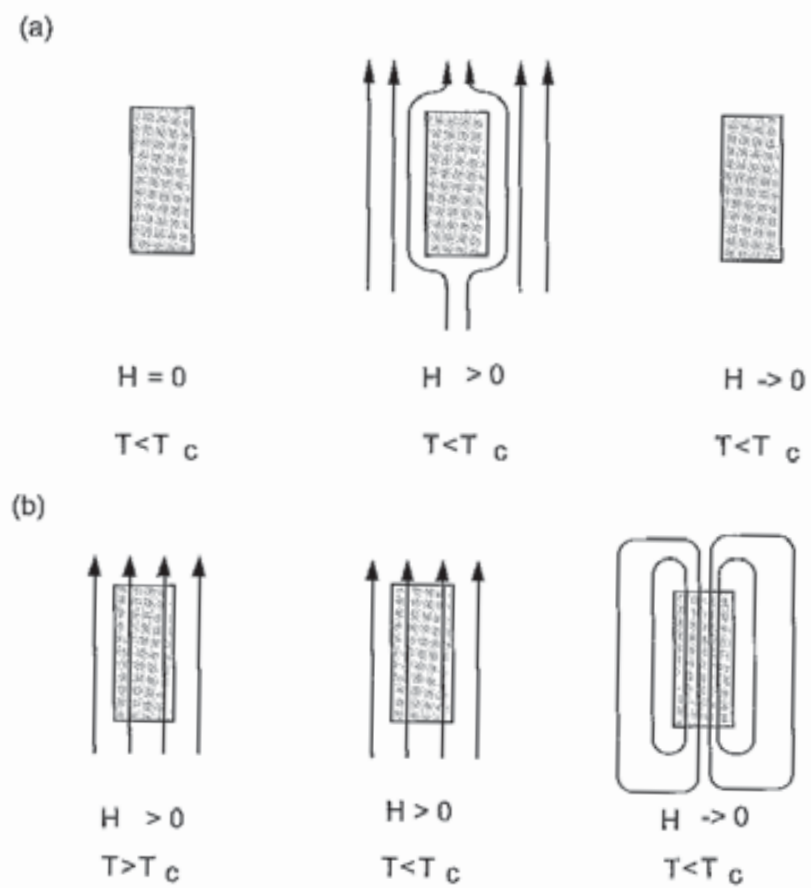

Figure 4.3: (a) Screening of external magnetic field by a perfect conductor. (b) Flux trapping in a perfect conductor.

Superconductivity

Tc = Critical temperature

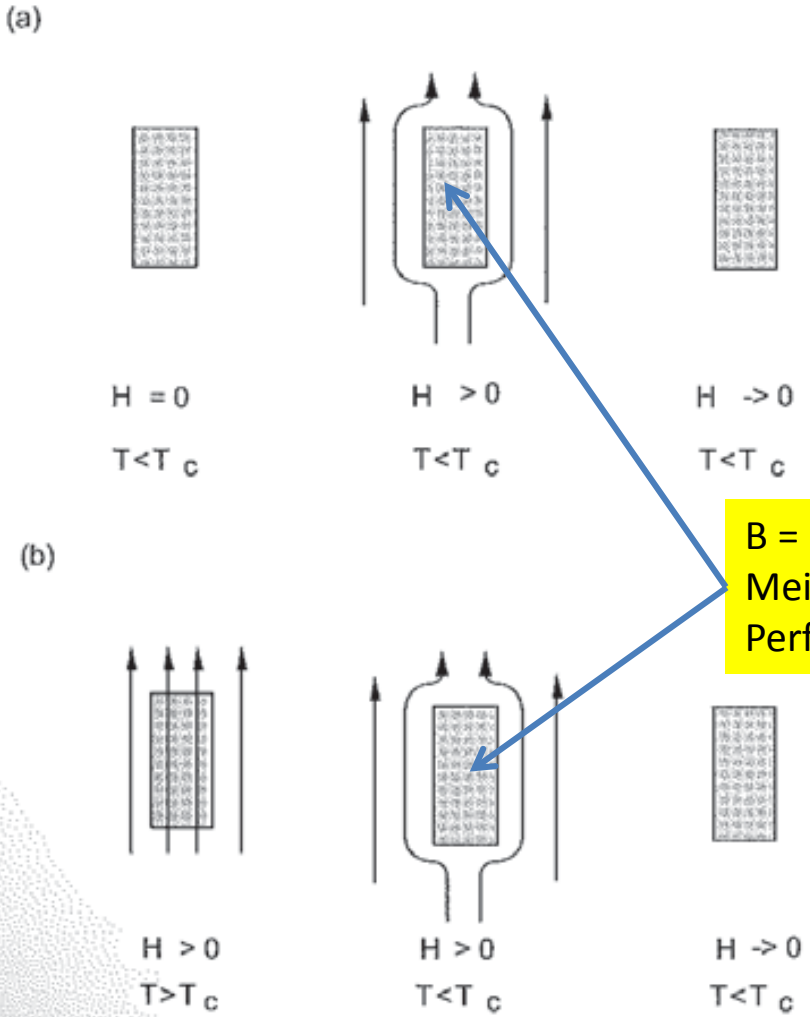

$B = \mu_0 H + \mu_0 M = 0$
Meissner effect
Perfect diamagnetism

Figure 4.4: (a) Screening of external magnetic field by a superconductor. (b) Meissner effect (flux expulsion) in a superconductor.

Superconductivity

Superconductivity is the thermodynamic state.
If you give the thermodynamic parameters: T and H, the state is defined exactly.

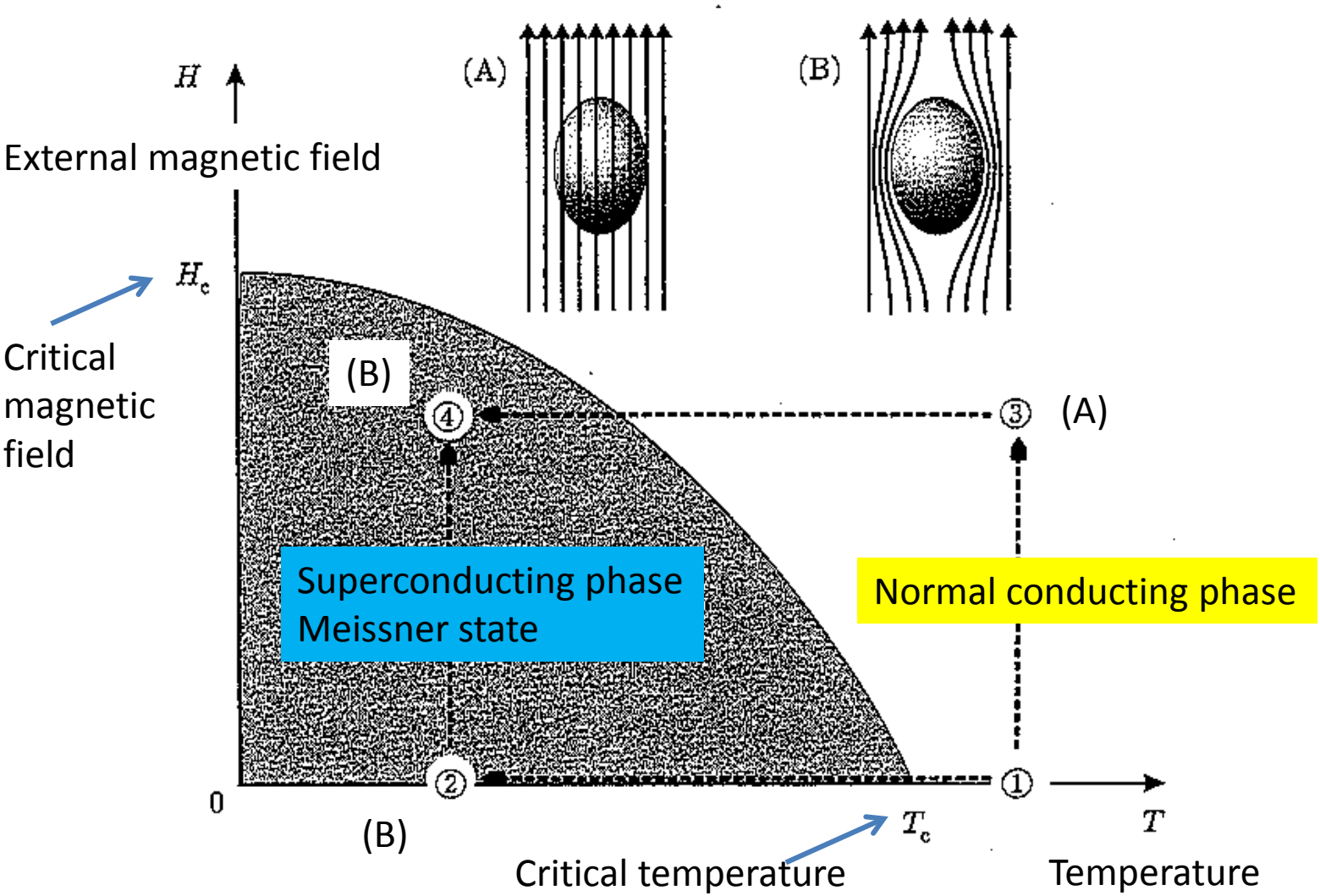

Thermodynamic properties

Entropy

Specific Heat

Energy

Free Energy

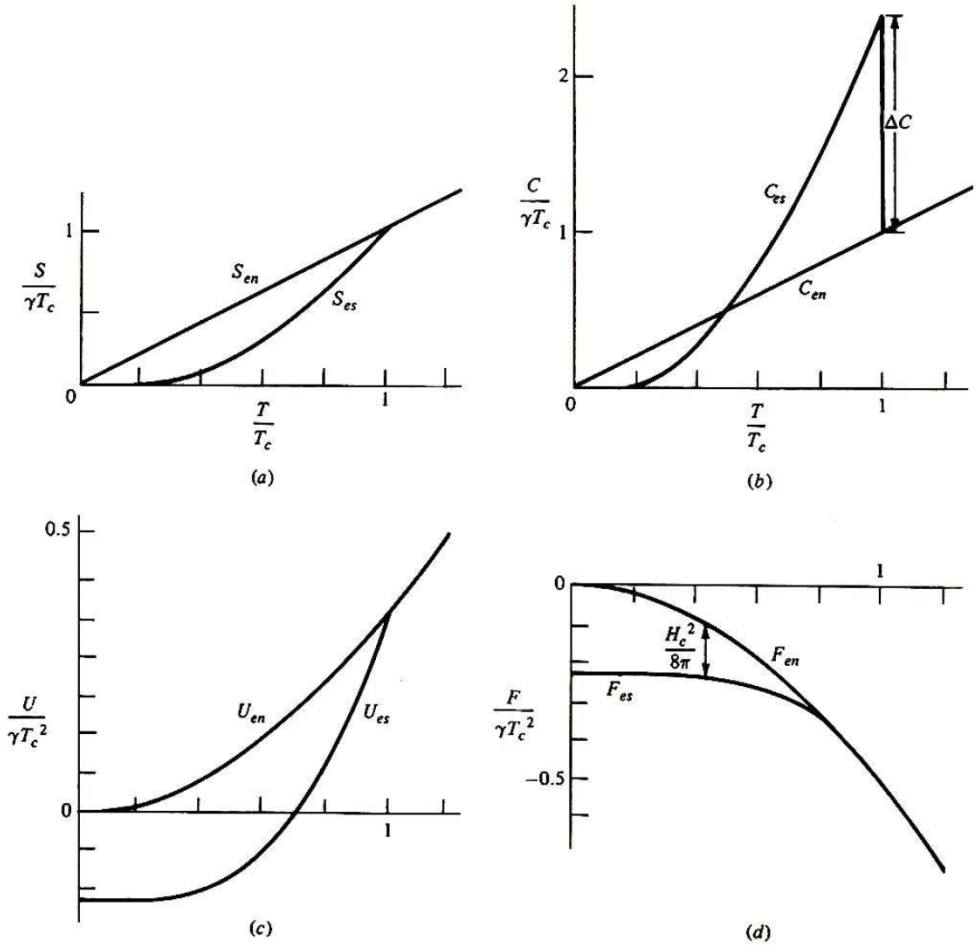

FIGURE 2-3
Comparison of thermodynamic quantities in superconducting and normal states. $U_{en}(0)$ is chosen as the zero of ordinates in (c) and (d). Because the transition is of second order, the quantities S, U, and F are continuous at T_c. Moreover, the slope of F_{es} joins continuously to that of F_{en} at T_c, since $\partial F/\partial T = -S$.

Type-I and Type-II superconductors

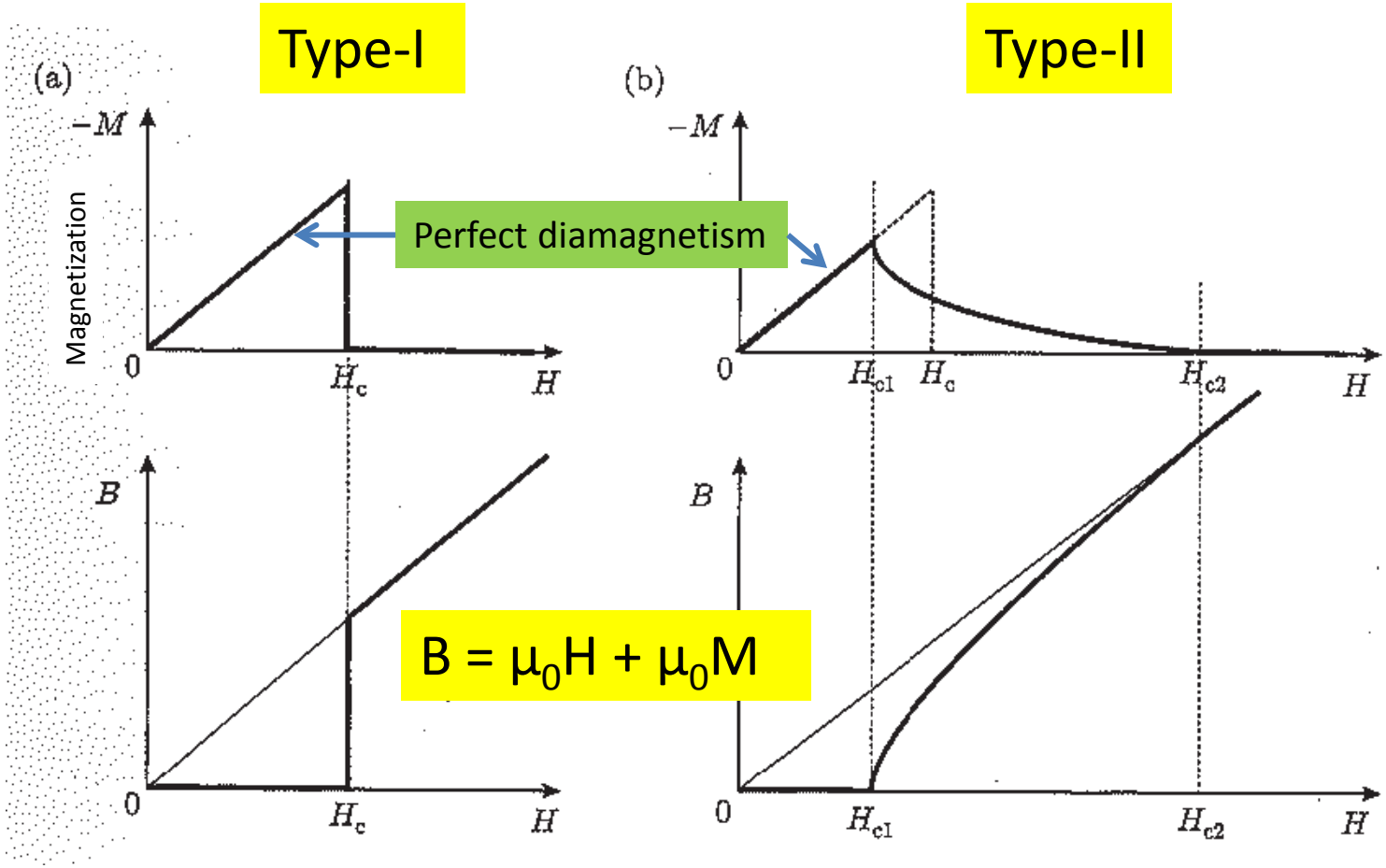

H = External magnetic field

Empirical expression of Hc(T)

It was found empirically that Hc(T) is quite well approximated by a parabolic law.

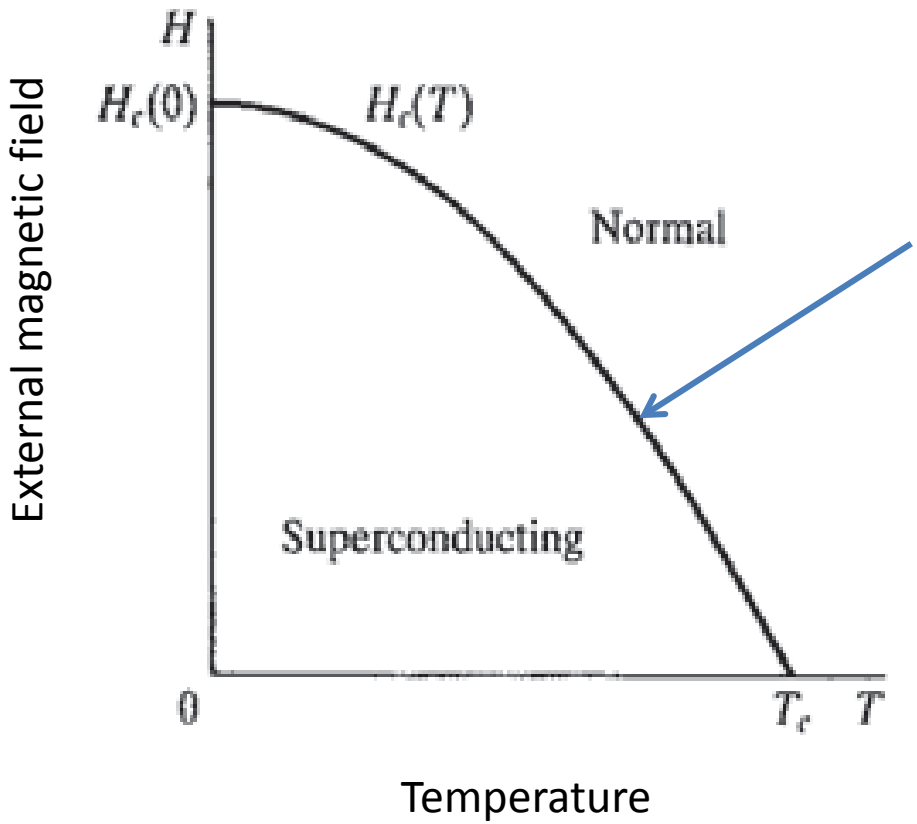

$$H_c(T) \approx H_c(0)[1 - (T/T_c)^2]$$

BCS theory

- What needed to be explained and what were the clues?
  - Energy gap (exponential dependence of specific heat)
  - Isotope effect (the lattice is involved)
  - Meissner effect

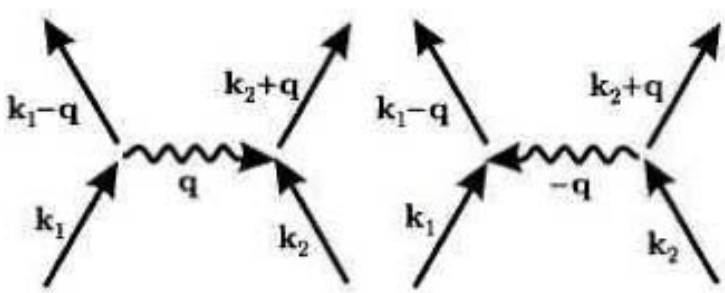

Interaction of two electrons via phonon

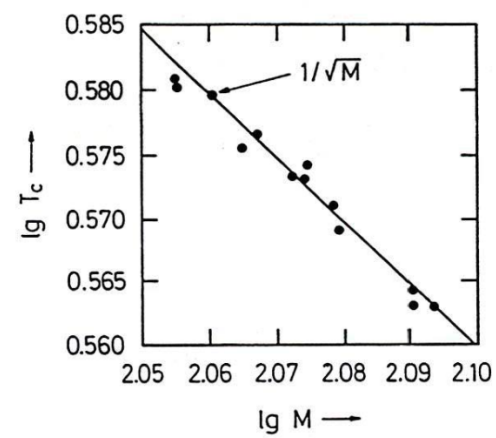

Figure 26: The critical temperature of various tin isotopes.

BCS theory

Assumption: Phonon-mediated attraction between electron of equal and opposite momenta located within $\hbar\omega_D$ of Fermi surface

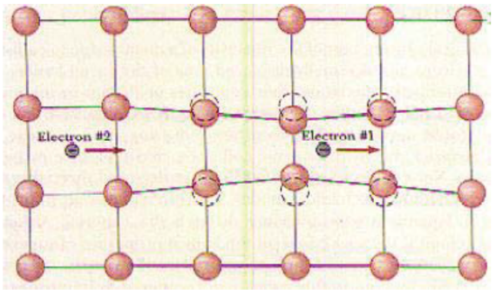

Moving electron distorts lattice and leaves behind a trail of positive charge that attracts another electron moving in opposite direction

Fermi ground state is unstable

Electron pairs can form bound states of lower energy

Bose condensation of overlapping Cooper pairs into a coherent Superconducting state

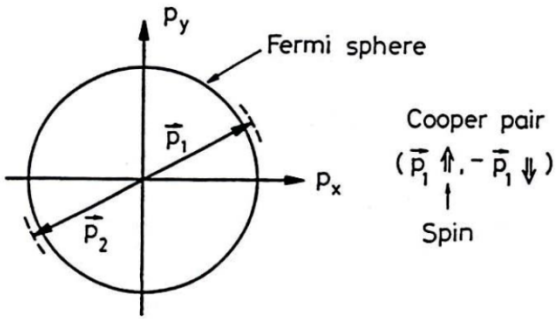

Figure 20: A pair of electrons of opposite momenta added to the full Fermi sphere.

BCS theory

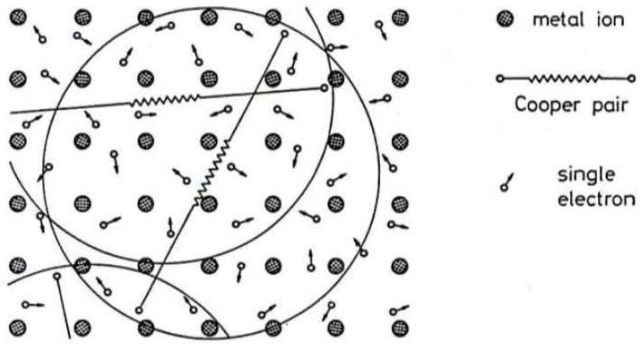

Figure 22: Cooper pairs and single electrons in the crystal lattice of a superconductor. (After Essmann and Träuble [12]).

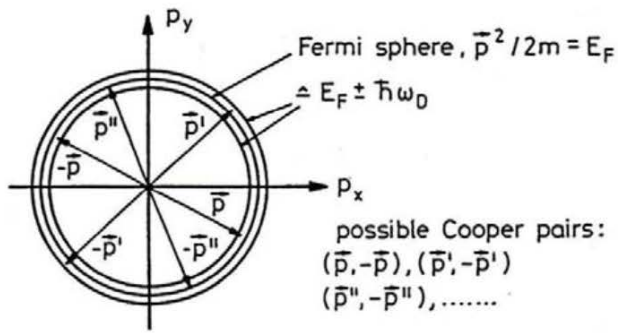

Figure 23: Various Cooper pairs $(\vec{p}, -\vec{p})$, $(\vec{p}', -\vec{p}')$, $(\vec{p}'', -\vec{p}'')$, ... in momentum space.

The size of the Cooper pairs is much larger than their spacing

They form a coherent state

BCS theory

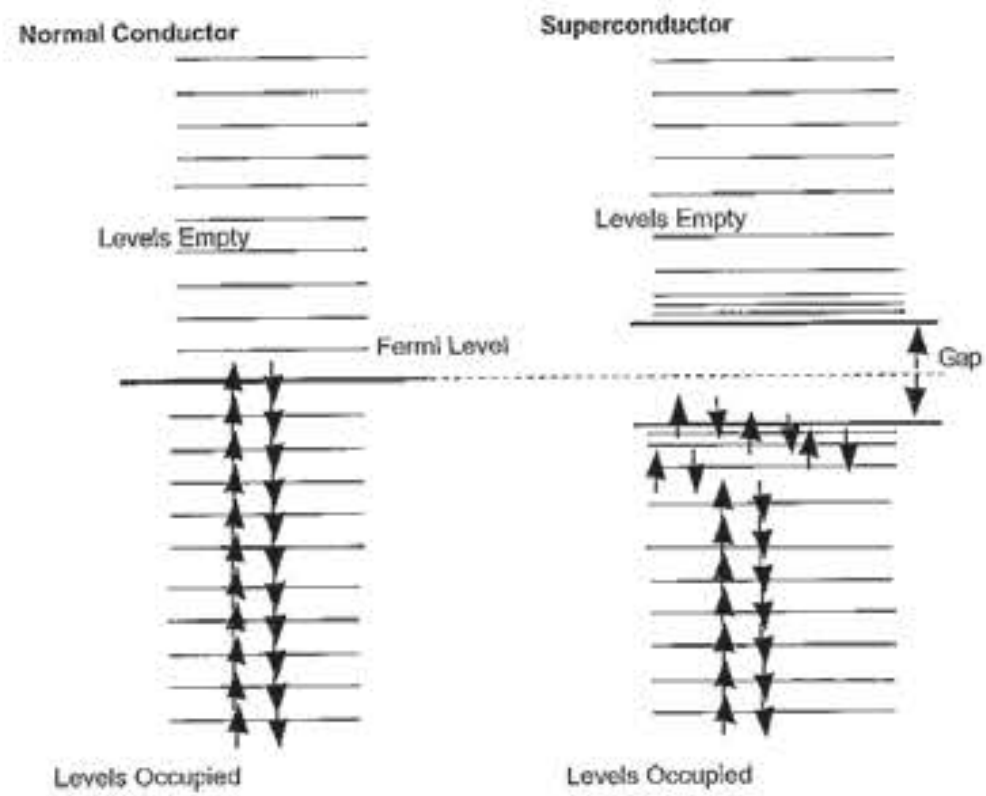

Figure 3.7: The change in the density of states that accompanies the superconducting state, showing the gap in the energy levels.

BCS theory

- The BCS model is an extremely simplified model of reality
  - The Coulomb interaction between single electrons is ignored
  - Only the term representing the scattering of pairs is retained
  - The interaction term is assumed to be constant over a thin layer at the Fermi surface and 0 everywhere else
  - The Fermi surface is assumed to be spherical

- Nevertheless, the BCS results (which include only a very few adjustable parameters) are amazingly close to the real world

BCS theory

At finite temperature:

Implicit equation for the temperature dependence of the gap:

$$\frac{1}{V\rho(0)} = \int_0^{\hbar\omega_D} \frac{\tanh\left[(\varepsilon^2+\Delta^2)^{1/2}/2kT\right]}{(\varepsilon^2+\Delta^2)^{1/2}} d\varepsilon$$

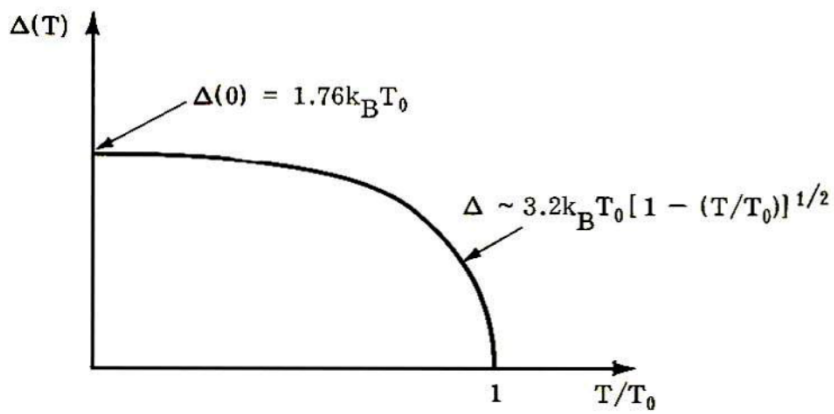

Figure 4-4
Variation of the order parameter Δ with temperature in the BCS approximation.

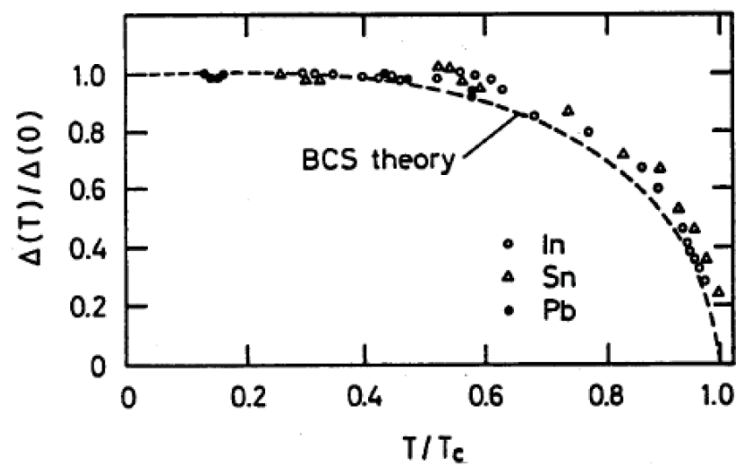

BCS theory

Specific heat

$$C_{es} \simeq \exp\left(-\frac{\Delta}{kT}\right) \quad \text{for} \quad T < \frac{T_c}{10}$$

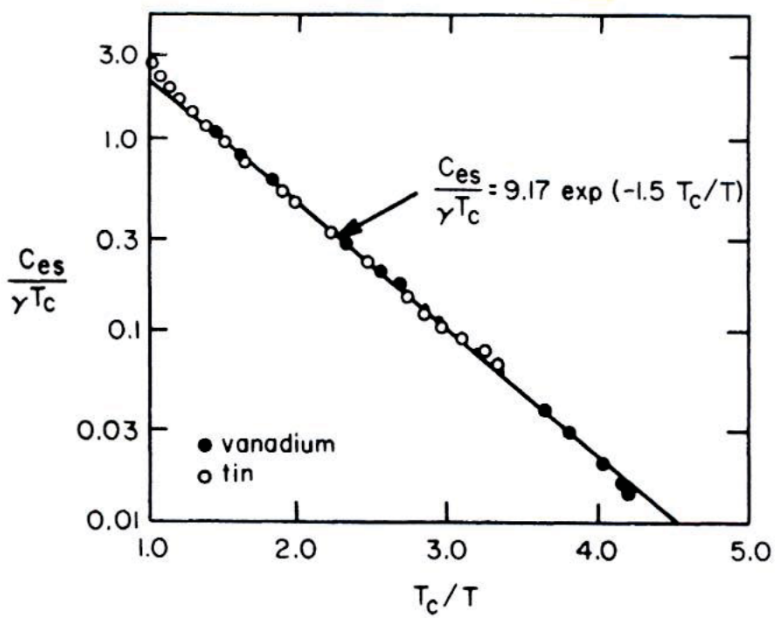

Fig. 22. Reduced electronic specific heat in superconducting vanadium and tin. [From Biondi et al., (*150*).]

BCS theory

$$H_0\phi + H_{ex}\ \phi = i\hbar\frac{\partial\phi}{\partial t}$$

$$H_{ex} = \frac{e}{mc}\sum A(r_i,t)p_i$$

H_{ex} is treated as a small perturbation

$$H_{rf} << H_c$$

There is, at present, no model for superconducting surface resistance at high rf field

$$J \propto \int \frac{R[R\cdot A]I(\omega,R,T)e^{-\frac{R}{l}}}{R^4}dr$$

similar to Pippard's model

$$J(k) = -\frac{c}{4\pi}K(k)A(k)$$

$K(0) \neq 0$: Meissner effect

BCS theory / Surface resistance

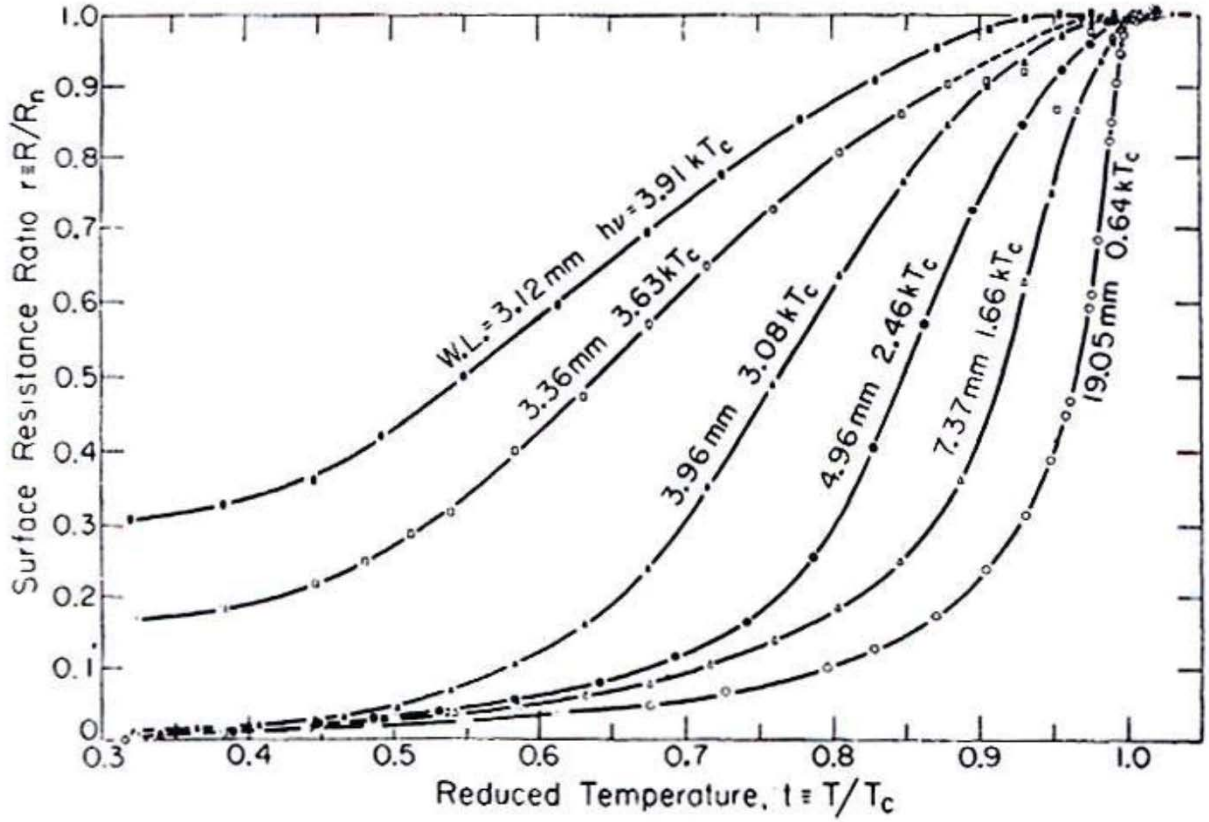

Fig. 1. Measured values of the surface resistance ratio r of superconducting aluminum as a function of the reduced temperature t at several representative wavelengths. The wavelengths and corresponding photon energies are indicated on the curves [After Biondi and Garfunkel (*15*).]

BCS theory / Surface resistance

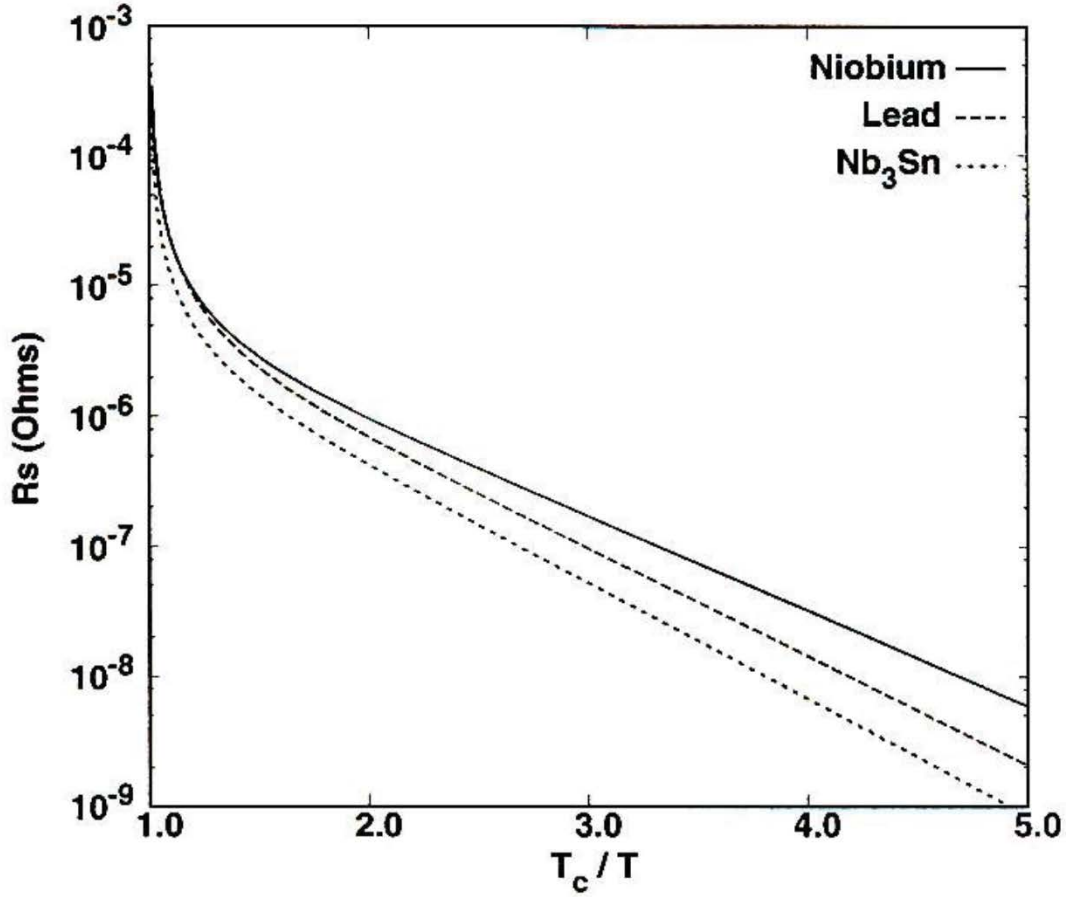

Figure 4.5: Theoretical surface resistance at 1.5 GHz of lead, niobium and Nb_3Sn as calculated from program [94]. The values given in Table 4.1 were used for the material parameters.

BCS theory / Surface resistance

Temperature dependence

–close to T_c :

dominated by change in $\lambda(t)$ $\quad \dfrac{t^4}{\left(1-t^2\right)^{3/2}}$

–for $T < \dfrac{T_c}{2}$:

dominated by density of excited states $\sim e^{-\Delta/kT}$

$$R_s \sim \frac{A}{T}\omega^2 \exp\left(-\frac{\Delta}{kT}\right)$$

Frequency dependence

ω^2 is a good approximation

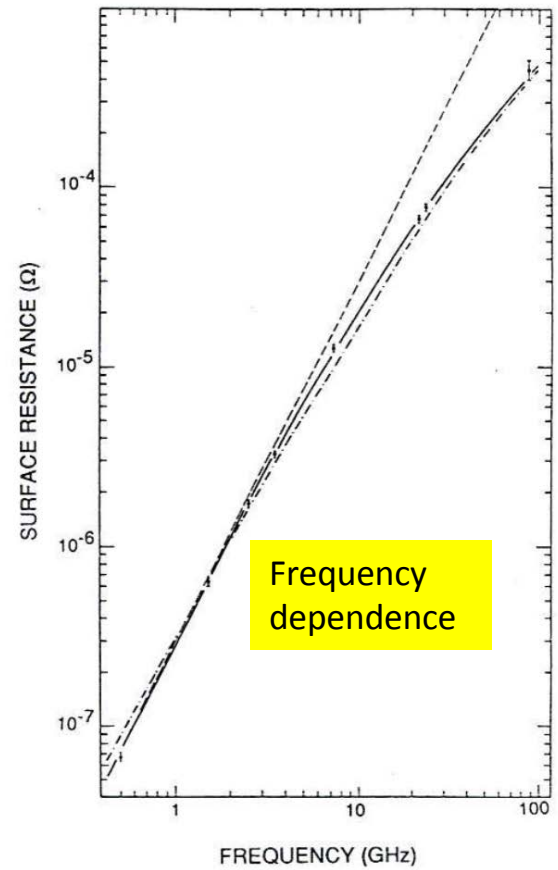

Fig. 5. The surface resistance of Nb at 4.2 K as a function of frequency [62,63]. Whereas the isotropic BCS surface resistance (– · – ·) resulted in $R \propto \omega^{1.8}$ around 1 GHz, the measurements fit better to ω^2 (– – –). The solid curve, which fits the data over the entire range, is a calculation based on the smearing of the BCS density-of-states singularity by the energy gap anisotropy in the presence of impurity scattering [61]. The authors thank G. Müller for providing this figure.

A reasonable formula for the BCS surface resistance of niobium is

$$R_{BCS} = 9 \times 10^{-5} \frac{f^2(\text{GHz})}{T} \exp\left(-1.83\frac{T_c}{T}\right)$$

BCS theory / Surface resistance

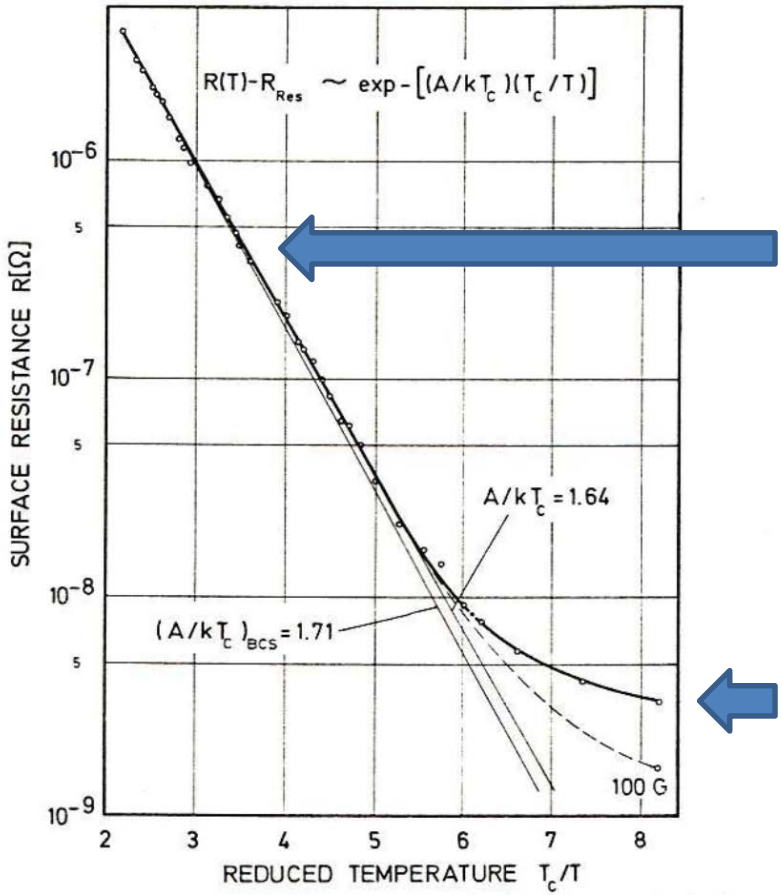

Fig. 2. Temperature dependence of surface resistance of niobium at 3.7 GHz measured in the TE_{011} mode at $H_{rf} \simeq 10$ G. The values computed with the BCS theory used the following material parameters:

$T_c = 9.25$ K; $\lambda_L(T=0, l=\infty) = 320$ Å;
$\Delta(0)/kT = 1.85$; $\xi_F(T=0, l=\infty) = 620$ Å; $l = 1000$ Å or 80 Å.

At around 4 – 3 K, the total resistance of SRF Nb cavity is dominated by BCS resistance. The fitting of these data gives the band-gap width of Nb material.

The total resistance of SRF Nb cavity at around 2 K is not dominated by the BCS resistance.
It is dominated by the residual resistance which is caused by impurity of Nb material and magnetic flux trapping.

BCS theory / Surface resistance

- The surface resistance of superconductors depends on the frequency, the temperature, and a few material parameters
  - Transition temperature
  - Energy gap
  - Coherence length
  - Penetration depth
  - Mean free path

- A good approximation for $T<T_c/2$ and $\omega<<\Delta/h$ is

$$R_s \sim \frac{A}{T}\omega^2 \exp\left(-\frac{\Delta}{kT}\right) + R_{res}$$

BCS theory / Surface resistance

- Normal Conductors
  - Skin depth proportional to $\omega^{-1/2}$
  - Surface resistance proportional to $\omega^{1/2 \rightarrow 2/3}$
  - Surface resistance independent of temperature (at low T)
  - For Cu at 300K and 1 GHz, R_s=8.3 mΩ

- Superconductors
  - Penetration depth independent of ω
  - Surface resistance proportional to ω^2
  - Surface resistance strongly dependent of temperature
  - For Nb at 2 K and 1 GHz, $R_s \approx 7$ nΩ

Lecture B and C3a: Superconductive RF

Cavity Fabrication

1.3 GHz elliptical 9-cell cavity

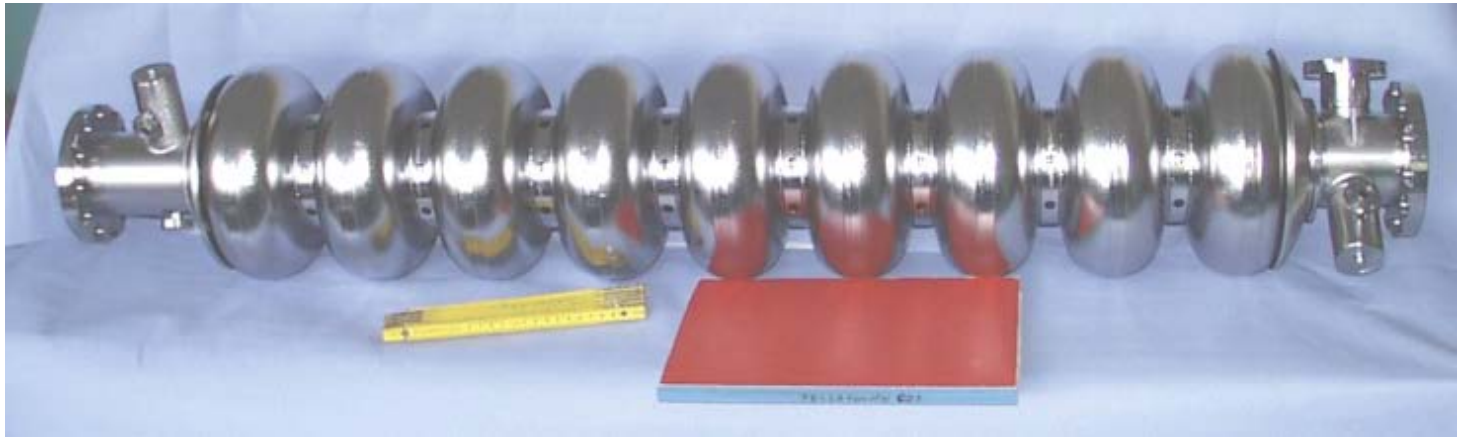

TESLA 9-cell Cavity
(Iris 70 mm)

Nb Mines in the world

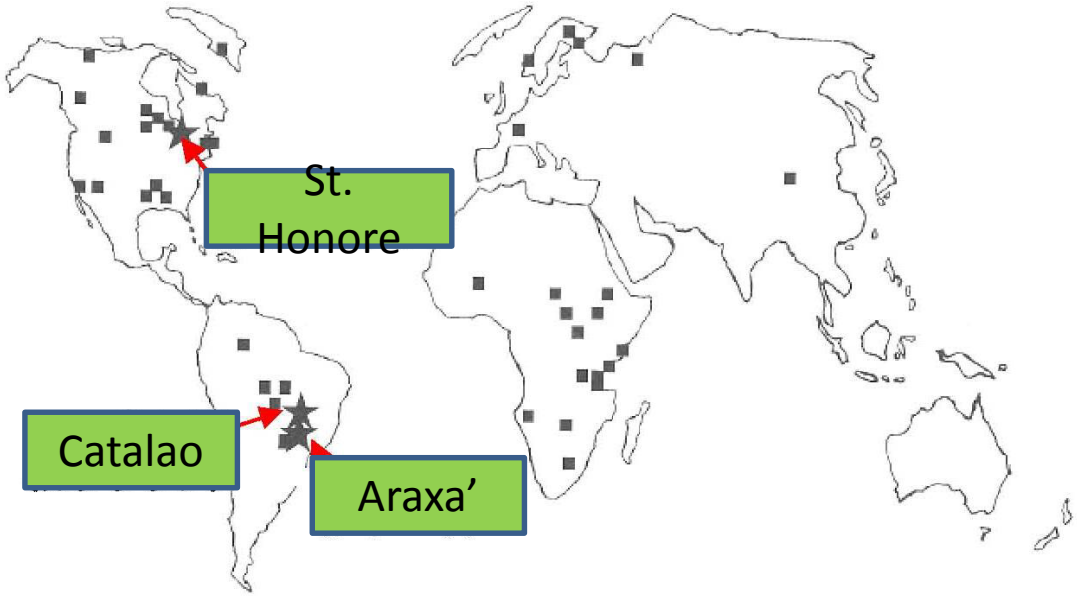

Ore of Nb:
Carbonite

Three largest mines in the world:
Araxa'
Catalao
St. Honore

■ Nb deposits
★ Nb Mines

金属 Vol.72 (2002) No.3

Niobium is the 33rd abundant/rich metal in the all existing metals in the earth.

Nb Mine

Process flow of the industrial Nb production

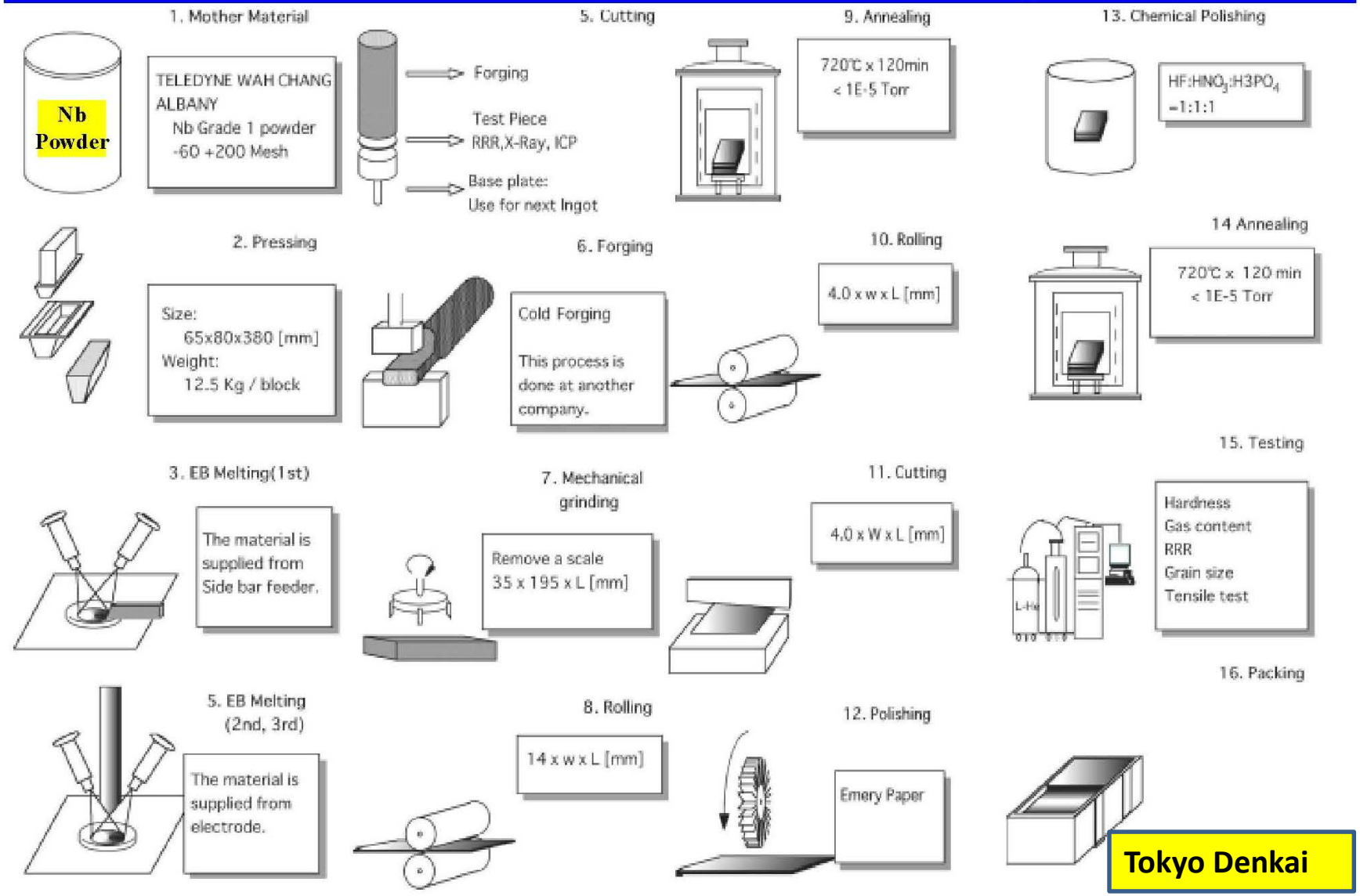

Electron Beam Melting (EBM) Furnace and Nb Ingots

Tokyo Denkai

Nb ingots

Electron Beam Melting

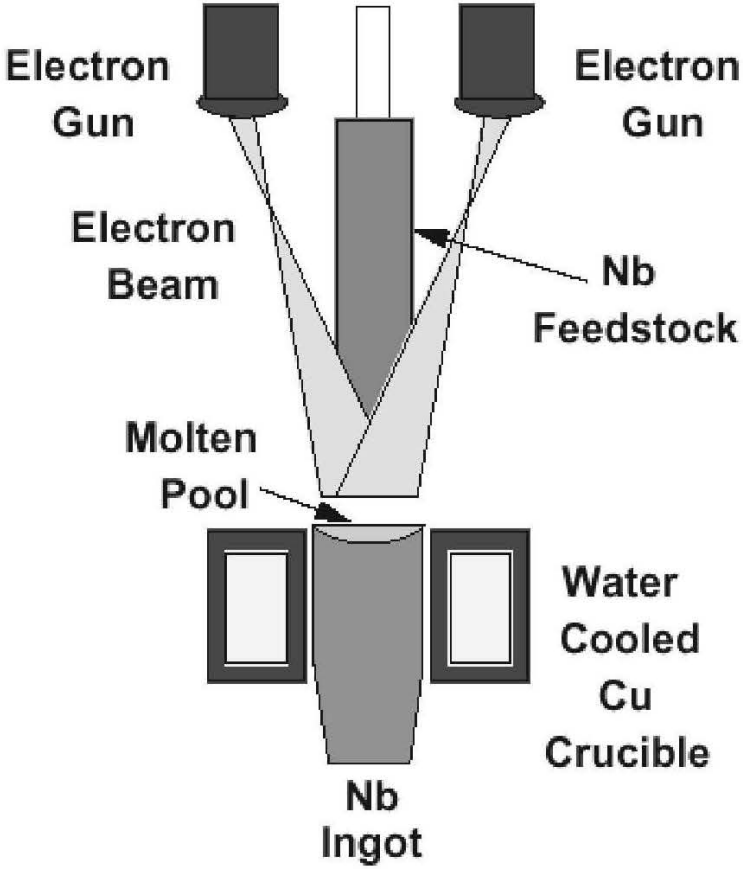

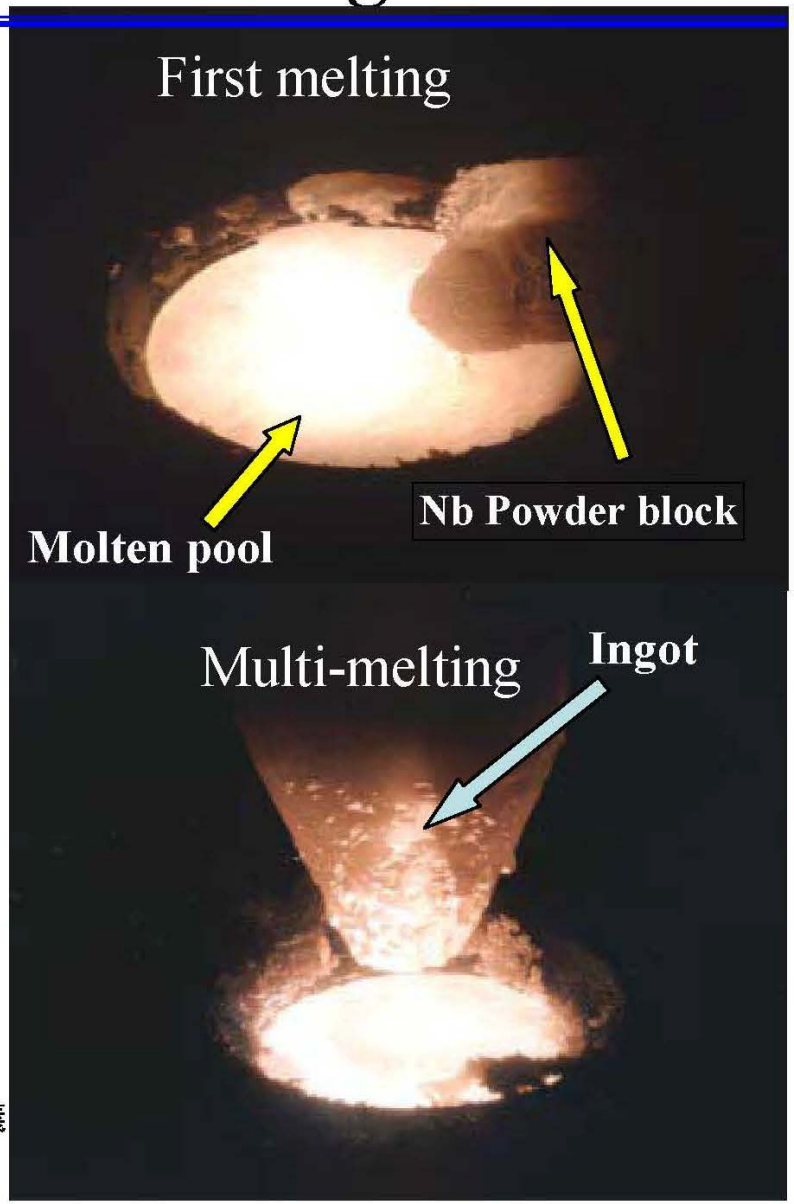

講義

Evaporation Pressure of Various Metals

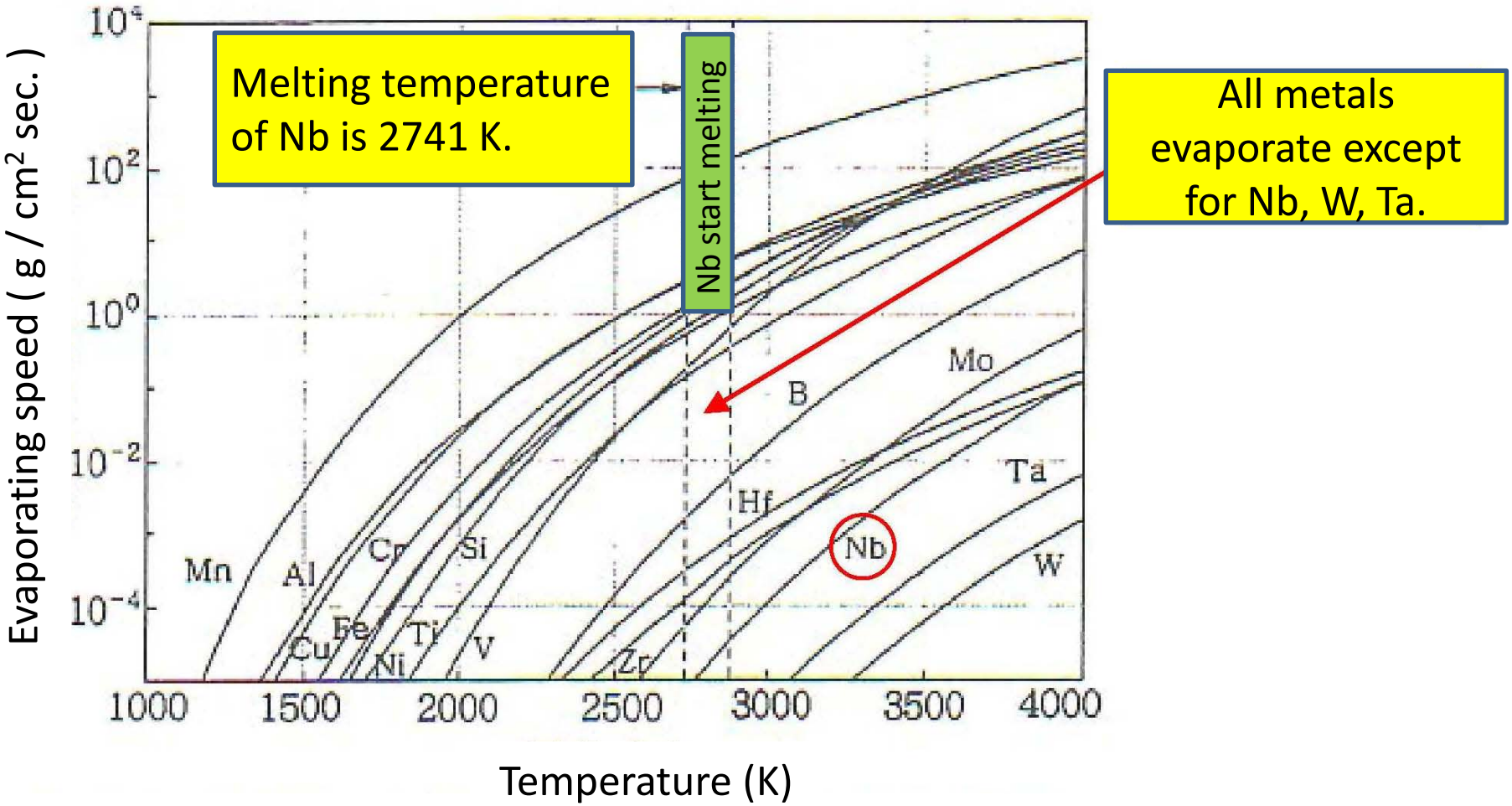

Relation between impurity in NB and RRR

Umezawa's calculation.

$$\frac{1}{RRR} = \frac{O}{5800} + \frac{N}{2273} + \frac{H}{16322} + \frac{C}{8911} + \frac{Ta}{604690} + \frac{1}{1249}$$

$$RRR \equiv \frac{R(300K)}{R(9.5K)}$$

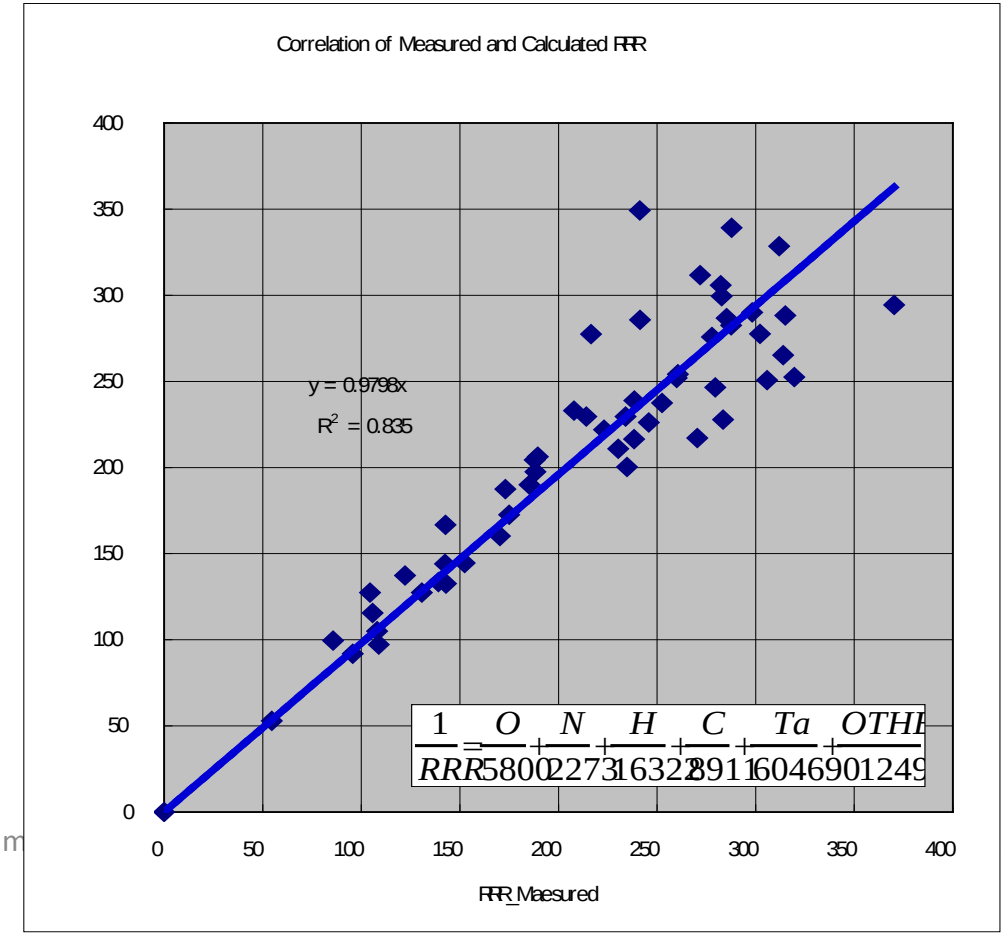

RRR Measurement

$$RRR \equiv \frac{R(300K)}{R(9.5K)}$$

4-terminal method

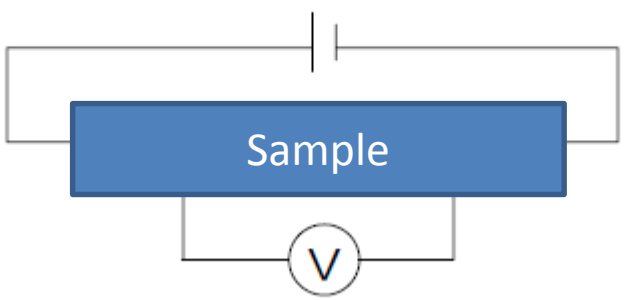

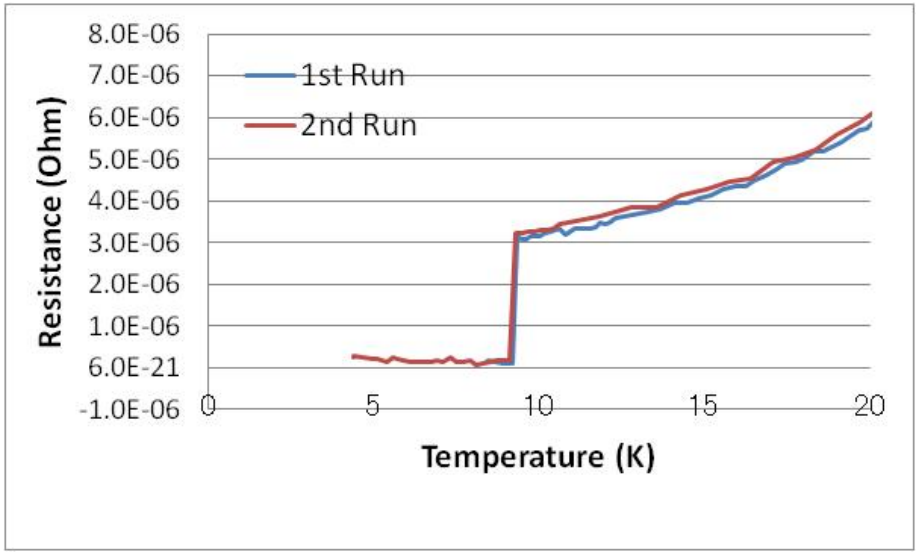

History of improvement with RRR

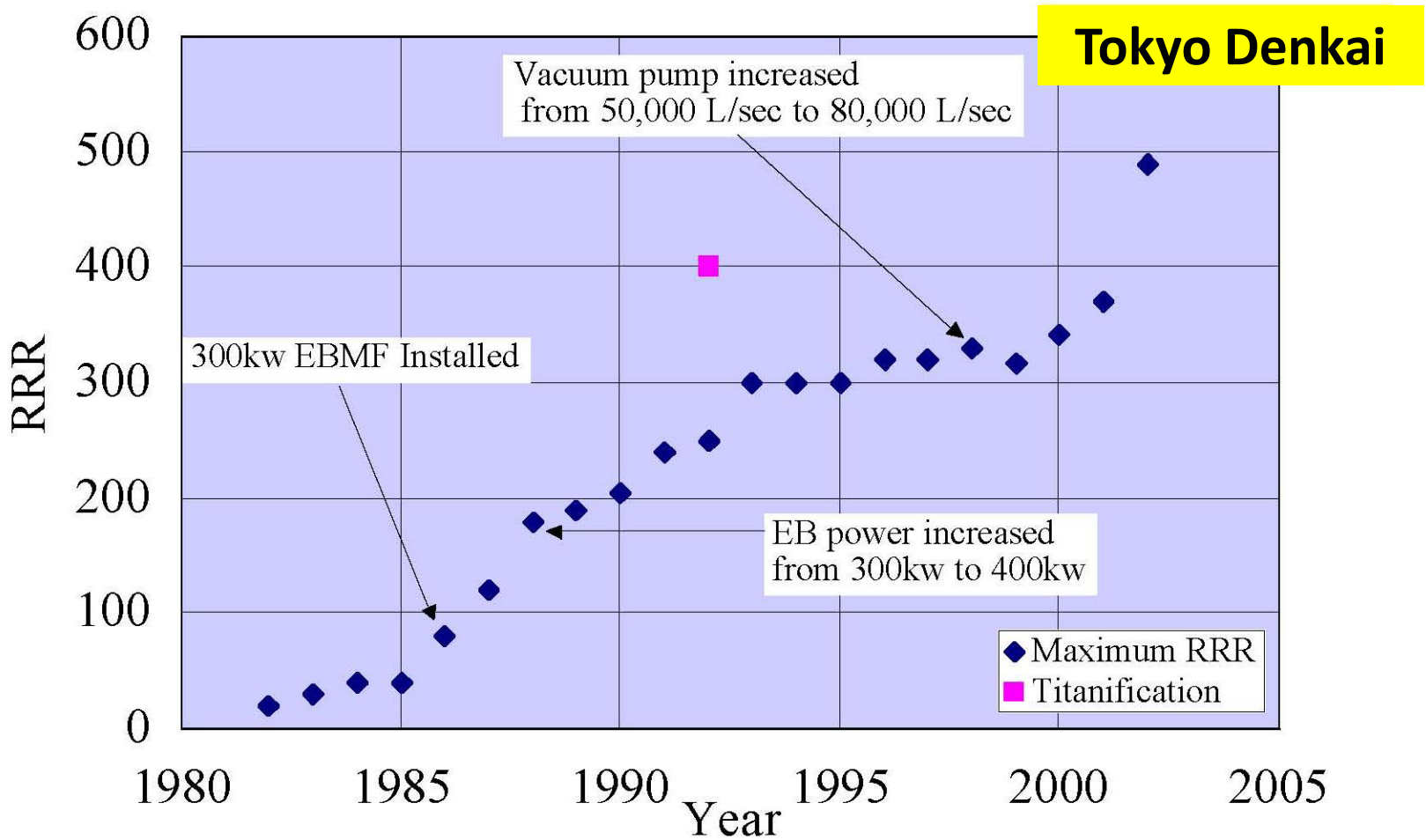

Nb materials for 9-cell cavity

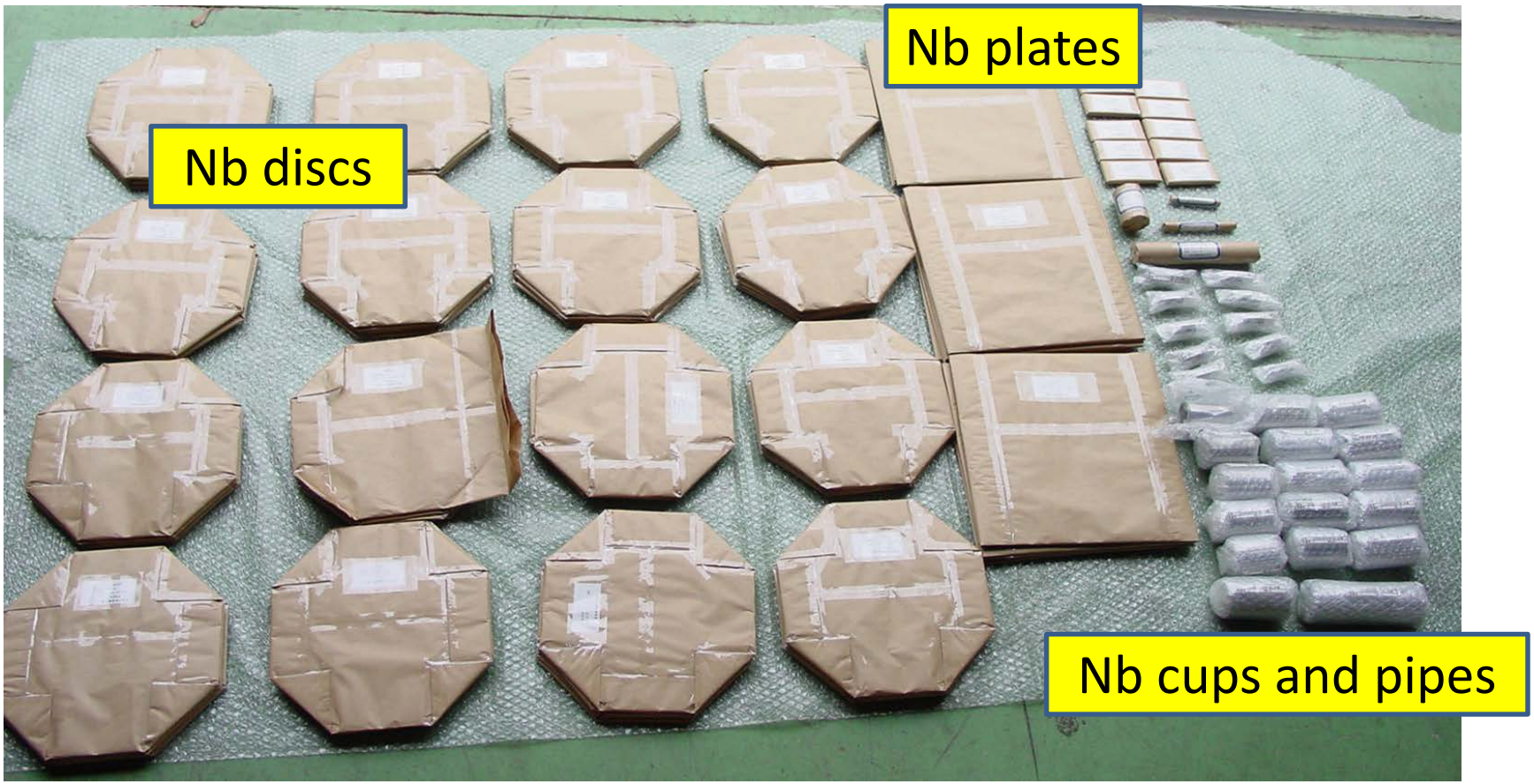

Material for four 9-cell cavities

Nb materials for 9-cell cavity

Nb plate for beam-pipe

HOM antenna and so on

Nb disc for half-cell cup

Overview over Fabrication of 9-cell cavity

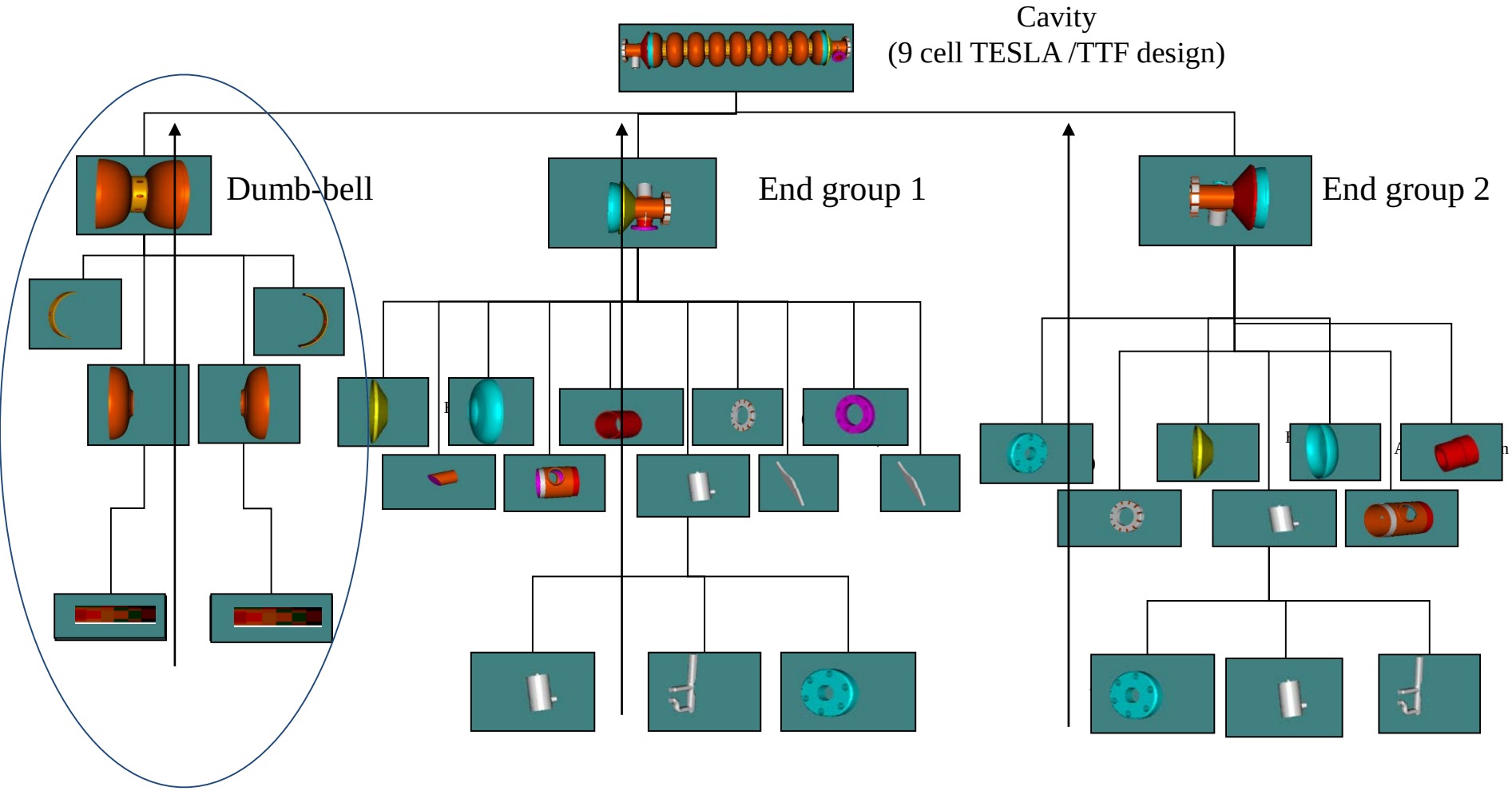

Overview over Fabrication of 9-cell cavity

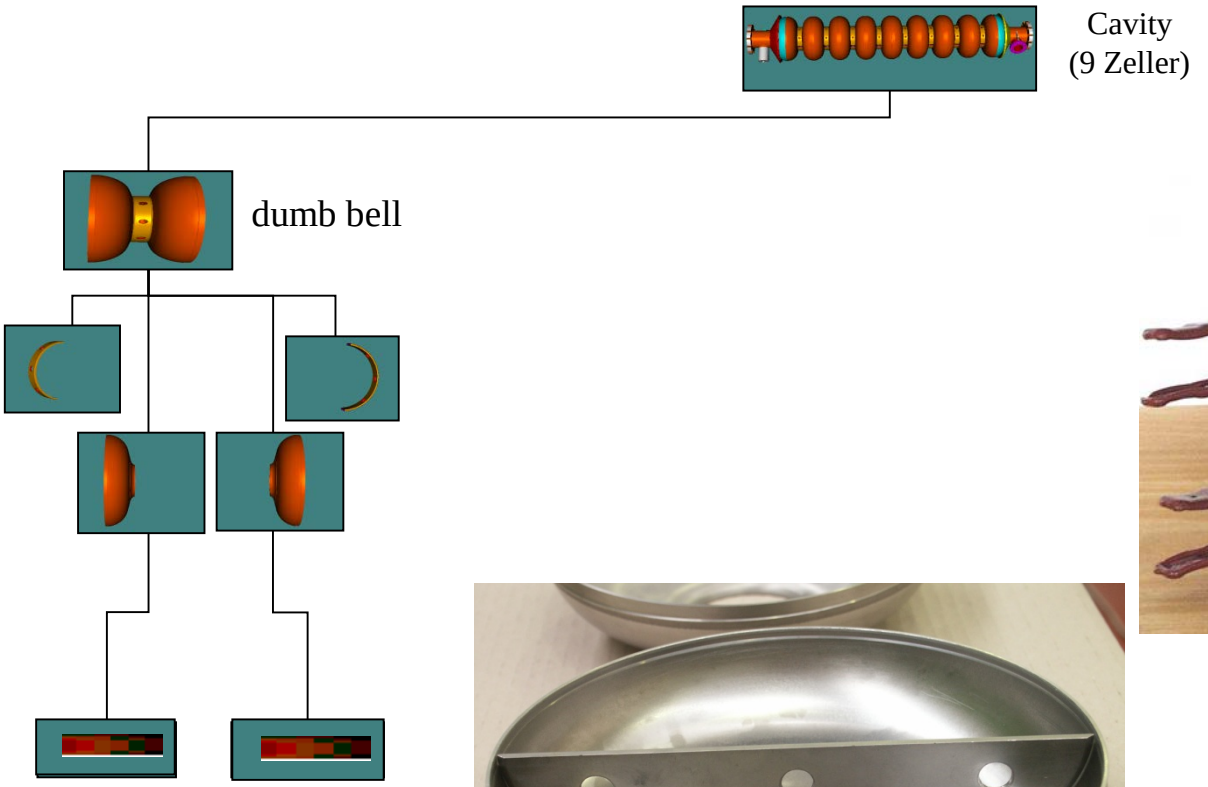

Fabrication Processes of half-cell

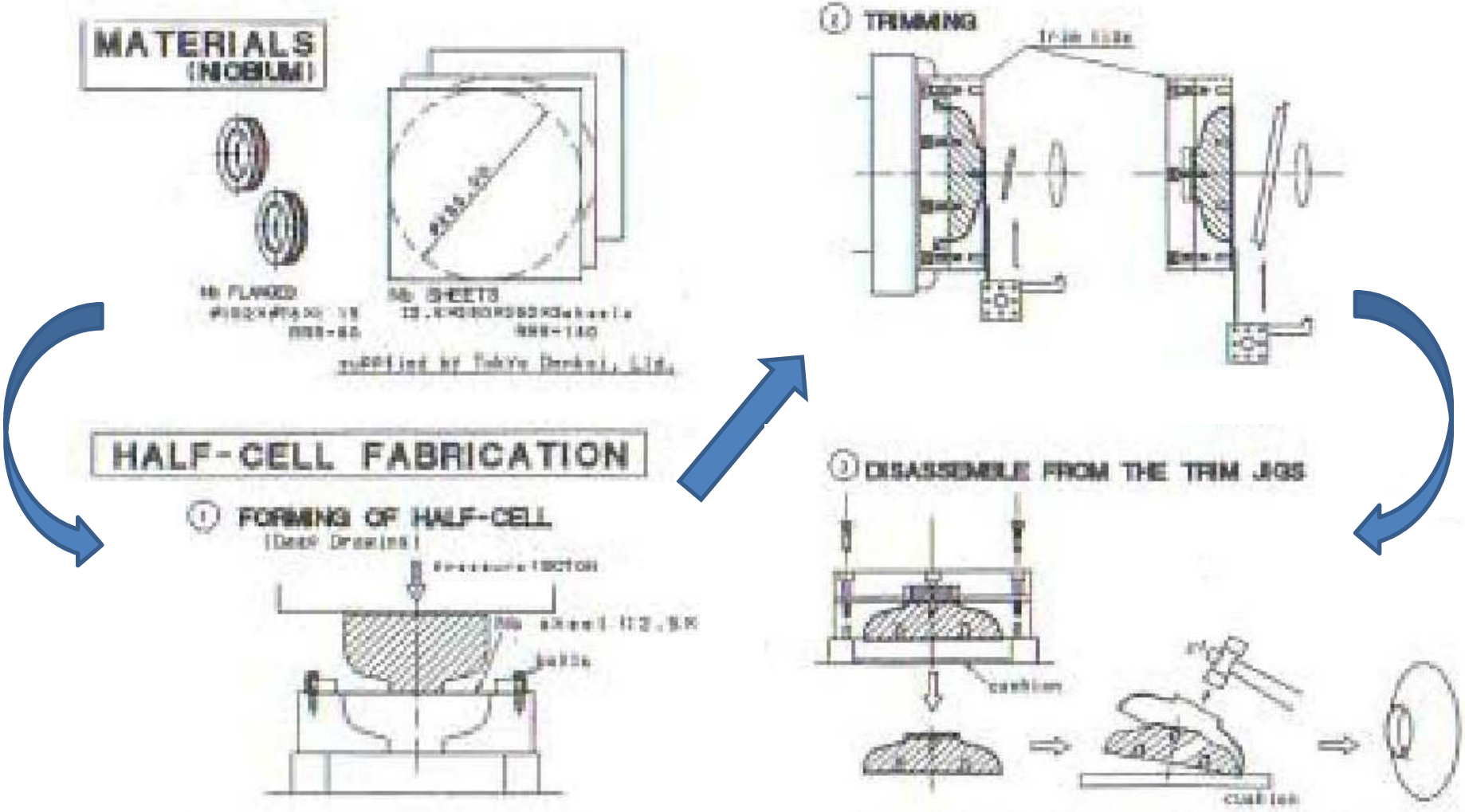

Deep-drawing of half-cell cups

Deep-drawing of Nb half-cell at 2.5 ton by a press-machine (80 ton).

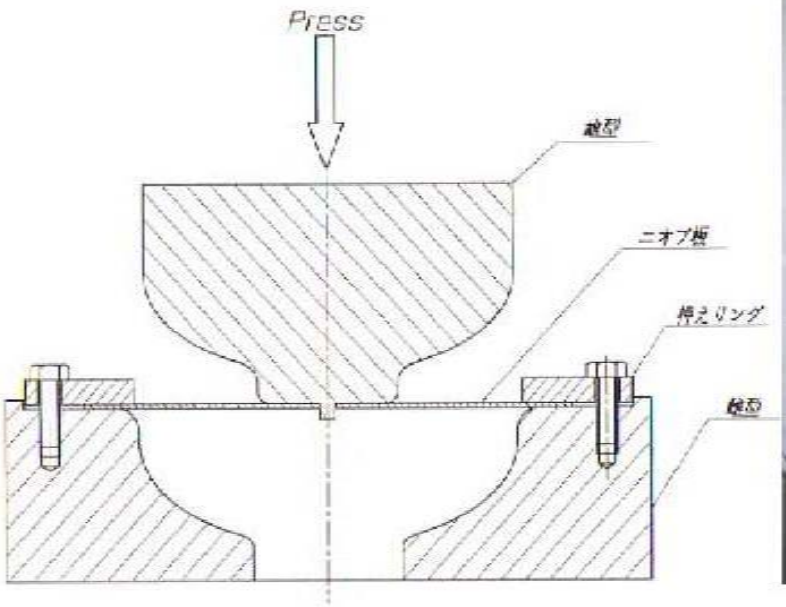

Fabrication of LL Cavity at KEK

Pressing Nb plate

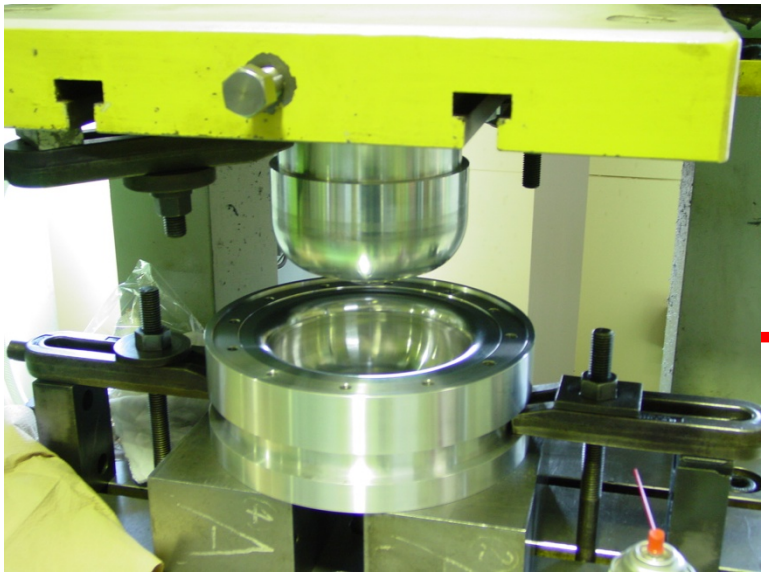

56 half-cells were pressed in a few hours

Fabrication of LL Cavity at KEK

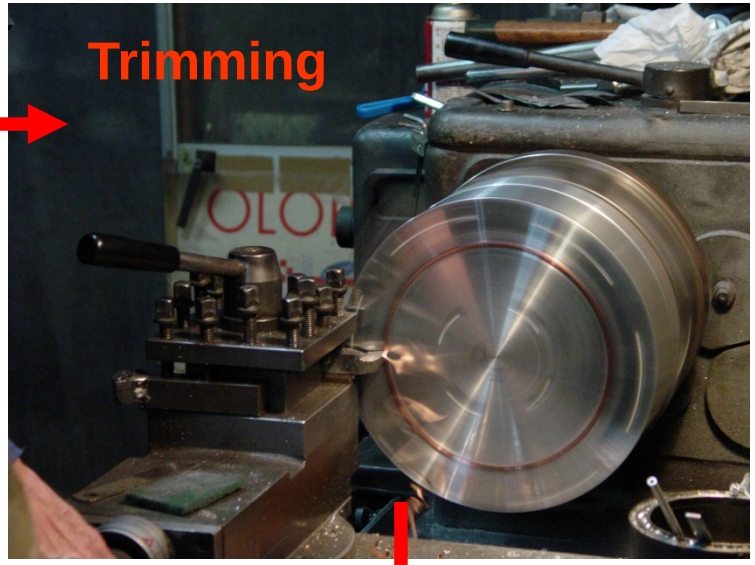

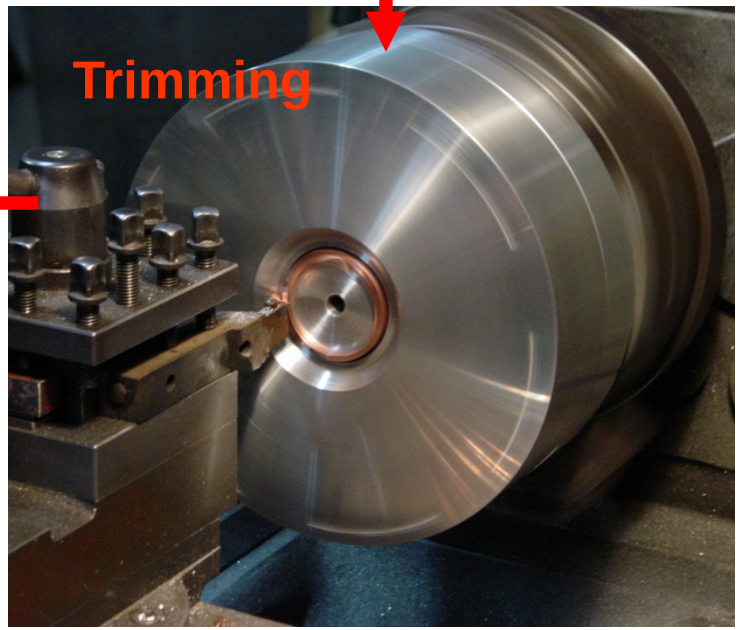

After trimming

Production procedure of 9-cell cavity for ILC

Dumbbell = EBW of two cups:

Dumbbell

8 dumbbells are needed for one cavity

EBW assembly of all parts:

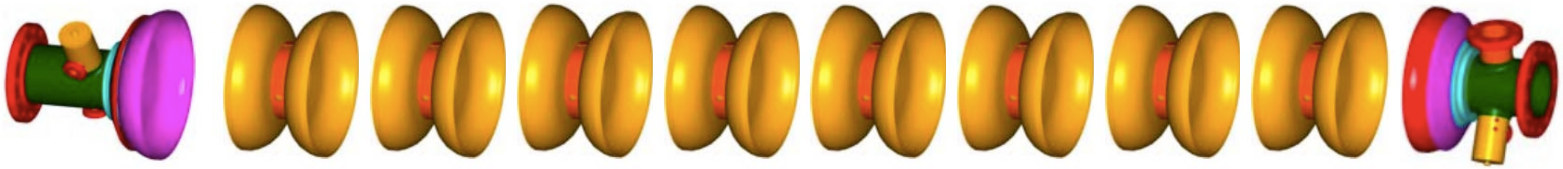

Welding of He tank:

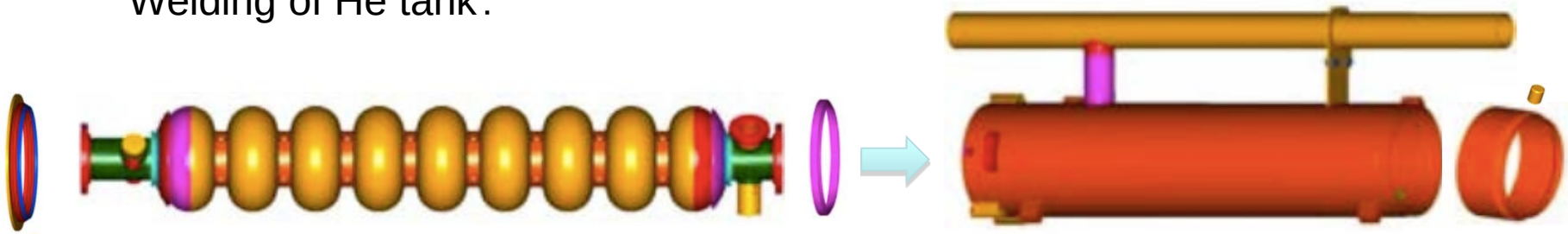

Fabrication of 9-cell Cavity

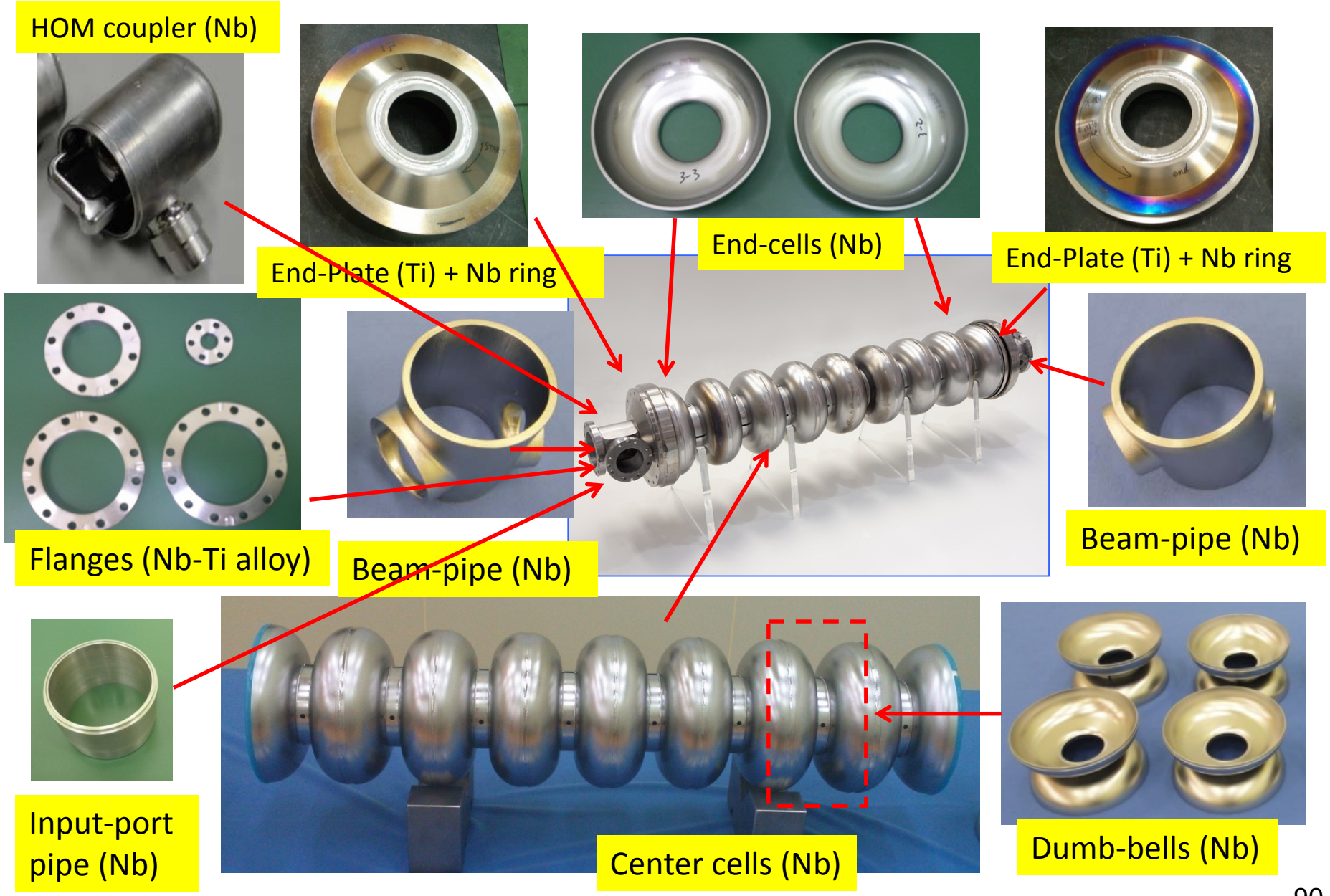

Electron Beam Welding (EBW) machine / KEK

Gun in vertical position

Gun in horizontal position

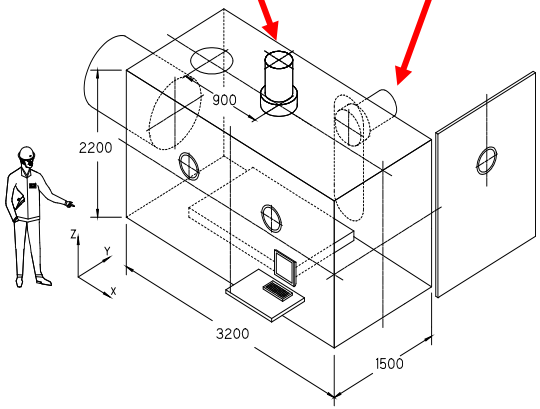

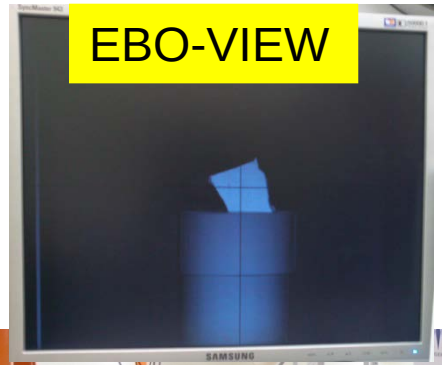

Steigerwald Strahl Technik

EBW machine : 150 kV, 15kW

Pressure : below 1×10^-2Pa within 20 min.
Inside material : SUS316L, Volume : 10.56 m³

Electron Beam Welding (EBW) Machine

Assembly of all Nb parts are done by EBW machine. This is because contamination of O2, N2, CO2, etc. degrade the SC performance of cavity.

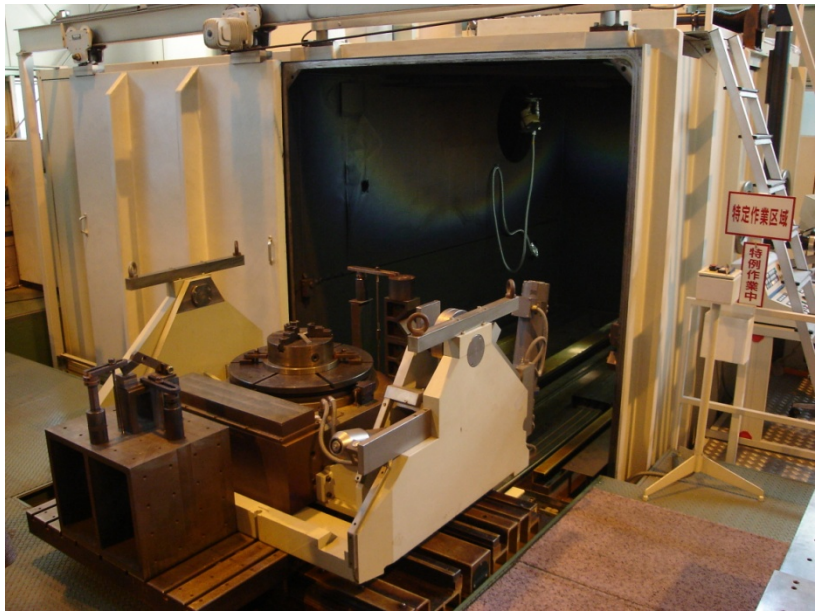

The chamber inside is pumped down to exclude the air before the EBW assembly.

Electron Beam Welding (EBW) Machine

Electron Gun

Operator

Electron Beam Welding (EBW) parameter search

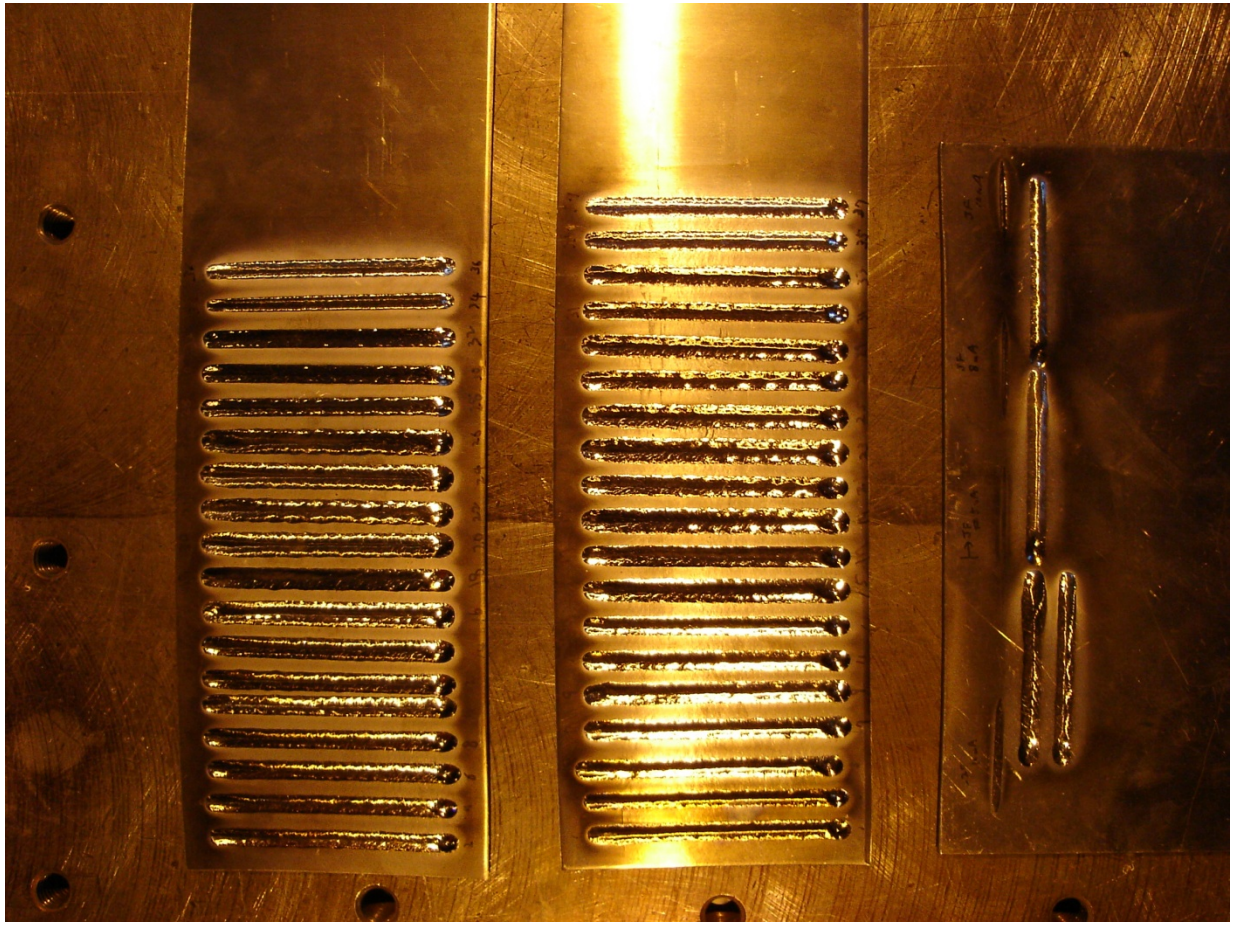

Beam-parameter search with Nb test-pieces.
Oscillation of beam was applied.

Electron Beam Welding (EBW) parameter search

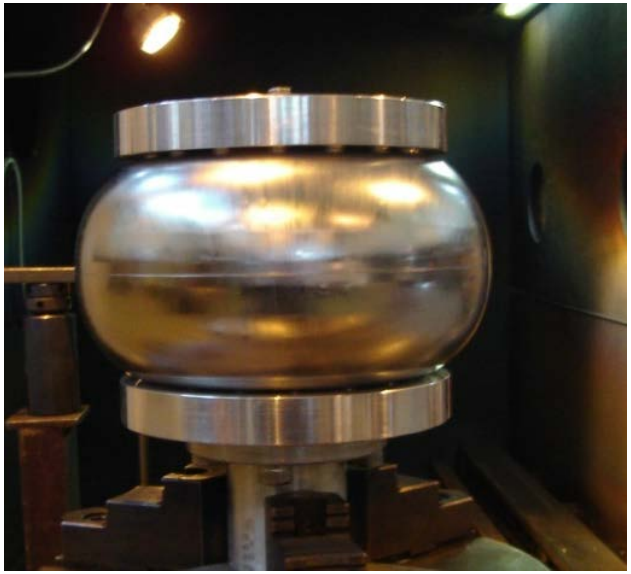

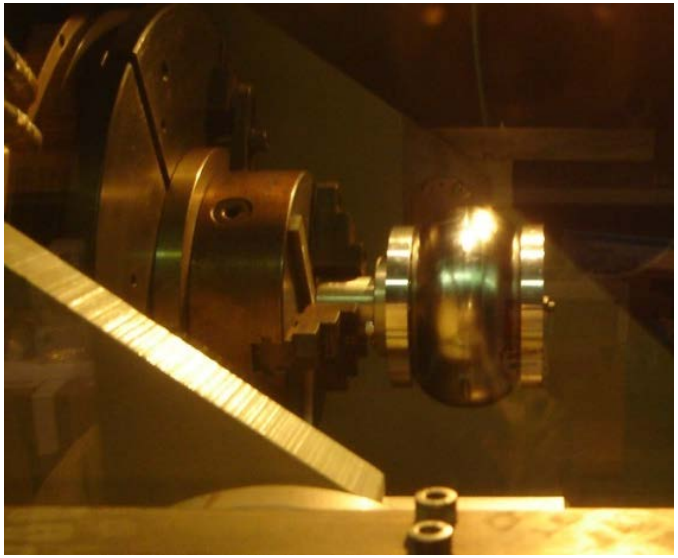

150 kV, 30 mA, 10 mm/s

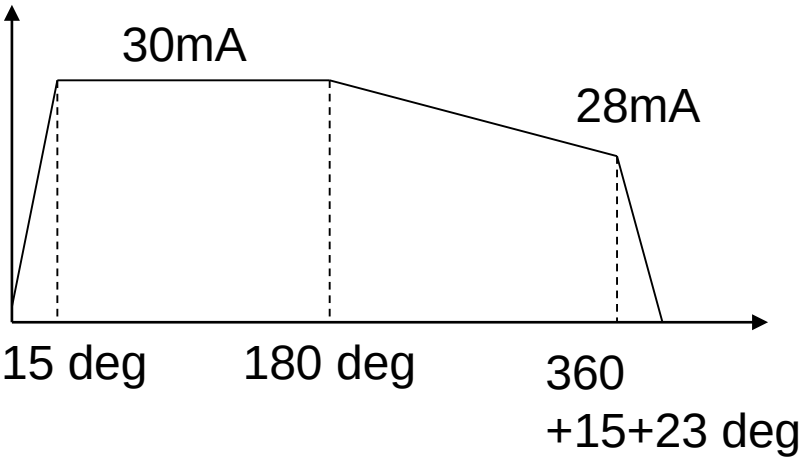

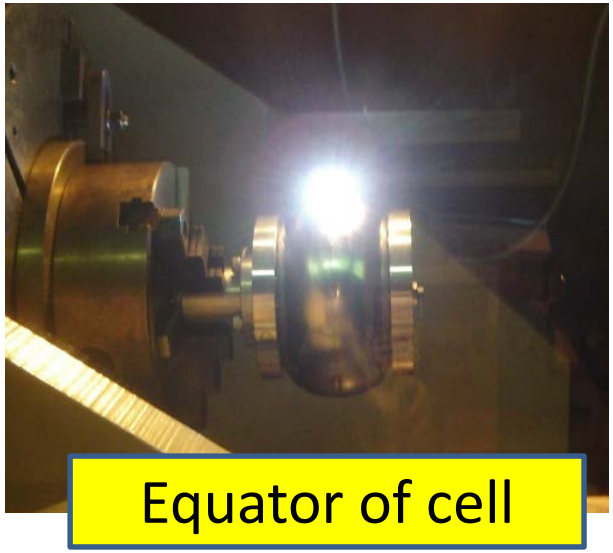

EBW of Dumbbell

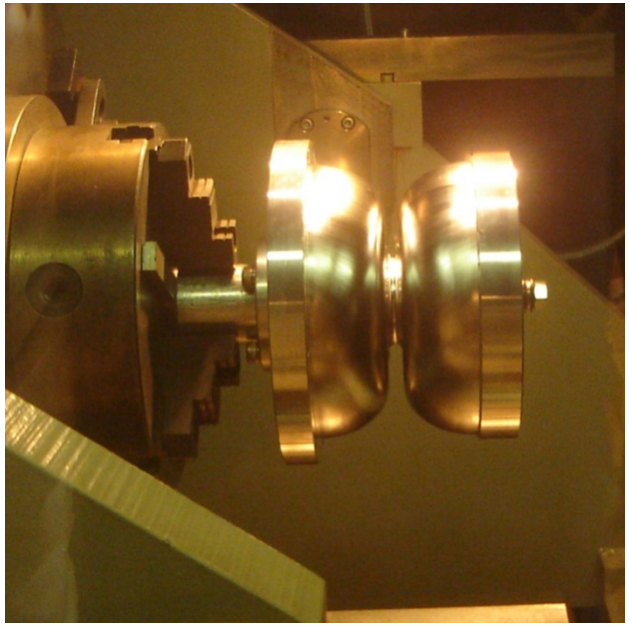

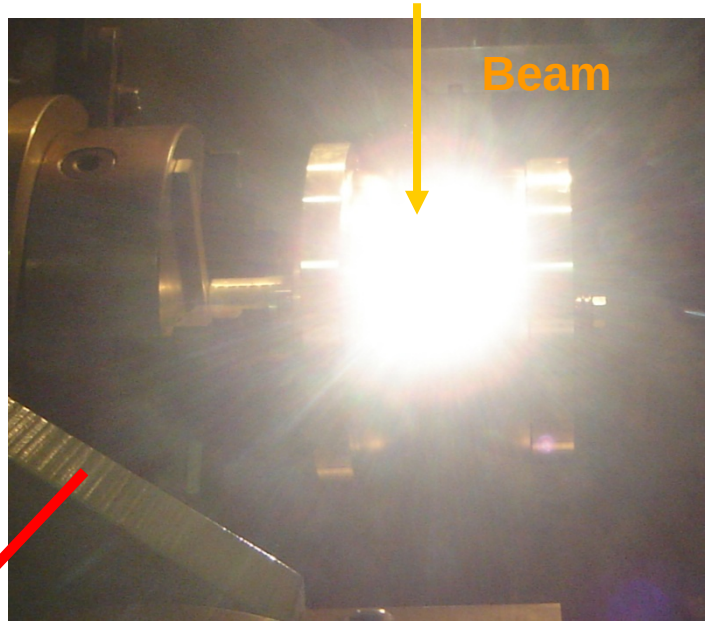

Outside, EBW depth = 70%
150kV, 18 mA, 10 mm/s

High electric field at iris.
The inner surface of iris should be smooth to avoid field-emission.

Overview over Fabrication of 9-cell cavity

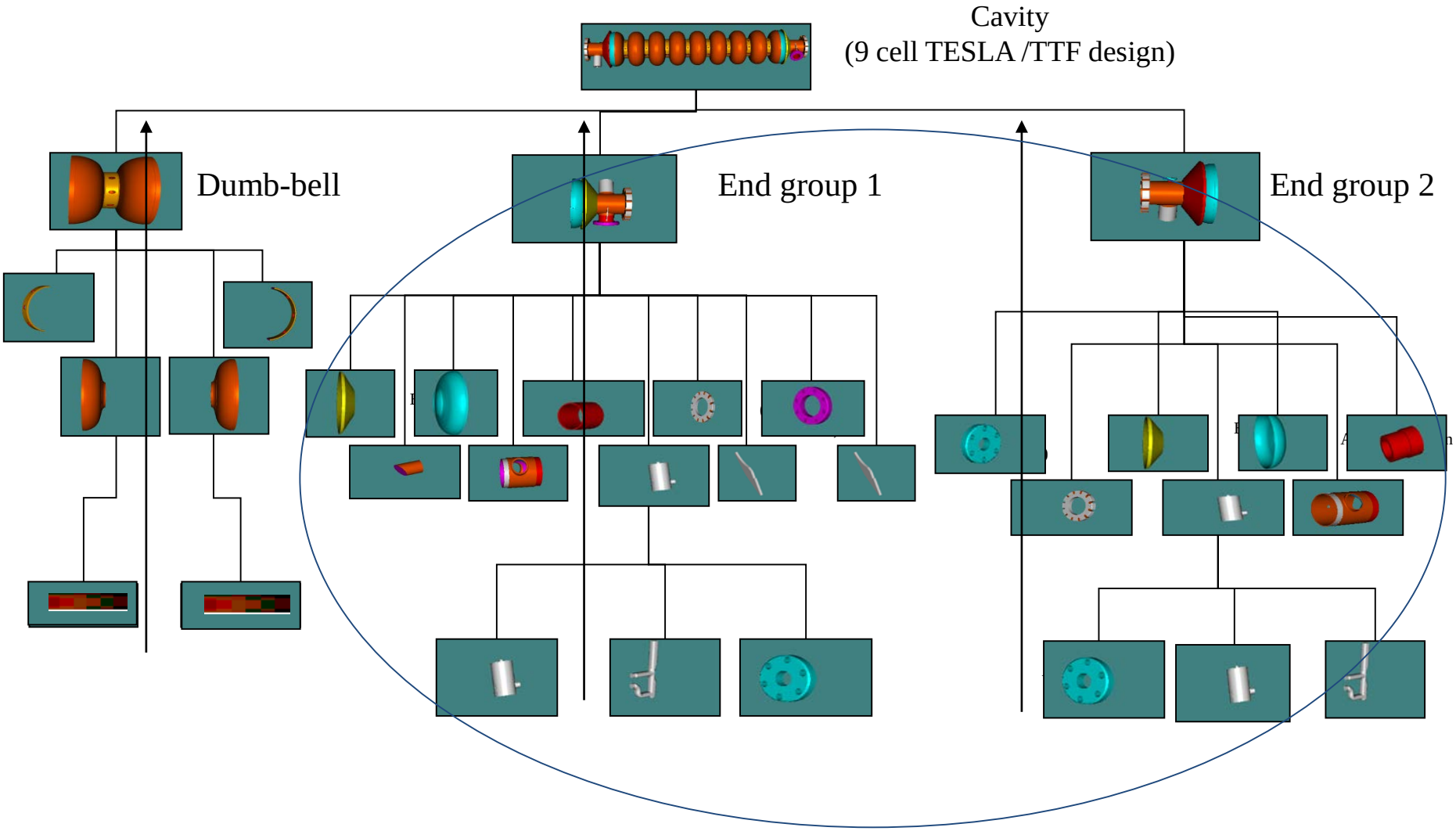

Fabrication Processes of beam-pipe

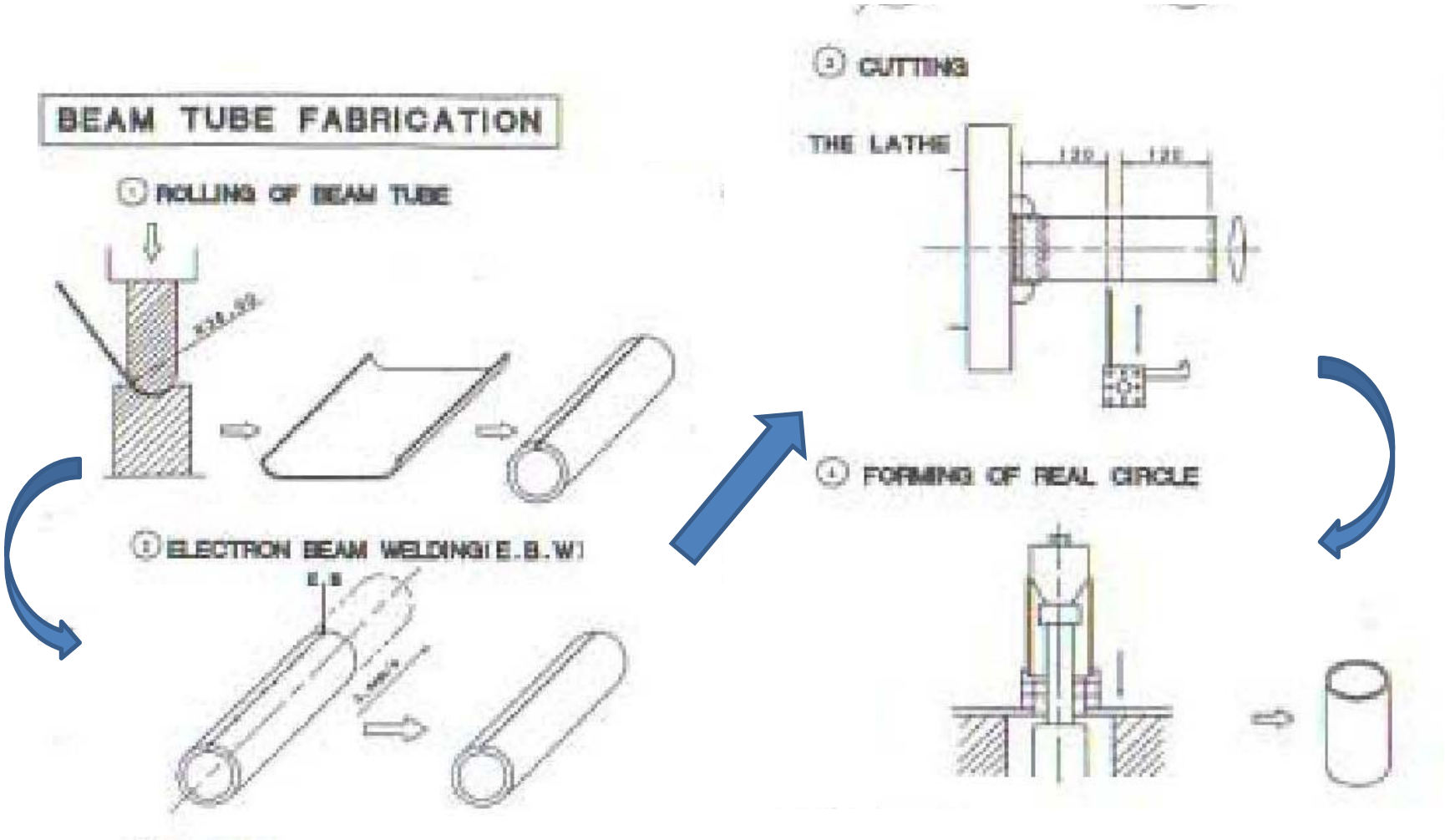

Rounding of Beam Pipe from Nb plate

Rounding of Beam Pipe from Nb plate

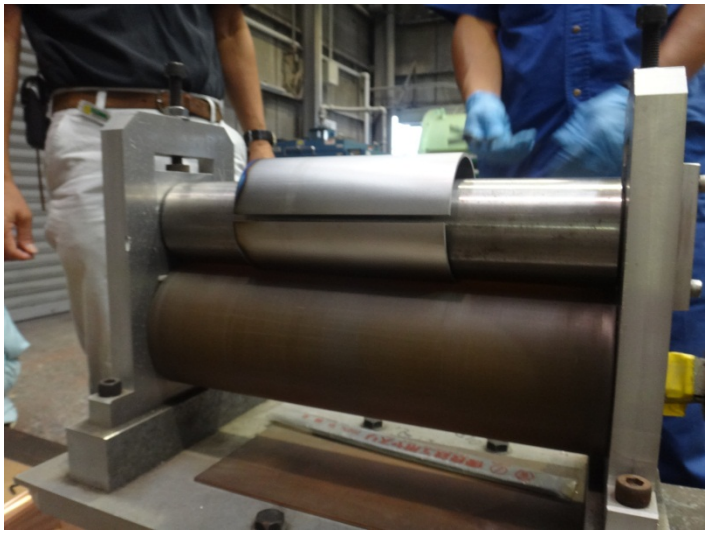

Final rounding

After rounding

Fixture for EBW

EBW of Beam Pipe

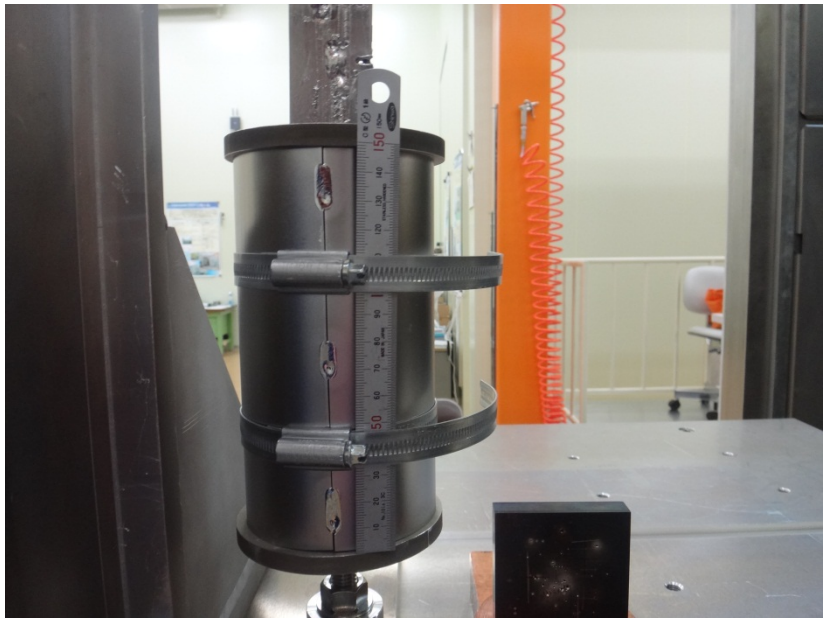

Point EBW

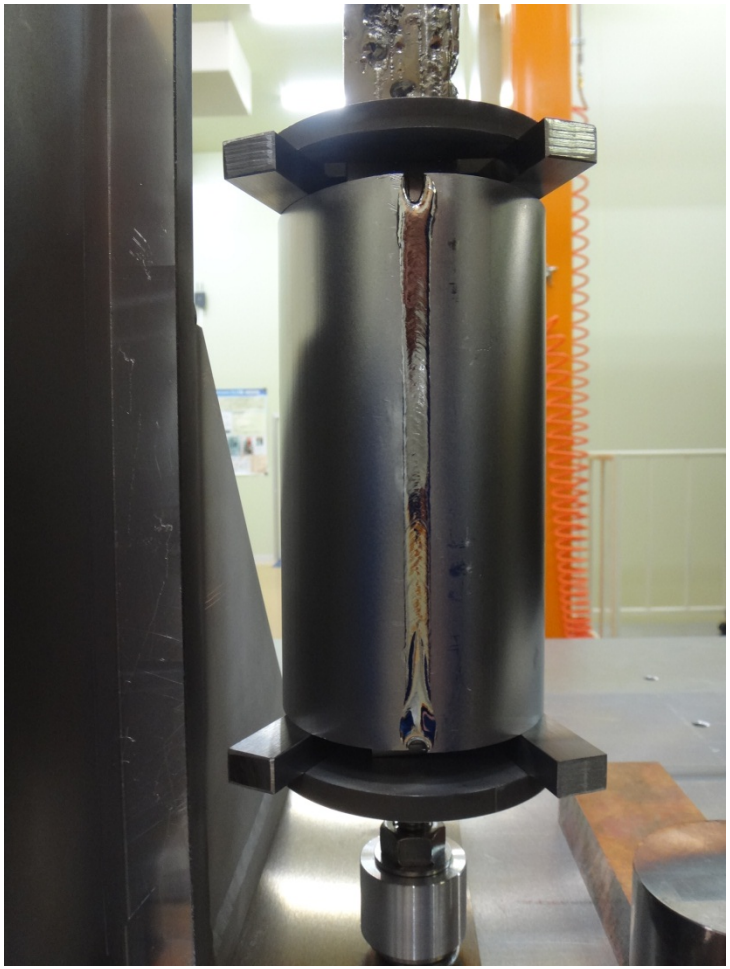

After EBW

Centering of Beam Pipe

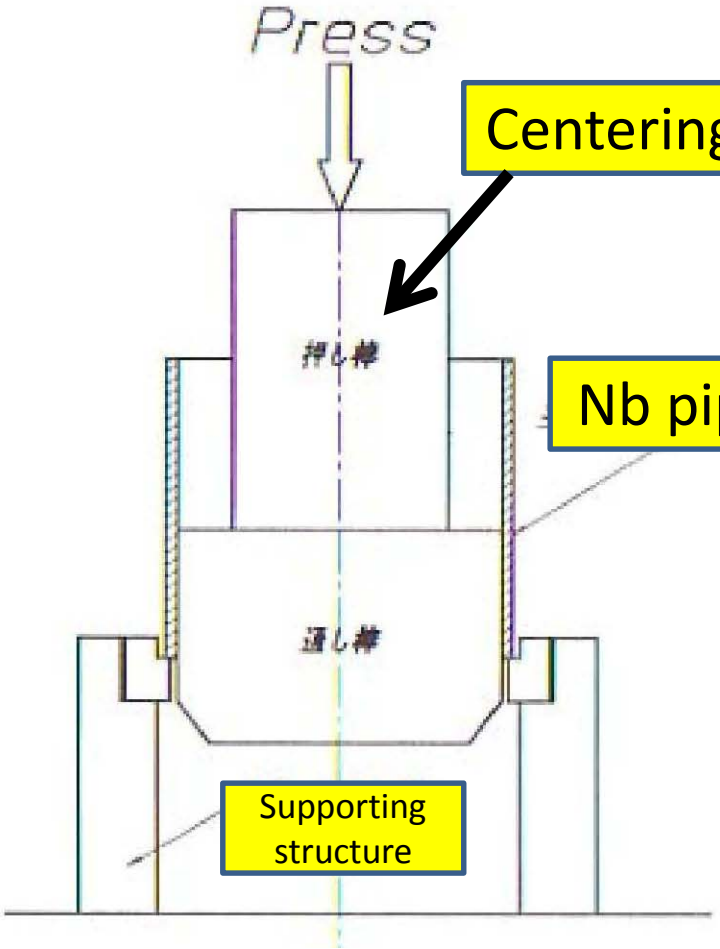

Fabrication Processes of beam-pipe

- The fabrication methods of beam-pipe are depending on the industries.
- Deep-drawing from a Nb plate to a pipe: For this process, several deep-drawing processes with different dies are needed with annealing process inbetween deep-drawing processes.
- Back-extrusion from a shaped Nb ingot to a pipe: Fabrication of Nb plate is skipped in this process, but you need a large press machine.

Beam Pipe

80 phi Nb Beam-pipe (input-coupler)

108 phi Nb Beam-pipe (pickup)

End-group

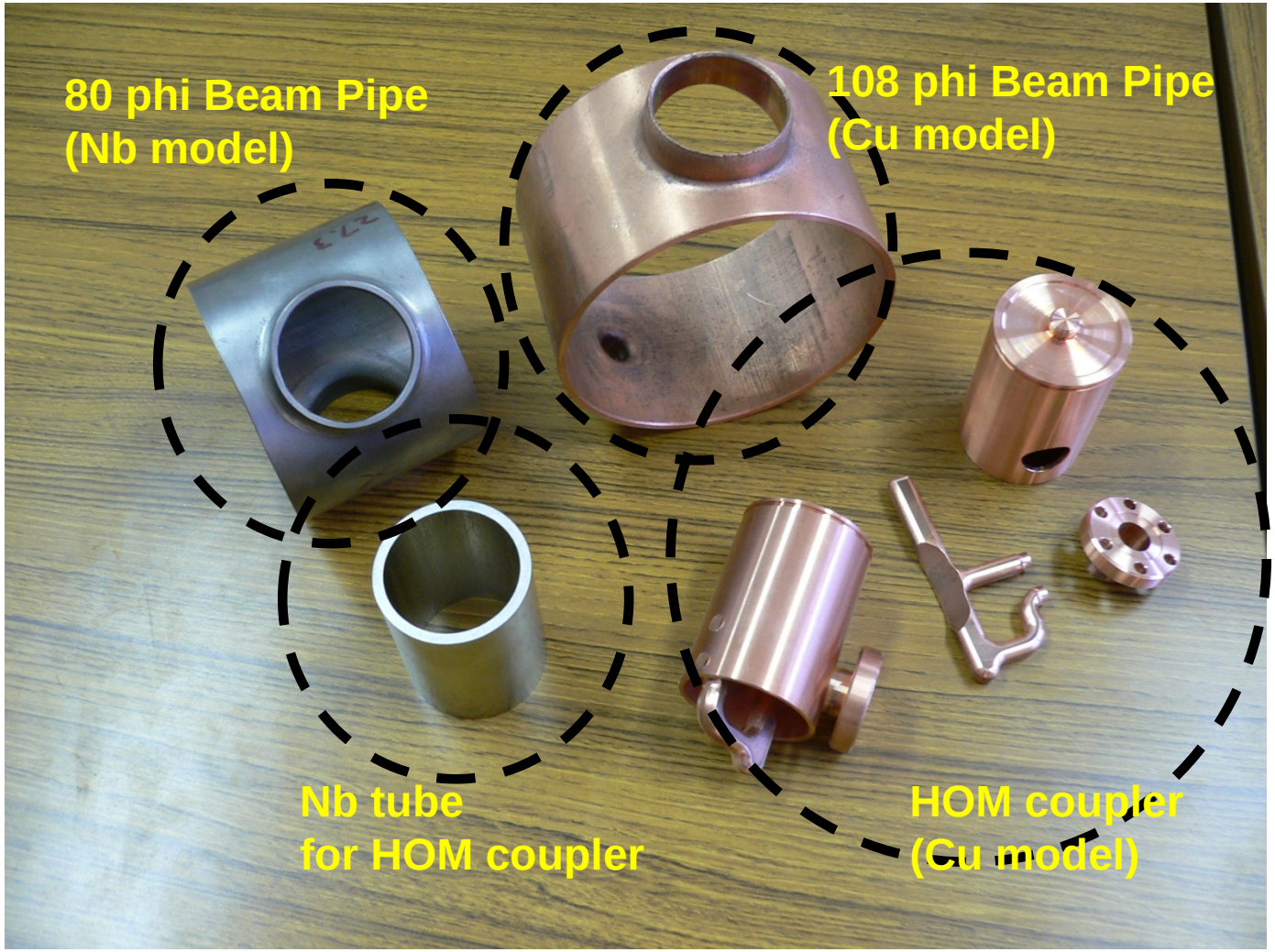
80 phi Beam Pipe
(Nb model)
108 phi Beam Pipe
(Cu model)
Nb tube
for HOM coupler
HOM coupler
(Cu model)

End-group

End-plates / joint to He jacket

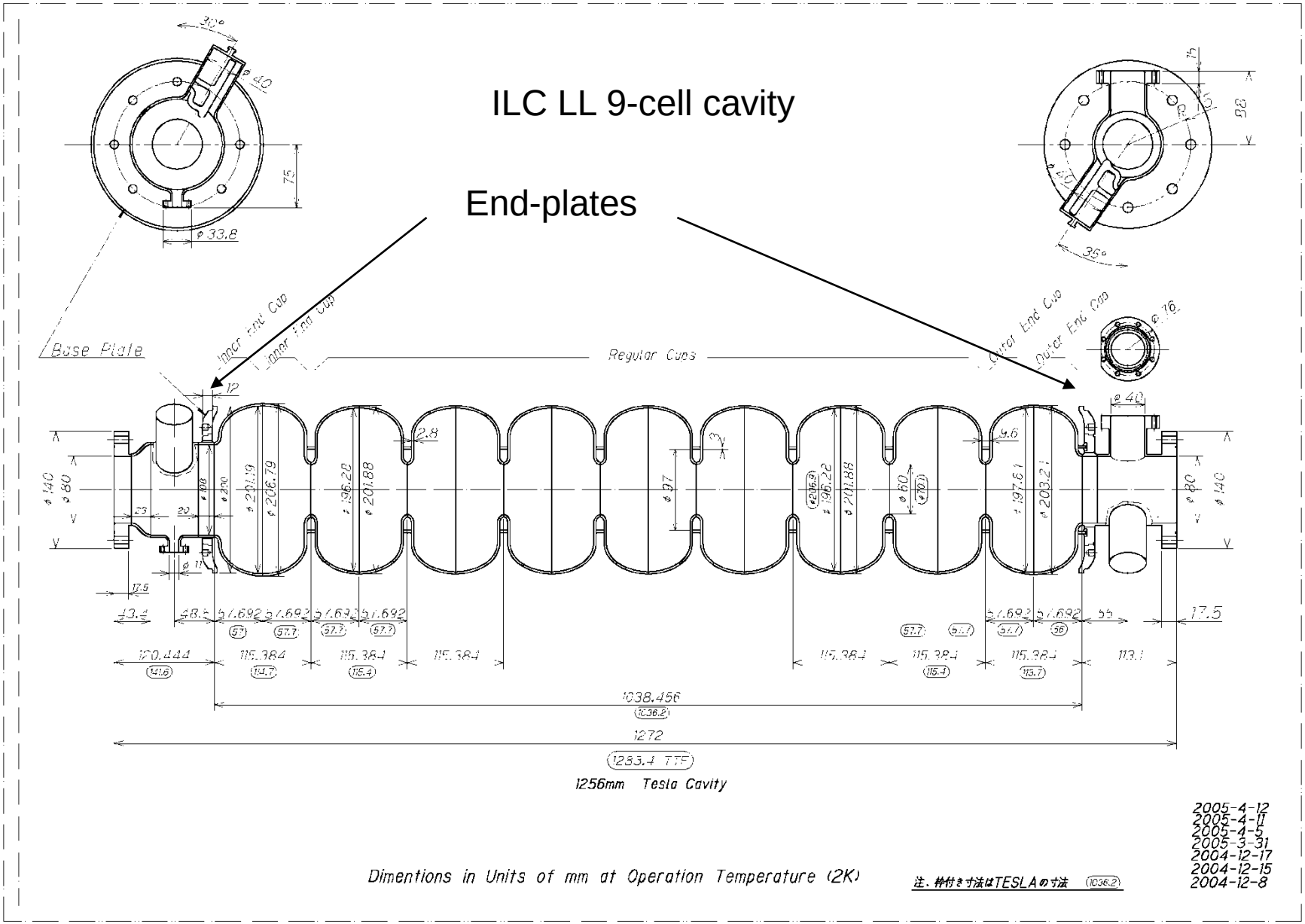

End-plates / joint to He jacket

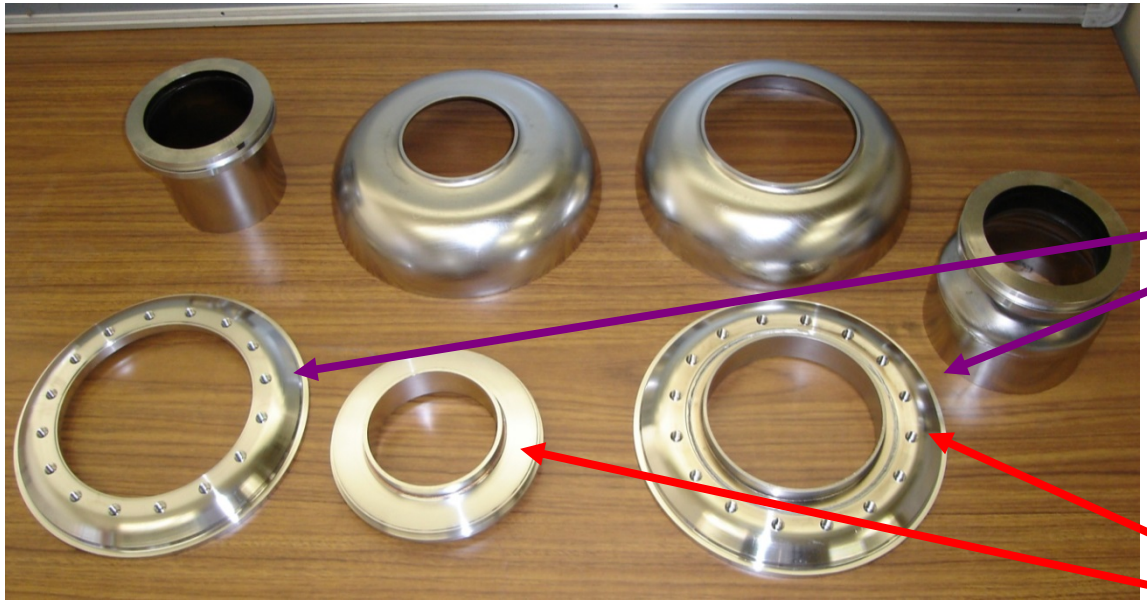

SUS Base-plate

HIP bonding

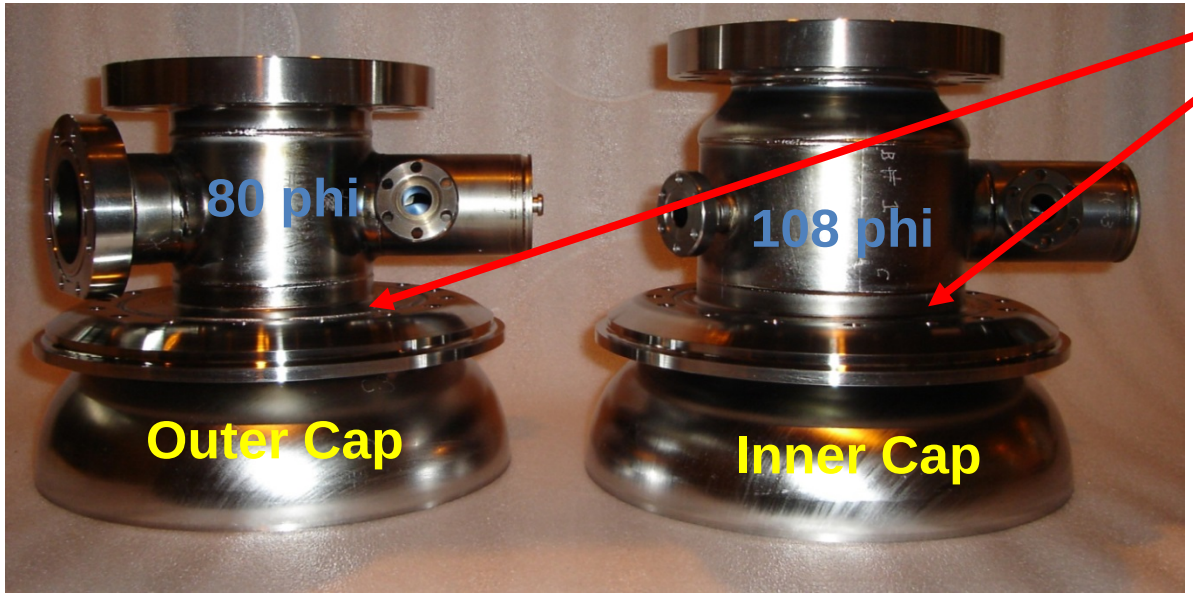

End-group EBW

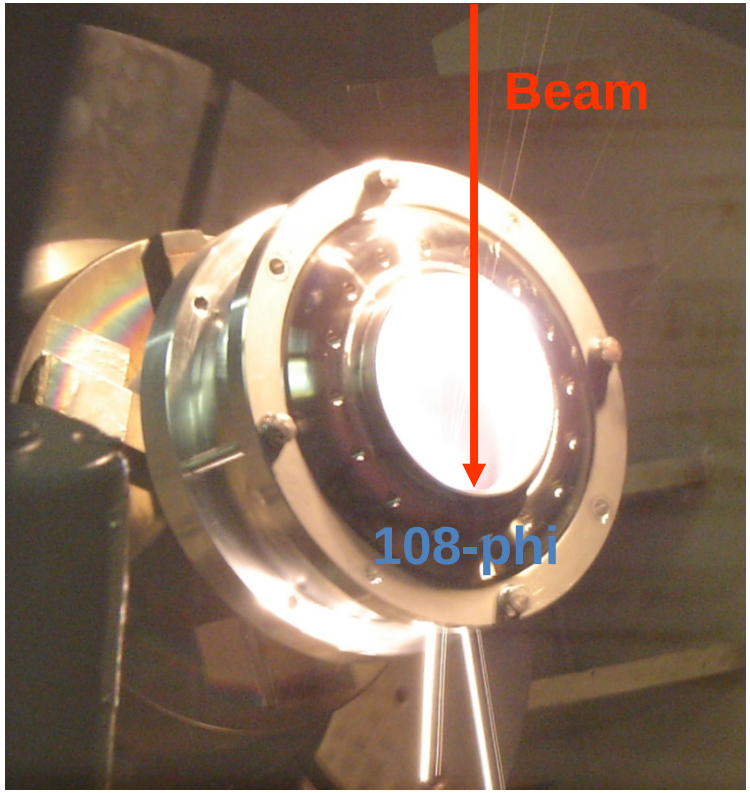

Base-plate 108-phi beam-pipe
+ Inner End-Cap

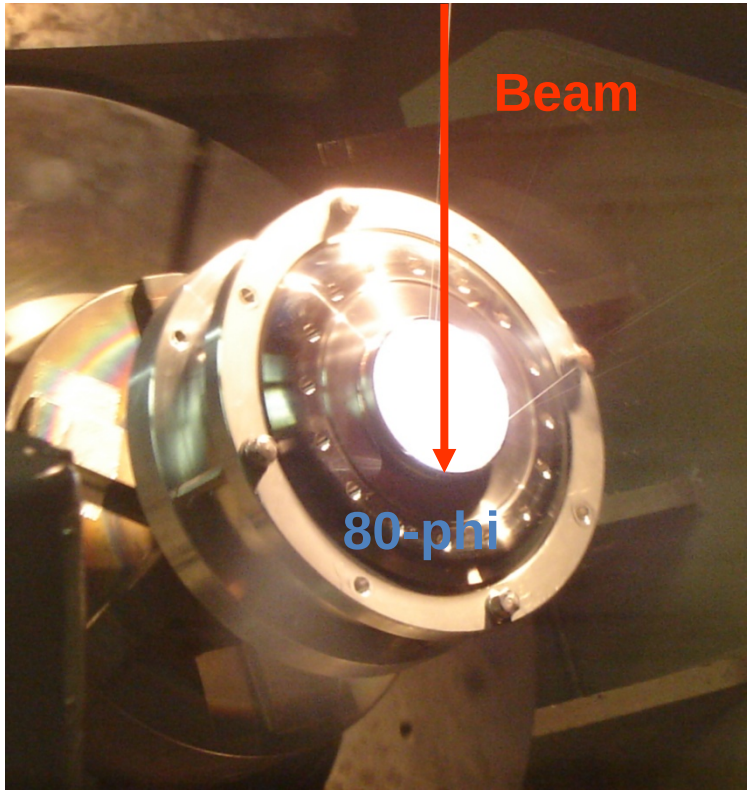

Base-plate 80-phi beam-pipe
+ Outer End-Cap

End-group EBW

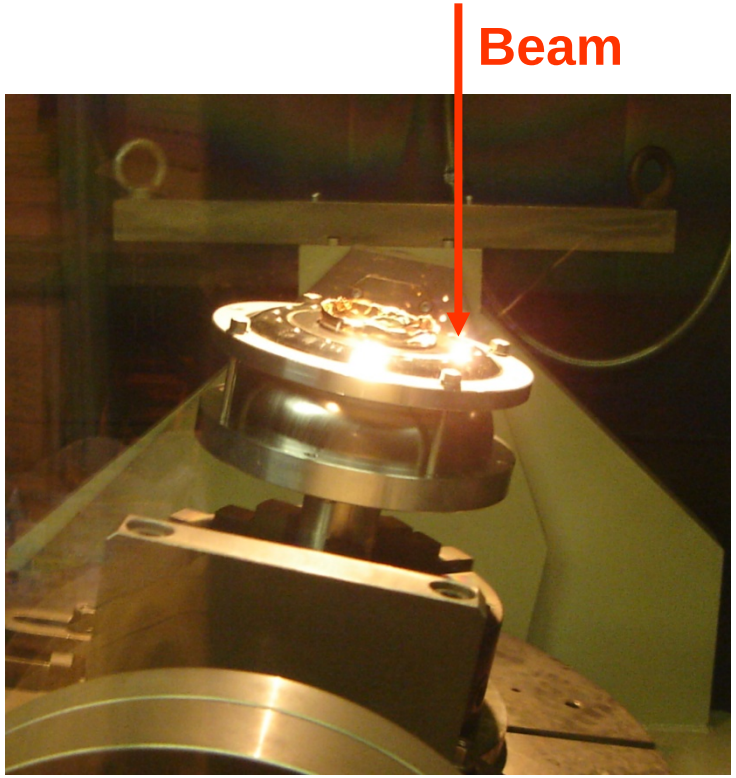

EBW of SUS Base-plate

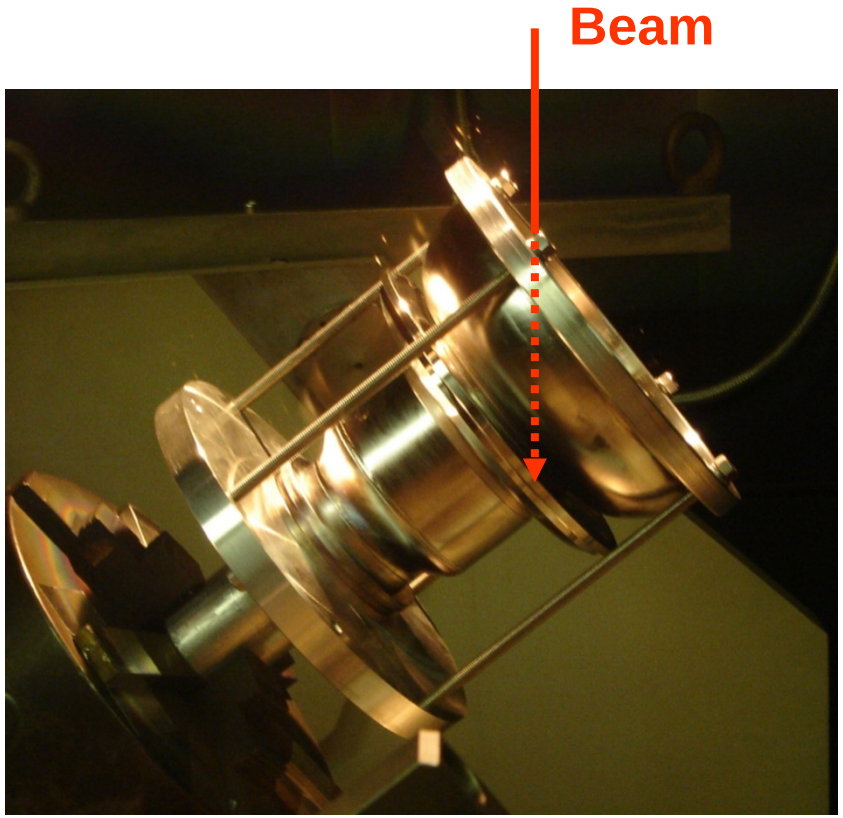

EBW of 108-phi beam-pipe

End-group assembled by EBW

EBW assembly of end-group + dummbells

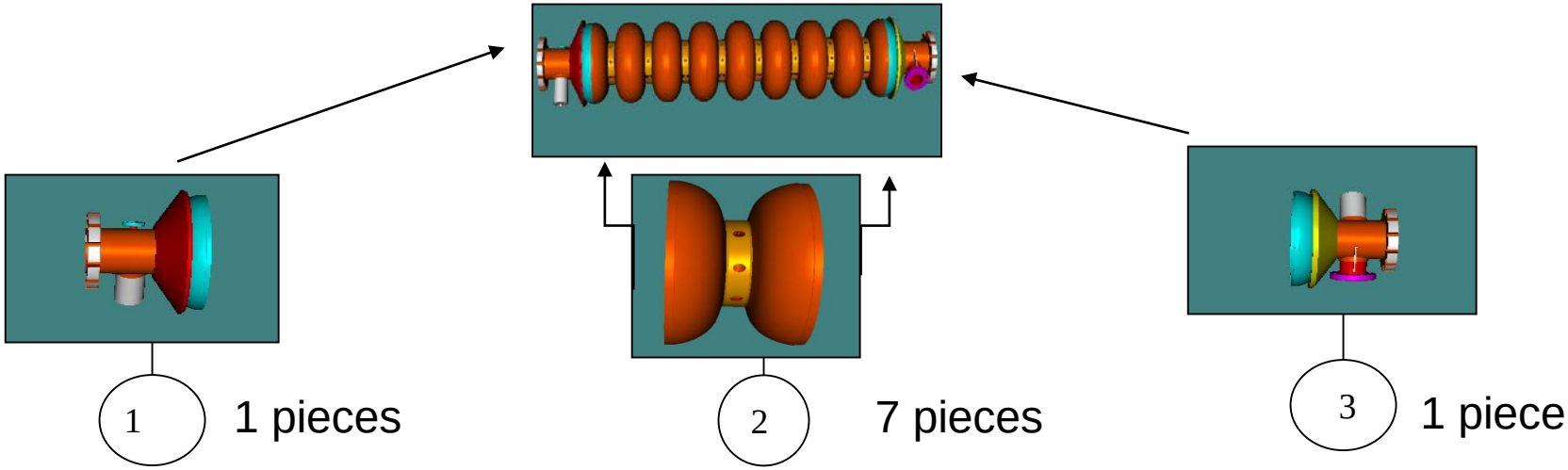

EBW of two dumbbells

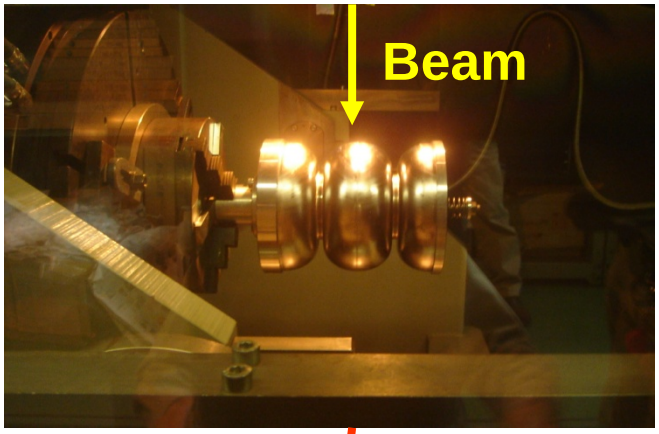

High magnetic field at equator.
The inner surface of equator should be defect-free.

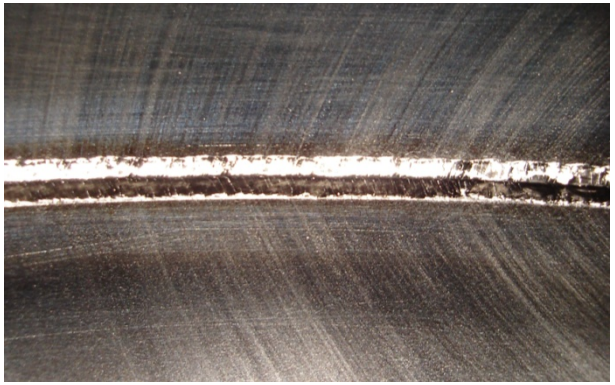

Good inner surface
(EBW with beam oscillation)

EBW of four dumbbells

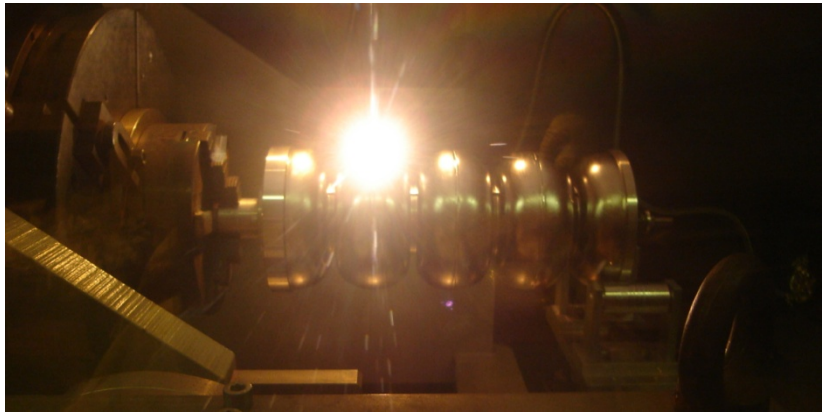

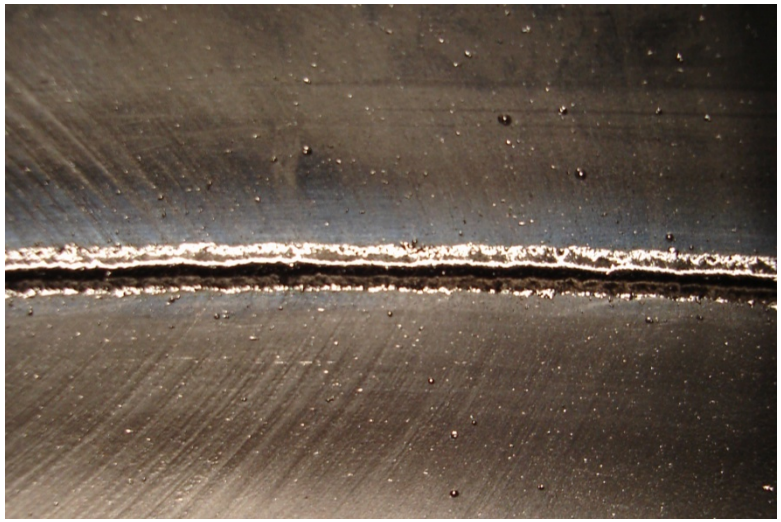

Bad EBW example

EBW of six dumbbells

Six dumbbells

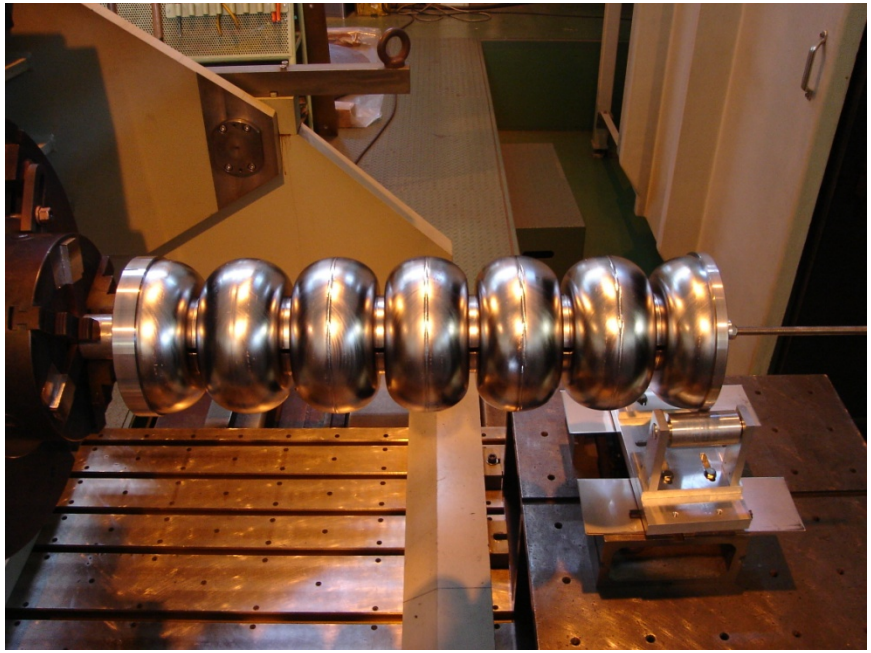

Beam

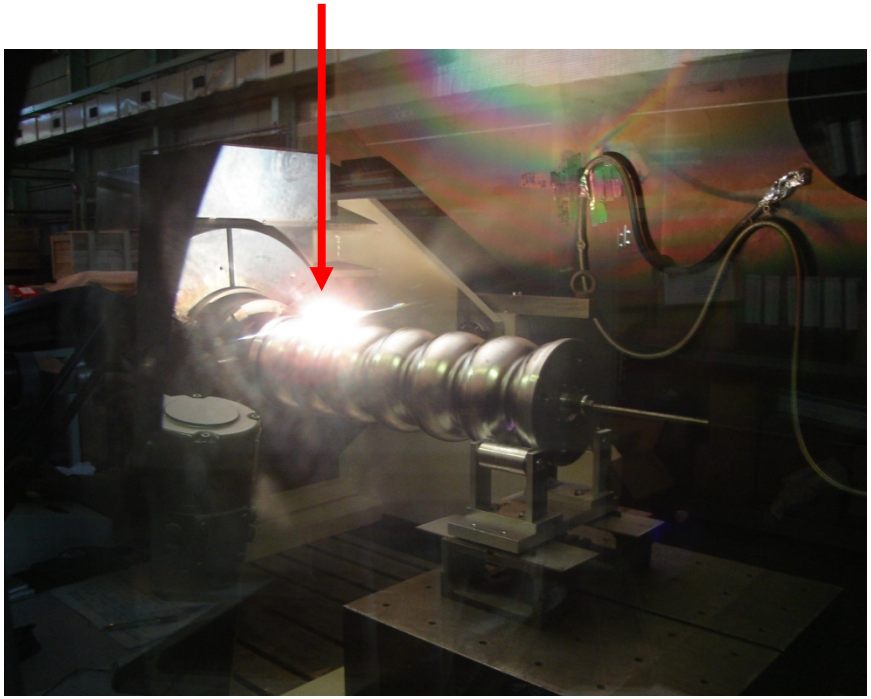

EBW of Center-cells + End-group

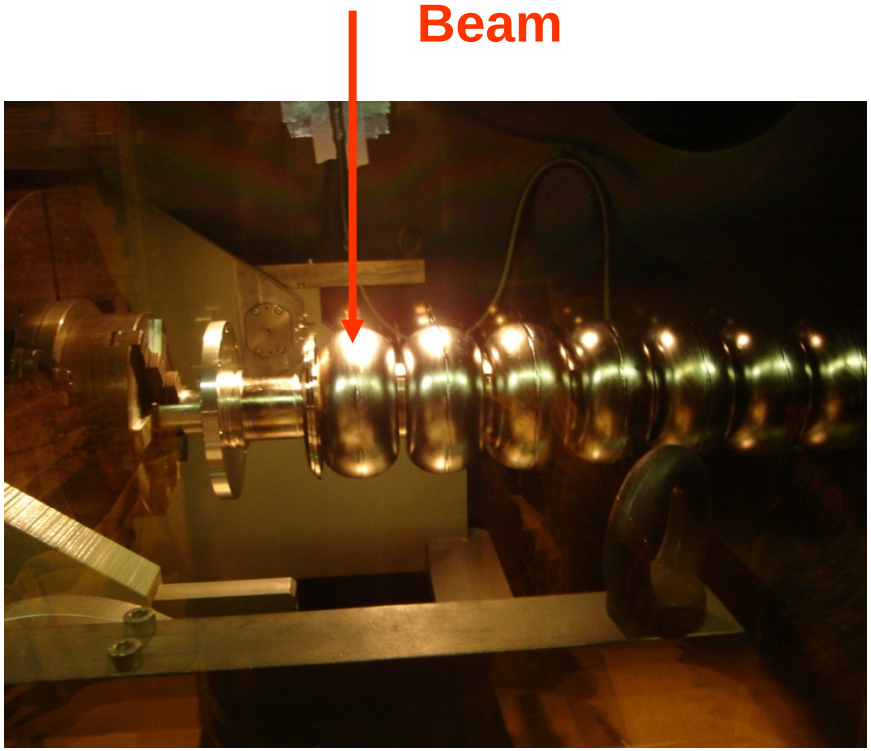

EBW of End-group + Center-cells

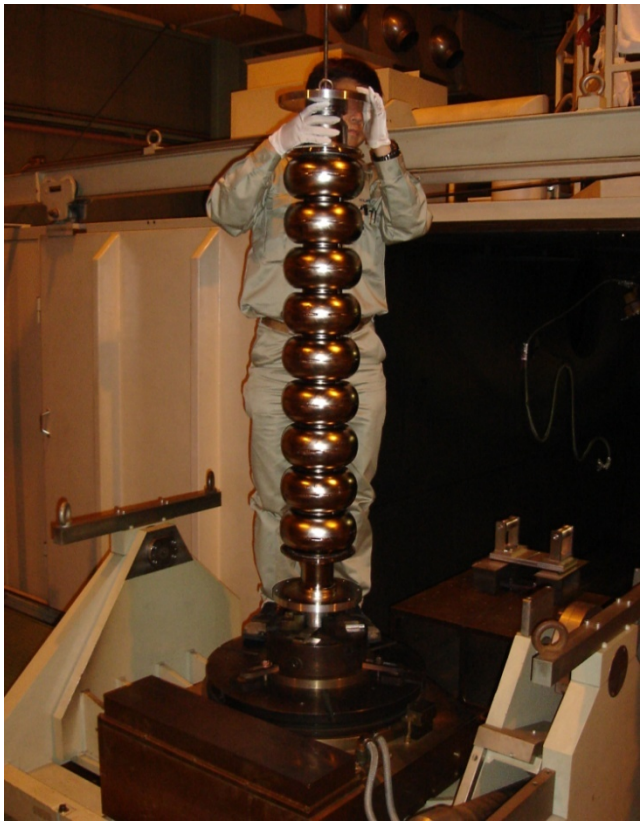

EBW completed

Fabrication of LL Cavity at KEK

EBW of dumbbells

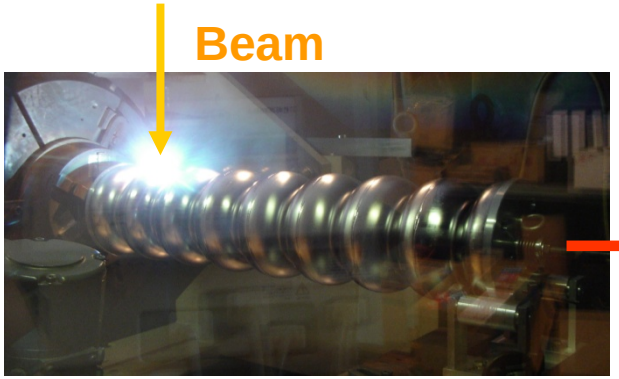

EBW of end-beam-pipe

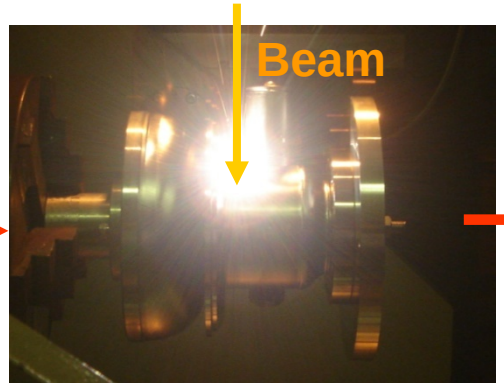

End-beam-pipes with HOM and flanges

EBW of end-beam-pipes and cell-part

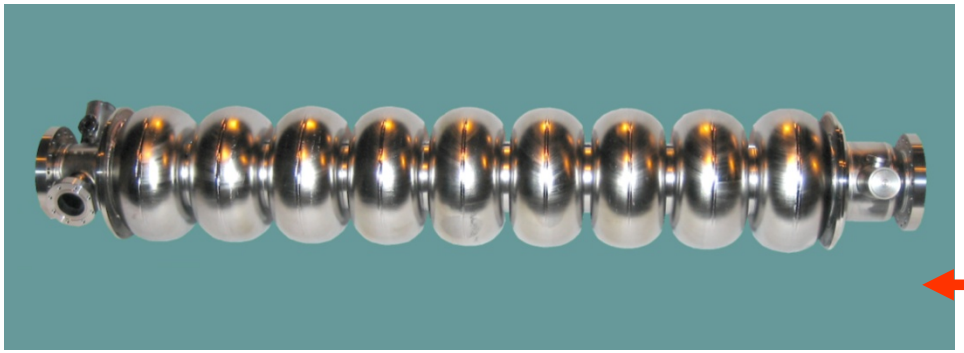

Delivery of 9-cell LL Cavities

1st, 2nd, 3rd, 4th LL 9-cell cavities

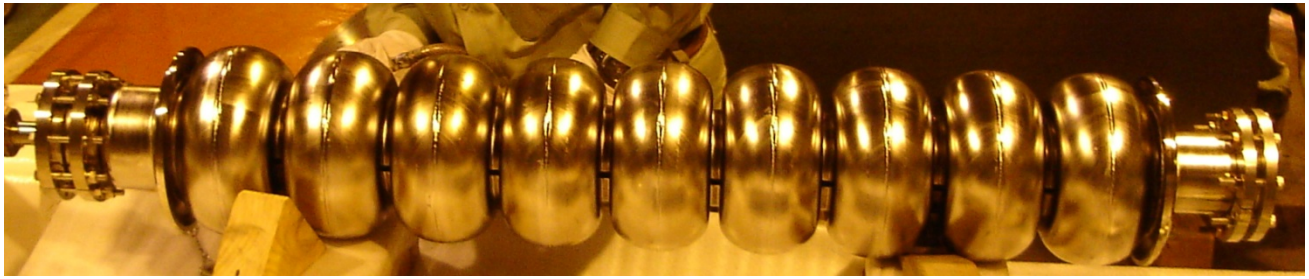

without
HOM coupler

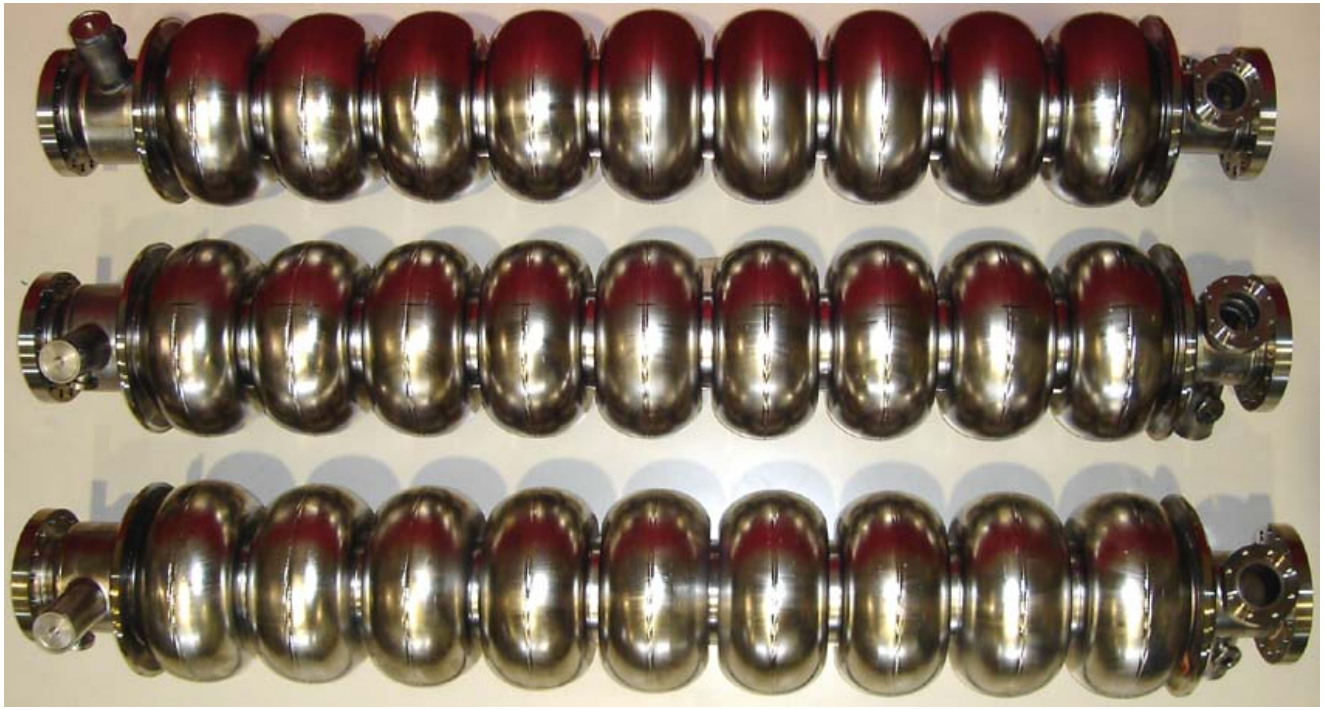

with
HOM coupler

with
HOM coupler

with
HOM coupler

Dimensional measurements

Length of the cavities were measured by 3D-measurement machine.

Dimensional deviation of length (only 9-cell part: 1038.5 mm)

- **-10 mm (1st 9-cell ICHIRO cavity)** ← Without dumbbell tuning
- **- 0.7 mm (2nd 9-cell ICHIRO cavity)**
- **- 0.1 mm (3rd 9-cell ICHIRO cavity)**
- **- 0.1 mm (4th 9-cell ICHIRO cavity)**

} With dumbbell tuning

Operator learned how to tune the dumbbells and fabrication error became less than 0.1 mm !

Straightness

3-D measurements of straightness of cavity

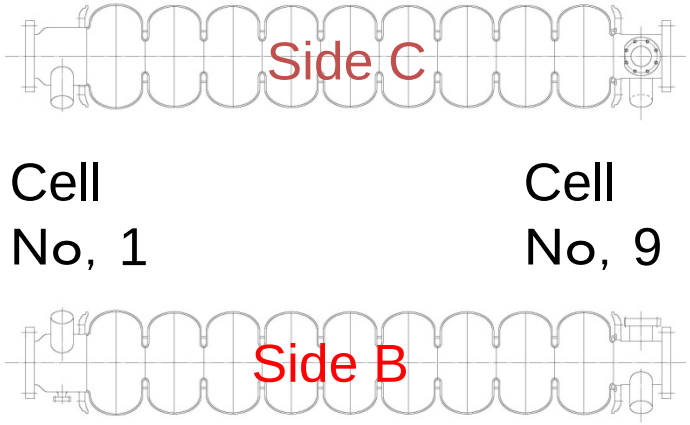

Cross-section view

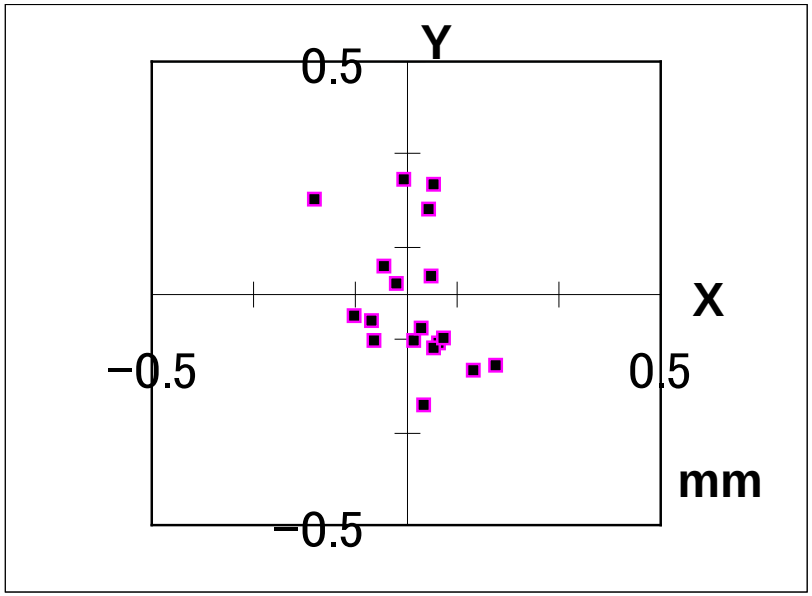

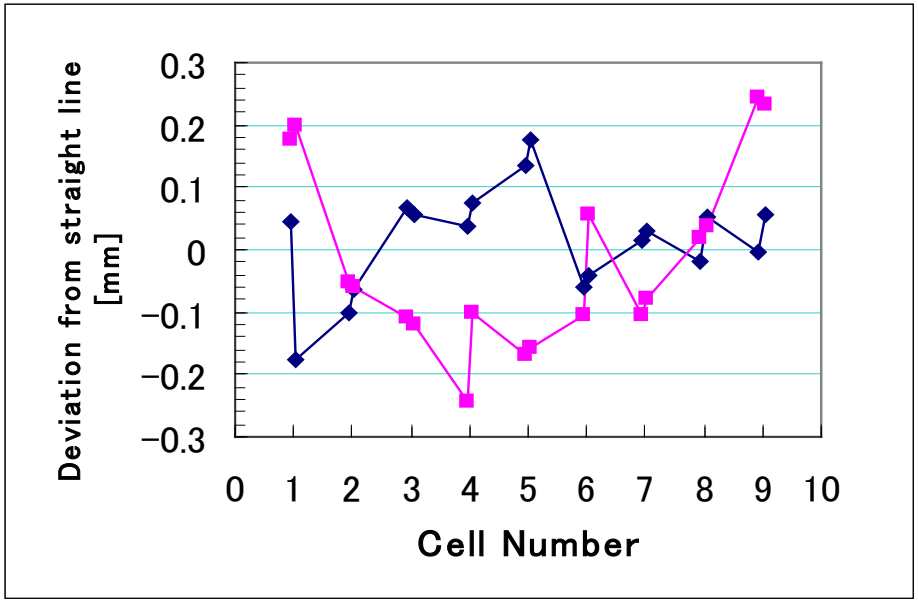

Pre-tuning for field flatness

Set-up for field profile measurements: a metallic needle is perturbing the rf fields while it is pulled through the cavity along its axis; the stored energy in each cell is recorded.

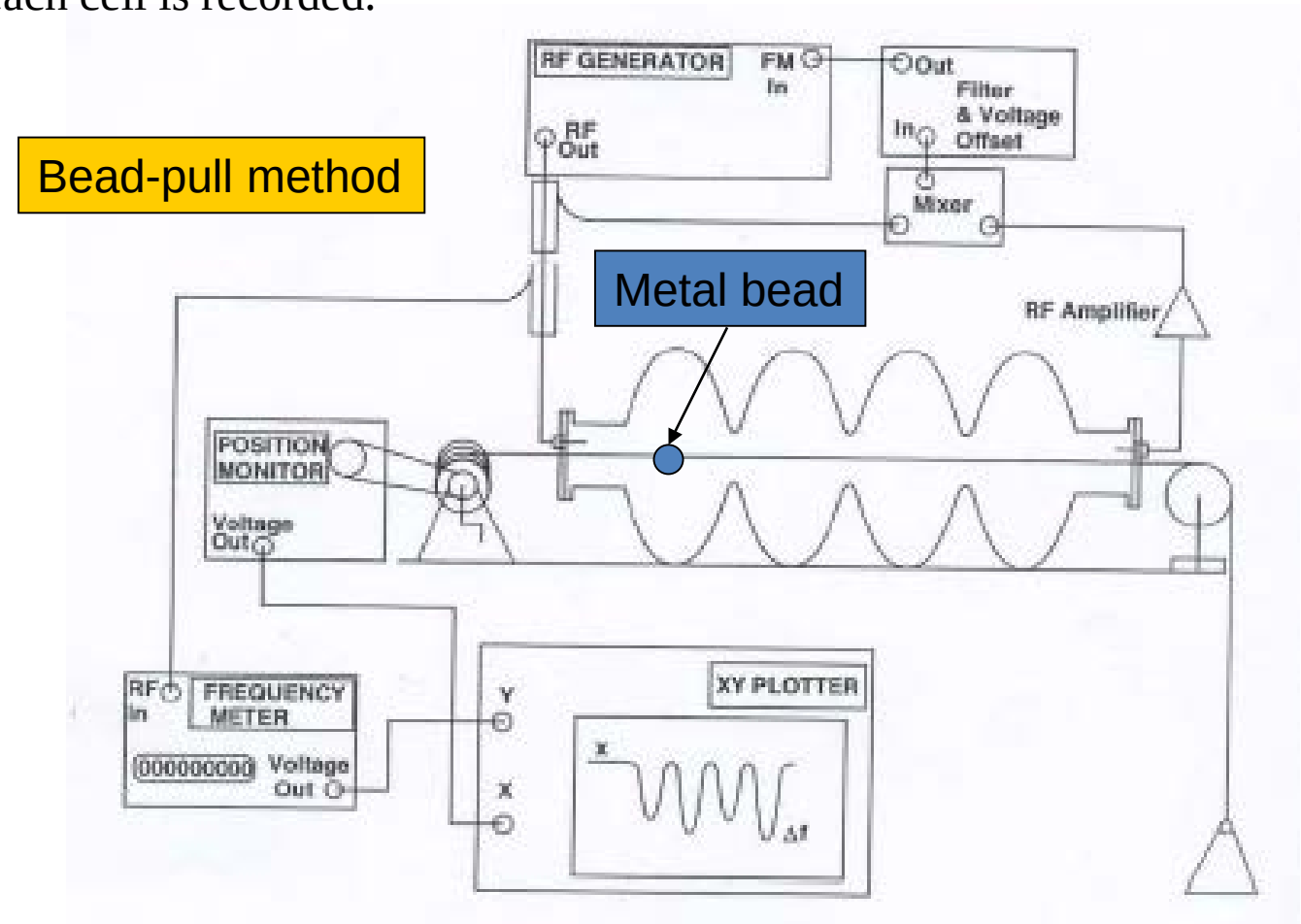

Filed flatness before/after pre-tuning

π mode frequency 1298.774 MHz

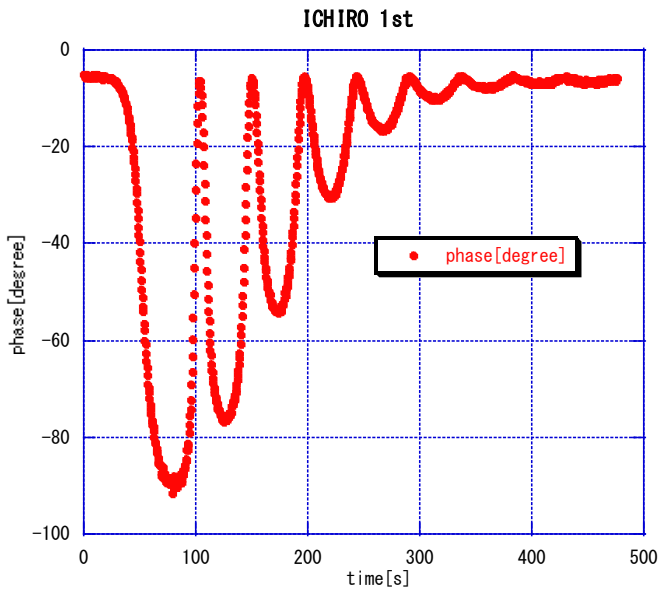

Field flatness = 0.1 %
(as delivered to KEK)

π mode frequency 1298.547 MHz

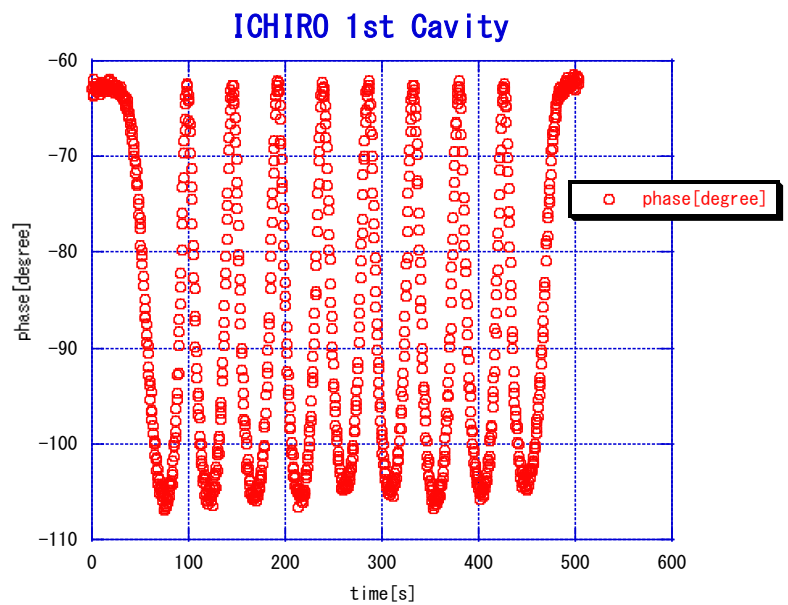

Field flatness = 98 %
(after pre-tuning)

Pre-tuning

Stepping-motor

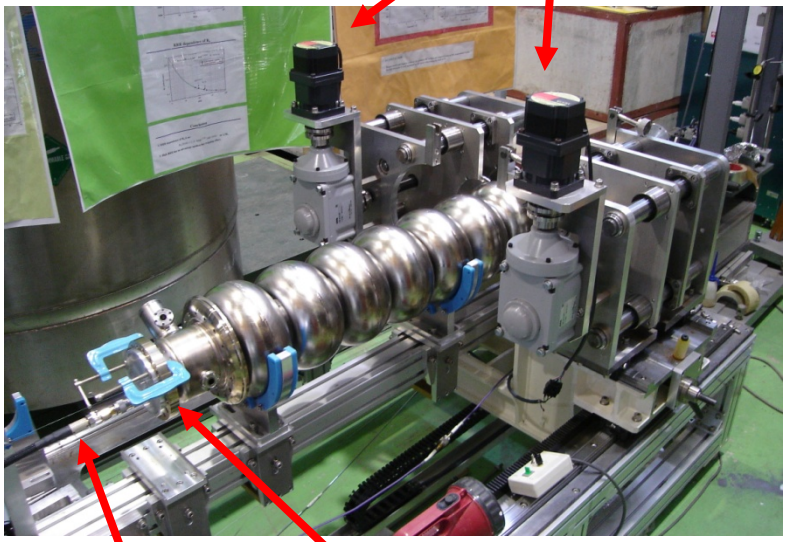

Flange with antenna

Line with metal bead

Blades are inserted into the iris

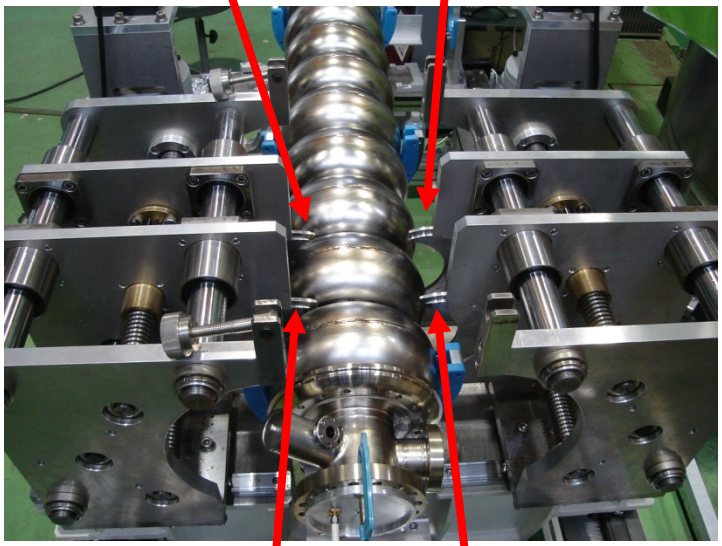

Blades are inserted into the iris

Pre-tuning

Metal bead

Antenna

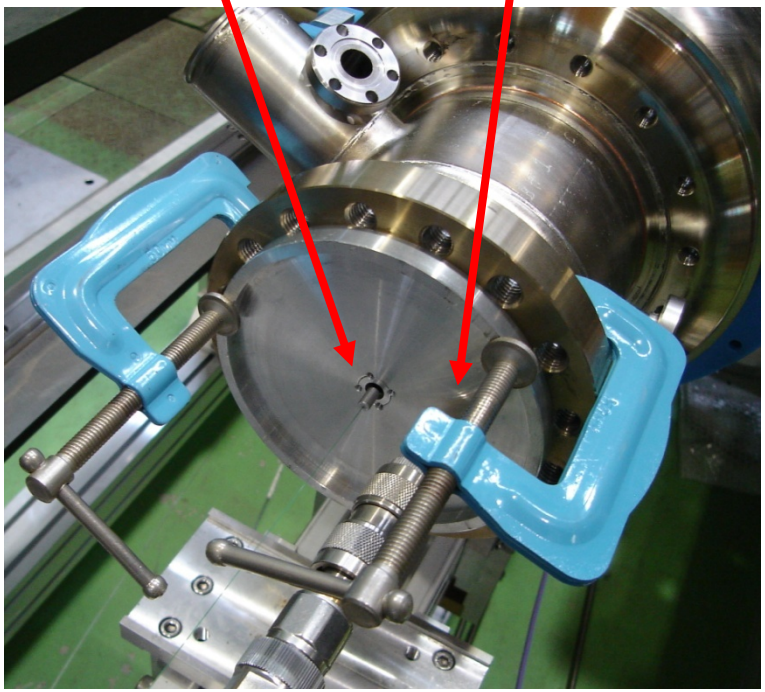

Pressing the cell by the blades